The University of Jordan
Authorization Form

I, Mouathe Ali Ameen authorize the University of Jordan to supply copies of my Thesis/Dissertation to libraries or establishments or individuals on request.

Signature:
Date:
16/10/2011

الجامعة الأردنيـــة
كلية الدراسات العليا

التاريـــخ: 2011/10/16

نموذج رقم (١٨)
اقرار والتزام بقوانين الجامعة الأردنية وأنظمتها وتعليماتها لطلبة الماجستير

أنا الطالب: معاذ علي حسن آمين   الرقم الجامعي: 8080969
التخصص: هندسة مدنية   الكلية: الهندسة والتكنولوجيا

اعلن بأنني قد التزمت بقوانين الجامعة الأردنية وأنظمتها وتعليماتها وقراراتها السارية المفعول المتعلقة باعداد رسائل الماجستير والدكتوراة عندما قمت شخصيا" باعداد رسالتي / اطروحتي بعنوان: Effect of Bridge Components on Live Load Distribution Factors in Prestressed Concrete Bridges.

وذلك بما ينسجم مع الأمانة العلمية المتعارف عليها في كتابة الرسائل والأطاريح العلمية. كما أنني أعلن بأن رسالتي /اطروحتي هذه غير منقولة أو مستلة من رسائل أو أطاريح أو كتب أو أبحاث أو أي منشورات علمية تم نشرها أو تخزينها في أي وسيلة اعلامية، وتأسيسا" على ما تقدم فانني أتحمل المسؤولية بأنواعها كافة فيما لو تبين غير ذلك بما فيه حق مجلس العمداء في الجامعة الأردنية بالغاء قرار منحي الدرجة العلمية التي حصلت عليها وسحب شهادة التخرج مني بعد صدورها دون أن يكون لي أي حق في التظلم أو الاعتراض أو الطعن بأي صورة كانت في القرار الصادر عن مجلس العمداء بهذا الصدد.

توقيع الطالب: ....   التاريخ: 2011/10/16

EFFECT OF BRIDGE COMPONENTS ON LIVE LOAD DISTRIBUTION FACTORS IN PRESTRESSED CONCRETE BRIDGES

By
MOUATHE ALI AMEEN

Supervisor
Dr. NAZZAL S. ARMOUTI

This Thesis was Submitted in Partial Fulfillment of the Requirements for the Master's Degree of Science in Structural Engineering

Faculty of Graduate Studies
The University of Jordan

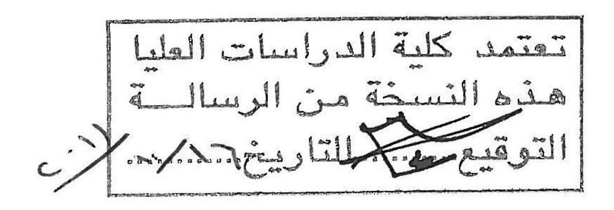

October, 2011

COMMITTEE DECISION

This Thesis **(Effect of Bridge Components on Live Load Distribution Factors in Prestressed Concrete Bridges)** was Successfully Defended and Approved on 10/10/2011

Examination Committee | **Signature**

Dr. Nazzal S. Armouti, (Supervisor)
Chairman of Civil Engineering Department,
Associate Professor of ~~Structural~~ Civil Engineering

Prof. Dr. Samih S. Qaqish, Member
Dean of the Faculty of Engineering and Technology,
Professor of Structural Engineering

Dr. Maha K. Alqam, Member
Assistant Professor of Structural Engineering

Prof. Dr. Musa R. Resheidat, External Member
Professor of Structural Engineering
Jordan University of Science and Technology

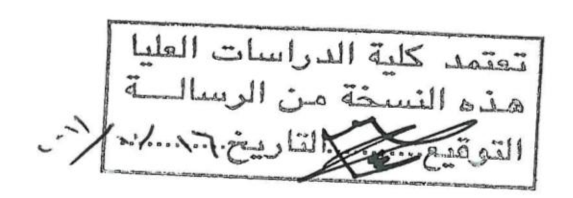

DEDICATION

This work is dedicated to soul of my graduate teacher Prof. Bassam Abu-Gazaleh, who died suddenly in summer 2009, and I would like to say, “We will never forget you”.

To my Mother, Safeyia who was passionate about discovering the science and for her unfailing support and expertise in helping me to prepare this Thesis.

To my father, Ali and my Brothers, Mohammed & Hasan who are a never-ending source of love, pride, and inspiration for me.

ACKNOWLEDGMENTS

I wish to express my appreciation to Prof. Bassam Z. Mahasneh of Mutah University, for his technical help and support in Computer Programs.

Special thanks to examining committee members, for their constructive comments and contribution to this work, Prof. Samih S. Qaqish, Dr. Maha K. Alqam, and Prof. Musa R. Resheidat.

Thanks also to my fellow graduate students for their assistance throughout this research.

My sincere thanks and gratitude goes to Dr. Nazzal S. Armouti for his support and help throughout this research and for guidance and encouragement as my graduate advisor. Thanks also for directing me with his knowledge and experience in many long discussions on various topics related to my research.

TABLE OF CONTENTS

	Page
COMMITTEE DECISION	ii
DEDICATION	iii
ACKNOWLEDGEMENT	iv
TABLE OF CONTENTS	v
LIST OF TABLES	vii
LIST OF FIGURES	viii
ABSTRACT	xi
1 INTRODUCTION	1
1.1 Load Distribution Factors of PC Bridges	2
1.2 Literature Review	8
1.3 Objectives of the Study	15
2 METHODOLOGY AND ANALYSIS METHODS	16
2.1 Method No. 1: Full 3D Finite Element Method	17
2.1.1 Compatibility between Shell and Beam Elements	18
2.1.2 Finite Element Model of Vehicular Live Loads	22
2.2 Method No. 2: Grillage Analysis of Bridges	24
2.2.1 Advantages and Disadvantages of Grillage Method	27
2.3 Nonlinear Analysis of Bridges under Plastic Stages	29
3 FINITE ELEMENT MODEL OF PC BRIDGES	32
3.1 Description of Bridge Models	33
3.2 Finite Element Modeling by ADINA	36
3.2.1 An Overview	36

3.2.2 Modeling of Prestressing Tendons 42

3.2.3 Modeling of Vehicular Loads 45

3.2.4 Modeling of RC Diaphragms 51

3.3 Structural Nonlinearity of PC Bridge 53

3.3.1 An Overview 53

3.3.2 Material Nonlinearity – Plastic Models 55

3.3.4 Material Nonlinearity – Concrete Models 57

3.3.5 Contact Nonlinearity 59

3.4 Nonlinear Analysis of PC Bridge 62

4 DISCUSSION OF MODELING AND RESULTS 64

4.1 An Overview 65

4.2 Behavior of Concrete and Plastic Material Models 67

4.3 Calculation of Load Distribution Factors 70

4.3.1 An Overview 70

4.3.2 FEA Results of Analyzed Bridges 71

4.4 Discussion of Results 85

4.4.1 Effect of Diaphragms on LDF 89

4.4.2 Effect of Girder Types on LDF 90

4.4.3 Effect of Structural Nonlinearity on LDF 92

4.5 General Checks on ADINA 94

5 CONCLUSIONS AND RECOMMENDATIONS 95

REFERENCES 100

ABSTRACT (IN ARABIC) 103

LIST OF TABLES

Number	Table Caption	Page
Table 4.1	Max. Stresses and Moments for Bridge Model No.1: BT54 Girders Bridge	71
Table 4.2	Max. Stresses and Moments for Bridge Model No.2: BIV Girders Bridge	72
Table 4.3	Max. Shears for Bridge Model No.1: BT54 Girder Bridge	72
Table 4.4	Max. Shears for Bridge Model No.2: BIV36 Girders Bridge	73
Table 4.5	Comparison of LDF–Moments in Bridge Model No.1	74
Table 4.6	Comparison of LDF–Moments in Bridge Model No.2	75
Table 4.7	Comparison of LDF–Shears in Bridge Model No.1	75
Table 4.8	Comparison of LDF–Shears in Bridge Model No.2	76
Table 4.9	Comparison of LDF-Moments at Elastic and Ultimate Stages for Diaphragms Models in Bridge Model No.1	79
Table 4.10	Comparison of LDF-Moments at Elastic and Ultimate Stages for Non-Diaphragms Models in Bridge Model No.1	79
Table 4.11	Comparison of LDF-Moments at Elastic and Ultimate Stages for Diaphragms Models in Bridge Model No.2	80
Table 4.12	Comparison of LDF-Moments at Elastic and Ultimate Stages for Non-Diaphragms Models in Bridge Model No.2	80
Table 4.13	Comparison of LDF-Shears at Elastic and Ultimate Stages for Diaphragms Models in Bridge Model No.1	81
Table 4.14	Comparison of LDF-Shears at Elastic and Ultimate Stages for Non-Diaphragms Models in Bridge Model No.1	81
Table 4.15	Comparison of LDF-Shears at Elastic and Ultimate Stages for Diaphragms Models in Bridge Model No.2	82
Table 4.16	Comparison of LDF-Shears at Elastic and Ultimate Stages for Non-Diaphragms Models in Bridge Model No.2	82

LIST OF FIGURES

Number	Figure Caption	Page
Figure 1.1	Characteristics of AASHTO Design Truck	4
Figure 1.2	Intermediate Diaphragms between PC Girders	6
Figure 1.3	Intermediate Diaphragms between PC Girders	7
Figure 2.1	Full 3D Finite Element Model	17
Figure 2.2	Bridge Cross-Section at Midspan	18
Figure 2.3	Cross-Section of Finite Element Model of Two Girders	19
Figure 2.4	Typical Bending DOFs and Node Numbering of Shell Elements	21
Figure 2.5	View of Tire Contact Area of AASHTO HS20 Truck	22
Figure 2.6	Discretization of Patch Load	23
Figure 2.7	Grillage Model (a) Prototype Deck and (b) Equivalent Grillage	24
Figure 2.8	(a) Grillage Model, (b) Crossing with Translational Continuity, (c) Crossing with Translational and Rotational Continuity, and (d) Degrees of Freedom in Grillage (Plane Grid) Modeling	26
Figure 2.9	Stress Contour for Bridge Model Under Live Load	30
Figure 3.1	Cross-Section of Bridge Model No.1: Slab on BT54 Girders Bridge	33
Figure 3.2	Cross-Section of Bridge Model No.2: Slab on BIV36 Girders Bridge	34
Figure 3.3	Posttensioned AASHTO-PCI Girder BT54, A_g = 425000 mm^2	35
Figure 3.4	Posttensioned AASHTOBox Girder BIV36, A_g = 458000 mm^2	35
Figure 3.5	Mesh Generation of Bridge Model No.1_Configuration No.1	36
Figure 3.6	Mesh Generation of Bridge Model No.1_Configuration No.2	37
Figure 3.7	Mesh Generation of Bridge Model No.2_Configuration No.1	38
Figure 3.8	Some 3D Solid Elements	39

Figure 3.9	Mesh Generation of Bridge Model No.2_Configuration No.2	40
Figure 3.10	Solid Deck Model	41
Figure 3.11	Eccentric Beam Model Including Prestressing Tendon	42
Figure 3.12	Prestressed Concrete Bridge Model	43
Figure 3.13	Profile of Harped Tendons, defined as Truss Element in Bridge Model No.1	44
Figure 3.14	Profile of Straight Tendons, defined as Truss Element in Bridge Model No.2	44
Figure 3.15	Exterior Girder Loading in Bridge Model No.1_Configuration No.1	45
Figure 3.16	Interior Girder Loading in Bridge Model No.1_Configuration No.2	46
Figure 3.17	Interior Girder Loading in Bridge Model No.2_Configuration No.1	47
Figure 3.18	Exterior Girder Loading in Bridge Model No.2_Configuration No.2	48
Figure 3.19	Single Concentrated Wheel Load on Shell Element	49
Figure 3.20	Typical Diaphragm Details	51
Figure 3.21	Mesh Generation of RC Diaphragm in Bridge Model No.1	52
Figure 3.22	RC Diaphragm in Bridge Model No.2	52
Figure 3.23	Degree of Freedom and Nodal Forces for a framed Member, (a) 2D Member, (b) 3D Member	54
Figure 3.24	Isotropic and Kinematic Hardening	55
Figure 3.25	Uniaxial Compressive and Tensile Stress-Strain Curve of Concrete	57
Figure 3.26	Normal Vectors in Contact Conditions between BT54 Girder and Prestressing Tendons in Bridge Model No.1	60
Figure 3.27	Normal Vectors in Contact Conditions between BIV36 Girder and Prestressing Tendons in Bridge Model No.2	61
Figure 3.28	Different Type of Nonlinear Analysis	63
Figure 4.1	Stress Contour for Bridge Model No.1 under Exterior Girder Loading	65
Figure 4.2	Stress Contour for Bridge Model No.1 under Interior Girder Loading	66
Figure 4.3	Uniaxial Stress-Strain Curve for Prestressing Tendons, by ADINA Program	67
Figure 4.4	Uniaxial Compressive and Tensile Stress-Strain Curve of PC Girder, by ADINA Program	68

Figure 4.5	Uniaxial Compressive and Tensile Stress-Strain Curve of Deck Slab and Diaphragms, by ADINA Program	69
Figure 4.6	Determination of Load Distribution Factors (LDF)	70
Figure 4.7	Comparison of FEA Max. Moments between All Bridge Models	73
Figure 4.8	Comparison of FEA Max. Shears between All Bridge Models	74
Figure 4.9	Comparison of FEA LDFs_Moments to AASHTO LDFs_Moments between All Bridge Models for Interior Loading	76
Figure 4.10	Comparison of FEA LDFs_Moments to AASHTO LDFs_Moments between All Bridge Models for Exterior Loading	77
Figure 4.11	Comparison of FEA LDFs_Shears to AASHTO LDFs_Shears between All Bridge Models for Interior Loading	77
Figure 4.12	Comparison of FEA LDFs_Moments to AASHTO LDFs_Moments between All Bridge Models for Exterior Loading	78
Figure 4.13	Nonlinear Curve (Load Steps Vs Displacement) at Midspan, by ADINA Program. The Jump at the Final Point Indicates the Failure Point of Bridge Model	78
Figure 4.14	Comparison of LDFs_Moments at Elastic and Ultimate Stages between All Bridge Models for Interior Loading	83
Figure 4.15	Comparison of LDFs_Moments at Elastic and Ultimate Stages between All Bridge Models for Exterior Loading	83
Figure 4.16	Comparison of LDFs_Shears at Elastic and Ultimate Stages between All Bridge Models for Interior Loading	84
Figure 4.17	Comparison of LDFs_Shears at Elastic and Ultimate Stages between All Bridge Models for Interior Loading	84
Figure 4.18	Displacement Contour for Bridge Model No.2 under Interior Loading	85
Figure 4.19	Crack Stress for Bridge Model No.1 under Interior Girder Loading	86
Figure 4.20	Crack Stress for Bridge Model No.2 under Exterior Girder Loading	87
Figure 4.21	Reactions Plots for Bridge Model No.1 under Interior Loading	89

EFFECT OF BRIDGE COMPONENTS ON LIVE LOAD DISTRIBUTION FACTORS IN PRESTRESSED CONCRETE BRIDGES

By
MOUATHE A. AMEEN

Supervisor
Dr. NAZZAL S. ARMOUTI

ABSTRACT

Load Distribution Factor (LDF) for moment and shear in multi-grider bridges is investigated under various conditions. Effect of girder type and presence of diaphragms on the LDF is evaluated. Two girder types are considered in the investigation, namely, prestressed concrete bulb-tee girder bridge, and spread box girder bridge.

Finite element model is developed for the bridges using ADINA software. The bridge slab is modeled as 3D solid elements, whereas the girders as well as the diaphragms are modeled as nonlinear shell elements. The analysis is carried out through the inelastic range.

It has been found, as expected that AASHTO load distribution formulas are conservative with respect to finite element analysis. AASHTO formulas seem to yield higher values of loading up to 20% over the finite element results.

It has also been found that the effect of presence of diaphragms on the moment LDF depends on the type of girders and their location. For interior girders, the presence of diaphragms decreases the LDF in tee girders, while increases the LDF in the box girders. For exterior girders, the presence of diaphragms increases the LDF in tee girders, while decreases the LDF in the box girders.

If desired, bridge reserved capacity due to inelastic behavior may be utilized. Due to its nonlinearity, inelastic behavior can only be utilized on case by case basis as LDF concept will not be valid for this stage of behavior.

CHAPTER ①: INTRODUCTION

CHAPTER 1
INTRODUCTION

1.1 Load Distribution Factors of PC Bridges

The AASHTO Standard Specifications for Highway Bridges have contained live load distribution factors (LDF) since 1931. The early values were based on the work done by Westergaard (1930) and Newmark (1948), but the factors were modified as new research results became available. For a bridge constructed with a concrete deck on prestressed concrete I or Bulb-Tee girders and carrying two or more lanes of traffic, the current distribution factor for moment in the AASHTO (2002) Standard Specifications, in SI unit is (S/1676), and for concrete deck on spread box girders is (S/2134), where S is the girder spacing (mm), this factor multiplied by the moment on a single girder, caused by one line of wheels, gives the girder design moment.

A more accurate LDF equation was introduced in the AASHTO (2010) LRFD Specifications, as an alternative to the Standard Specifications. This equation was based on Finite Element Analysis and Probability Theory.

The load distribution factor for moment from AASHTO LRFD for concrete slab on prestressed concrete BT girder bridges under *interior girder loading* with two or more design lanes loaded in SI unit is

$$0.075+\left(\frac{S}{2900}\right)^{0.6}\left(\frac{S}{L}\right)^{0.2}\left(\frac{K_g}{Lt_s^{\,3}}\right)^{0.1} \qquad (1.1)$$

For shear, the load distribution factor under interior girder loading with two or more design lanes loaded is

$$0.2+\frac{S}{3600}-\left(\frac{S}{10\ 700}\right)^{2.0} \qquad (1.2)$$

While the load distribution factor for moment in spread box girders under interior girder loading with two or more design lanes loaded is

$$\left(\frac{S}{1900}\right)^{0.6}\left(\frac{Sd}{L^2}\right)^{0.125} \tag{1.3}$$

For shear, the load distribution factor under interior girder loading with two or more design lanes loaded is

$$\left(\frac{S}{2250}\right)^{0.8}\left(\frac{d}{L}\right)^{0.1} \tag{1.4}$$

where L is span length (mm), $K_g = n(I+Ae^2)$ is longitudinal stiffness (mm^4), t_s is slab thickness (mm), n is modular ratio between steel and concrete, I is girder stiffness (mm^4), A is girder area (mm^2), e is eccentricity between centroids of girder and slab (mm), and d is the overall depth of the girder.

The lever rule method can be used to determine the load distribution factors for *exterior girder loading.* It involves a statical distribution of load based on the assumption that each deck panel is simply supported over the girder, except at the exterior girder that is continuous with the cantilever. Because the load distribution to any girder other than one directly next to the point of load application is neglected, the lever rule is a conservative method of analysis.

The load distribution factor by AASHTO LRFD is the number of design lanes per girder, while other load distribution factors are in terms of the number of wheel lines per girder.

With the development of computational tools, engineers are increasingly using a grillage or finite element models to analyze the entire bridge. However, there are still many reasons that bridge engineers need to simplify a bridge system into individual components, which uncouples the longitudinal and transverse load effects with the so-called load distribution factors (LDF).

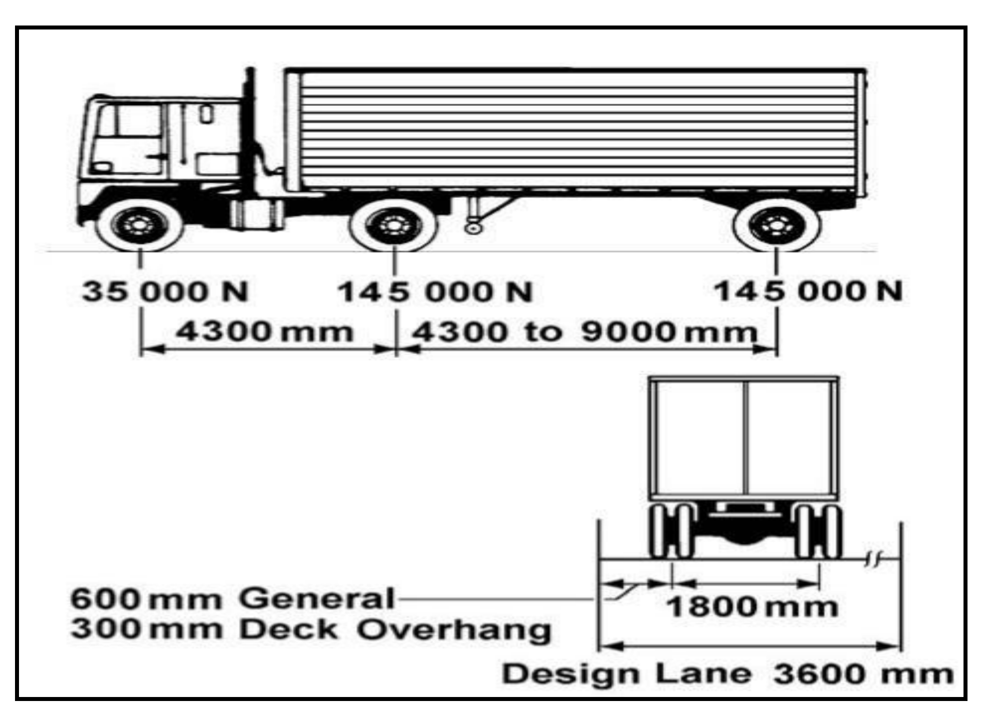

Figure 1.1 Characteristics of AASHTO Design Truck (AASHTO LRFD Specifications, 2010).

To simplify the design process, many bridge codes, such as the AASHTO LRFD Specifications, and the AASHTO Standard Specifications, treat the longitudinal and transverse effects of wheel loads as uncoupled phenomena. The design live load moment caused by a truck (or lane of traffic) is first estimated by obtaining the maximum truck (or lane of traffic) moment on a single girder. A designer then obtains the design moments for each girder by multiplying the maximum single girder moment by a factor, which is usually referred to as the live load distribution factor.

Load distribution among girders reflects the bridge response to applied loads and has been studied extensively in the last few decades (Heins and Kuo 1975, Kim and Nowak 1997, Mabsout et al. 1999, among many others). The LDF is a function of many parameters, such as the bridge geometry, the relative stiffness of the components, and the nature of the loads. The load distribution is different in different situations, such as service versus ultimate strength state, moment versus shear, and positive versus negative moment. The current AASHTO (2010) LRFD Specifications recognize that the

LDF is a function of girder spacing, span length, slab thickness, and beam stiffness. The LDFs are specified differently for exterior and interior girders, for shear and moment, and for one-lane loaded and two-or-more-lane loaded cases. The LRFD expressions for live-load distribution are based on the results of a parametric study by Zokaie et al. (1991), which considers variations in girder spacing, girder stiffness, span length, skew, and slab stiffness.

The finite-element models used to develop the AASHTO LRFD Specifications equations were detailed, but the models did not include all of the components of a typical bridge. For example, Zokaie et al. considered the effects of diaphragms in a pilot study but not in the main parametric study. In addition, the factor that Zokaie et al. proposed to account for girder continuity was not included in the LRFD Specifications.

Consequently, the LRFD code expressions are based on the results of analyses for HL-93 loading (Figure 1.1) of simply supported bridges without lifts (the effect of concrete layer between the top of the girder and the bottom of deck), intermediate diaphragms, or end diaphragms.

The AASHTO LRFD Specification equations for the distribution factors are more accurate than those provided in the Standard Specifications (Mabsout et al. 1997). However, Chen and Aswad (1996) found that the LRFD code distribution factors can be uneconomically conservative for bridges with large span to depth ratios. Based on the results of finite-element analysis, Chen and Aswad found that this conservatism could be as much as 23% for interior beams and 12% for exterior beams. A reduction in the conservatism of the code would lead to more economical bridge designs.

Diaphragms have been thought to contribute to the overall distribution of live loads in bridges; cast-in-place concrete diaphragms are commonly used in prestressed concrete I-girder bridges. According to the AASHTO Standard Specifications, “A diaphragm is a

transverse stiffener, which is placed between girders in order to maintain section geometry."

Figure 1.2 Intermediate Diaphragms between PC Girders.

The AASHTO Standard Specifications recommend that Intermediate Diaphragms (IDs) as shown in Figure 1.2, be used at the point of the maximum positive moment for spans in excess of 40 ft (12 m). It is stated in AASHTO LRFD Specifications, that IDs can improve live load distributions, but this effect is not included in the design specifications.

Some of the arguments in favor of using IDs rely on the fact that they can transfer lateral loads to and from the deck, distribute vertical live loads between girders, thus reducing maximum deflection and moment for each individual girder, provide lateral supports to girders during construction; and distribute lateral impact loads from over-height trucks to all girders, thus reducing the total damage.

Figure 1.3 Intermediate Diaphragms between PC Girders.

1.2 Literature Review

One of the important components of this study is to conduct a thorough review of existing literature on various aspects of diaphragms for prestressed concrete (PC) girder bridges. Debate on the need for IDs in slab-over-prestressed-concrete-girder bridges started in the late 1960s, with some studies stating that in some cases, IDs are counterproductive.

The first of the reports which raised the question on the need for IDs in PC bridges was the report by Lin and Van Horn (1968). Results from their study were obtained from the field tests conducted on a bridge in Philadelphia and produced surprising conclusions, diaphragms were found to transmit the loads laterally. However, when various lanes were loaded at the same time, the experimentally determined distribution factors were not appreciably affected.

Moreover, the deflections in the girder reduced slightly with the provision of the IDs in the bridge structure, thereby putting the advantage of IDs in load distribution into question.

Burdette and Goodpasture (1973) performed experimental tests on four highway bridges. The tested bridges were subjected to exploratory loads, truck loads up to twice the HS20 loads, and finally to static loads up to failure. All bridges were two-lane deck-on-girder with four longitudinal girders. One of the four tested bridges was a composite simple span with AASHTO type III precast, prestressed concrete girders spaced 200-250 mm on center. This bridge was 20 m long and skewed by 70^o. In the tests performed, the ultimate loading was defined as the maximum load attained in a test to failure, and failure was said to occur when deflections continued to increase at sustained loads. It was observed that concrete diaphragms cracked at early loading steps. This early cracking, however, had no measurable effect on the load-deflection behavior on

any of the tested bridges. The prestressed concrete bridge failure occurred when interior girders failed in shear at total load equal to 5070 kN.

Kostem (1977) investigated the effect of diaphragms on the lateral distribution of live load in simple-span, beam-slab bridges with prestressed concrete I-beams without skew. Data from two field tested bridges were used to validate the finite element model. The bridges had span lengths of 22 m and 21 m. It was found that only 20 to 30% of the stiffness of midspan reinforced concrete diaphragms contributes to load distribution. This contribution becomes negligible when all lanes are loaded, in which case the bridge models behaved as if there were no diaphragms. The contribution of diaphragms to load distribution, contrary to intuitive beliefs, was not of relevant importance regardless of the loading pattern. Contrary to their expectations, the increase in the number of diaphragms did not necessarily correspond to a more even distribution of loads at mid-span. Overall, the contribution of intermediate diaphragms was not found to be significant. According to this study, these findings can be applied to bridges with moderate skew (0 to 30^o) as well as right continuous bridges. A recommendation was made that vehicle overload and large skew effects be considered before eliminating the use of IDs.

Cheung et al. (1986) found that previous researchers disagree not only on the effectiveness of IDs in the lateral distribution of vertical live loads, but also on the optimal position of the IDs.

Griffin (1997) studied the influence of intermediate diaphragms (IDs) on load distribution in prestressed concrete I-girder bridges. The studies included two bridges that were constructed with a 50^o skew angle along the coal haul route system of Southeastern Kentucky. One of the bridges has concrete intermediate diaphragms. Bridges of similar design along coal haul routes have experienced unusual concrete

spalling at the interface of the diaphragms and the bottom flange of girders. The IDs appeared to be contributing to the increased rate of deterioration and damage instead of reducing the moment coefficient and distributing the traffic loads as expected. Experimental static and dynamic field testing were conducted on both bridges. All field tests were completed prior to the opening of the bridges. Once the calibration of the finite element models was completed using the test data, analysis was conducted with actual coal haul truck traffic to investigate load distribution and the cause of the spalling at the diaphragm-girder interface. Based on the results obtained in the research study, IDs did not create a significant advantage in structural response. Although large differences were noted percentage-wise between the responses of the two bridges, analysis suggested that the bridge without IDs would experience displacements and stresses well within AASHTO and the American Concrete Institute (ACI-318) design requirements. The finite element analysis also revealed the cause of concrete spalling witnessed in the diaphragm girder interface region. The tendency of the girders to separate as the bridge was loaded played a large role in generating high stress concentrations in the interface region.

Cai et al. (1998) investigated six prestressed concrete bridges in Florida, and the results were compared with field measurement of these bridges. It was found that the finite element prediction that did not consider IDs had better agreement with field test results, implying that the effectiveness of IDs of these bridges are insignificant in distributing the live loads. Further examination of the details of these bridges found that the diaphragm connections are weak. Numerically, the diaphragms would have more significant effects on vertical live load distribution if a full moment connection is ensured between the diaphragms and girders where the ID stiffness is about 10% of that of the girder. It was also found that if no ID is in position, an increase in skew angle will

decrease the load distribution factor. However, when the ID is in position, the increase in skew angle tends to increase the load distribution factor. These results imply that, if a right bridge without IDs is safe in carrying the design loads, a skew bridge without IDs will be safer, given the other parameters are the same.

Barr et al. (2001) studied the evolution of flexural live-load distribution factors in a three span prestressed concrete girder bridge, where a bridge with three spans with lengths of 24 m, 42 m, and 24 m, and a skew angle of 40^o was tested. A finite element model was developed to assess the live-load distribution procedures recommended by the AASHTO code. For both interior and exterior girders, the addition of IDs had the least effect on the live-load distribution factor among the variables investigated in this study. For the exterior girders, IDs slightly increased the live-load distribution factor for low skew angles. For skew angles larger than 30^o, the addition of IDs was slightly beneficial. According to this study, for design consideration from a structural standpoint, the largest changes would be credited to the addition of end diaphragms, while almost no changes would occur due to the addition of intermediate diaphragms, since these showed almost no change in the distribution factors.

Eamon and Nowak (2002) studied the combined effects of secondary elements such as diaphragms, sidewalks, and barriers on load distribution in the elastic and inelastic domains, as well as their effects on the ultimate capacity of steel girder bridges. According to this study, diaphragms tend to be more effective at wider girder spacing and longer spans in terms of maximum girder moment reduction, and increasing the number of IDs does not significantly affect the results. Diaphragms showed to reduce the maximum girder moment up to 13% with an average reduction of about 4%. The ratio of girder stiffness to diaphragm stiffness was observed to be the most important factor effect load distribution. It was observed that the improvement of the ultimate

capacity due to IDs in the inelastic region was not very significant. They found that the girder spacing has very little effect on the moment capacity increase factor, and that the effect of diaphragms on the ultimate load carrying capacity in the inelastic region is insignificant.

Eamon and Nowak (2004) continued this work by assessing the effect of secondary elements on the reliability of bridges. According to them, the results suggested that a variation of reliability will exist on bridge structural systems if secondary elements are included, and this was found to be a function of span length and spacing. They also suggested that a structural system-based calibration of the LRFD code may be useful in providing a uniform level of reliability to bridge structures and their components, furthermore, if a right bridge with IDs is safe, a skew bridge with IDs may not necessarily be safer, given the other parameters are the same.

Green et al. (2002) analyzed bridge performance, considering temperature change effects on bridges of different skew angles with and without IDs. When full ID stiffness was considered in the analysis where diaphragms were modeled using solid finite elements, the diaphragms were found to have contributed up to a 15% reduction in load distribution. Both the intermediate diaphragm and the positive temperature gradient decreased the maximum girder moment and the stresses at the mid-span.

Green et al. (2004) have extended this research by making a study on the influence of skew and bearing stiffness on the maximum deflection of girder at mid-span. The results show that the influence of intermediate diaphragm decreases with an increase in skew angle. A decrease in deflection due to the presence of IDs for 0º, 15-30º, and 60º skew is about 18%, 11%, and 6%, respectively. By increasing the stiffness of bearing from 0.0 to 0.655 GPa, the maximum deflection reductions are of 11.5% and 5.9% for 30º and 60º, respectively. Increasing the bearing stiffness further to 6.895 MPa, the

girder deflections decreased by 14.3% and 10.2% for 30 and 60º skewed bridges, respectively.

Abendroth et al. (2003) focused their research on diaphragms. Their work incorporated a wide ranging literature review, survey of design agencies, the testing of a full scale, simple span, PC girder bridge model, and the finite element analysis of the bridge model considering pinned and fixed end conditions. They concluded that the vertical load distribution was independent of the type and location of the ID. The horizontal load distribution was found to be a function of the ID location and type. Constructional details at the girder supports formed substantial rotational end restraint for vertical and horizontal loading. It was also shown that the Finite Element Method (FEM) generally enveloped the experimental results.

Abendroth and Fanous (2003) developed a finite element model for skewed and non-skewed PC girder bridges. They analyzed the bridge model for a lateral impact load both at and away from the location of the diaphragm configurations. Dynamic loading with 0.1s impact duration was used, and a single impact load was applied on either exterior girder. An investigation on whether analysis for single span can effectively be replaced for a four-span bridge was carried out. Only a 15% maximum difference in strains was observed, which is within tolerable limits. Therefore, single span was used for further analysis. The following results were observed:

a. When the impact load was applied at the diaphragm location, the diaphragm reduced the strains effectively, and the performance was dependent on configuration of diaphragm, but when the impact was away from the diaphragm, the diaphragm did not distribute load effectively, and there was no significant difference in performance of different diaphragms.

b. When the impact load was applied at the diaphragm for both skewed and non-skewed

bridges, reinforced concrete diaphragms provided the largest degree of impact protection.

Khaloo and Mirzabozorg (2003) had taken skew angle, girder spacing, and span length for bridges as the parameters for carrying out a parametric study for skew bridges. They considered four kinds of configurations of bridges in their study, with the first type being without ID, the second type having an ID parallel to the supporting lines, and for the third and fourth configurations, the diaphragms were perpendicular to the girders. For the third type, IDs were provided as per AASHTO requirement, while for the fourth type, the diaphragms were provided at the quarter and mid-span. The following conclusions were drawn from this study:

a. The configuration of IDs in the bridges has a significant effect on the load distribution pattern and their effect varied for different skew angles.

b. Bridges with IDs perpendicular to the longitudinal girders are the best arrangement for load distribution.

c. The effect of girder spacing on the influence of IDs on load distribution was found to be insignificant.

Cai and Shahawy (2004) studied the effects of field factors, such as bearing restraints and non-structural members such as barriers and diaphragms, on prestressed concrete bridge performance. It was found that these field results collectively result in much less girder moment than that calculated according to AASHTO specifications (Standard, 2002 and LRFD, 2004). Therefore, the current AASHTO specifications are very conservative for prestressed concrete girders.

Other reviews included the work done by Zokaie et al. (1991) and Zokaie (2001) which gave the foundation of AASHTO LRFD Specifications.

1.3 Objectives of the Study

The Objectives of this study will be:

1) Investigation of the effects of girder types, end diaphragms, and intermediate diaphragms on live load distribution factors for both moment and shear in slab-on-girder prestressed concrete bridges, using Full 3D Finite Element Analysis by ADINA Program. Both AASHTO Specifications did not consider the effect of diaphragms on load distribution factors equations.
2) Comparison are made between two bridge models, the first model is slab on six AASHTO-PCI bulb tee girders BT54, and the second model is slab on six AASHTO spread box girder BIV36, considering both interior and exterior girder loading.
3) Understanding bridge systems performance in plastic stages, and to demonstrate how the load distribution affects the behavior of PC girder as the live load is increased to higher values in order to cause cracking of the concrete, yielding of prestressing tendons, and a consequent, nonlinear response.
4) Evaluation of the degree of conservatism of the AASHTO (2002) Standard Specifications, and AASHTO (2010) LRFD Specifications equations for load distribution factors in slab-on-girder PC bridges, which is based only on linear elastic analysis.

CHAPTER ②: METHODOLOGY AND ANALYSIS METHODS

CHAPTER 2
METHODOLOGY AND ANALYSIS METHODS

2.1 Method No. 1: Full 3D Finite Element Analysis

Finite Element Method (FEM) enables bridge engineers to determine the distribution of wheel loads more accurately than using empirical expressions of restricted code formulas, and to determine the overall behavior of structures by dividing them into several small finite elements (e.g. shell elements), with well-defined mechanical and physical properties.

In the full 3D finite element model, the loads are applied as uniform pressure simulating the contact area between truck wheels and pavement.

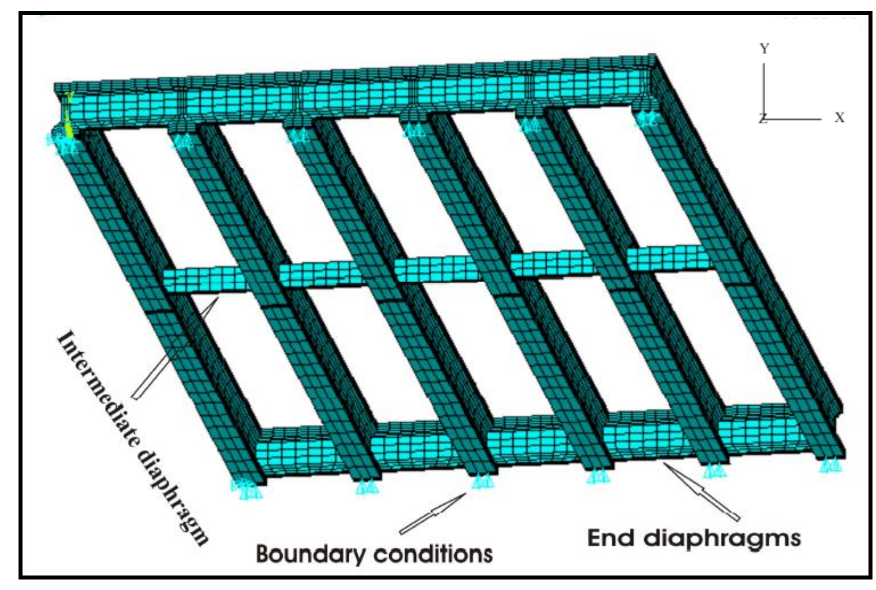

Figure 2.1 Full 3D Finite Element Model (Araujo, 2009).

A partial view of the full 3D finite element model is shown in Figure 2.1, displaying girders, both end and intermediate diaphragms, and boundary conditions. In the full 3D FE model, stresses, strains and deflections were obtained directly from the elements at the locations of interest. The postprocessing ADINA-PLOT of the finite element results is required.

2.1.1 Compatibility between Shell and Beam Elements

The girders are made composite with deck slab thickness, as shown in Figure 2.2. Directly above the girder, the deck thickness is increased to a sufficient thickness, the extra thickness referred to as the lift, is intended to compensate for camber differences among the girders.

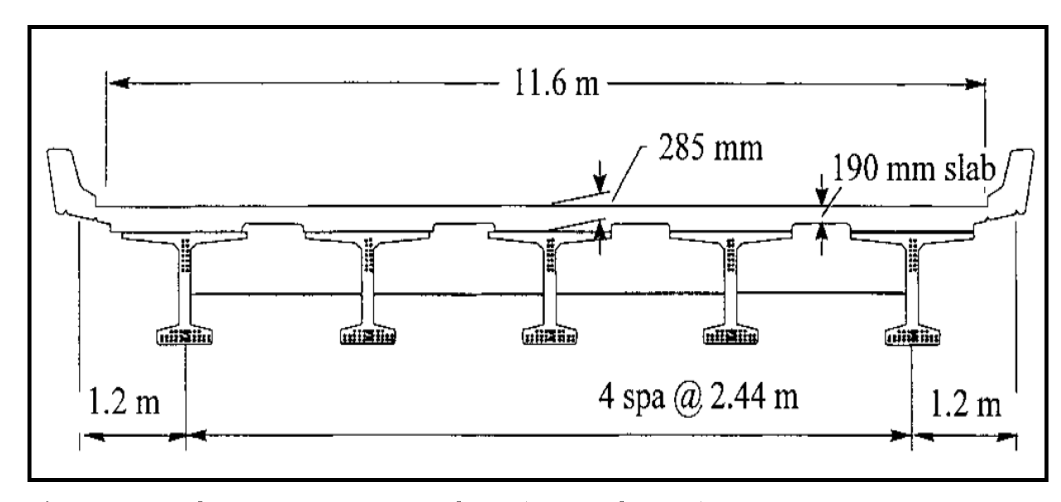

Figure 2.2 Bridge Cross-Section at Midspan (Barr et al., 2001).

The lift slightly increases the composite girder stiffness. More importantly, because the top flange width of the girder is a significant fraction of their spacing, the addition of lift increases the effective thickness of the deck and thus the transverse bending stiffness. This change leads to an increase in the ratio of transverse to longitudinal stiffness, which in turn implies a more uniform distribution of girder moments and a lower live-load distribution factor.

The eccentric beam model ensures full composite action between the deck slab and the girders. This model utilizes the non-composite section properties of two elements to model composite action by applying the rigid links between the centroid of the girder and the midsurface of the slab.

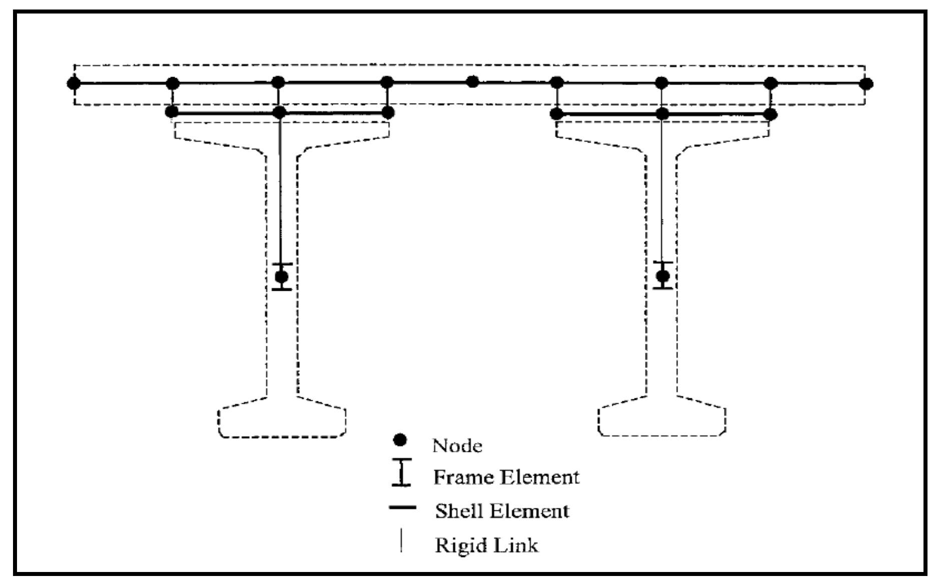

Figure 2.3 Cross-Section of Finite Element Model of Two Girders (Barr et al., 2001).

The concrete deck slab is usually modeled as shell elements, which combine plate bending and membrane elements. The effects of shear lag are automatically included since the elements used to model the slab consider membrane behavior as well as flexural behavior. Longitudinal girders are modeled using eccentrically connected beam elements.

As can be seen in Figure 2.3, the nodes of the beam do not coincide with the nodes of the shell. The beam and the shell should be connected in such a way that only shell degrees-of-freedom (DOFs) appear in the global structure. Imaginary weightless rigid links are added between the two pairs of nodes.

The transformation equation between a shell node and its corresponding beam node is given by

$$\begin{Bmatrix} u^b \\ w^b \\ \theta_y^b \end{Bmatrix} = \begin{bmatrix} 1 & 0 & e \\ 0 & 1 & 0 \\ 0 & 0 & 1 \end{bmatrix} \begin{Bmatrix} u^p \\ w^p \\ \theta_y^p \end{Bmatrix} \quad (2.1)$$

where the superscript b and p represent beam and plate/shell, respectively. The e is the eccentricity between the shell element and the beam element. It should be noted that beam axial deformations are activated by the shell rotations.

Typical bending elements make use of a linear shape for the axial displacement and a cubic shape for the transverse displacement. It has been reported that displacement incompatibility occurs at the interface of two typical bending elements (Gupta et al. 1977). The axial displacement in the beam of Eq. (2.1) is given as

$$u^b = u^p - e \cdot \theta_y^p \tag{2.2}$$

This causes a quadratic expression of rotation in the plate (θ_y^P). The incompatibility is noticeable since the axial displacements (u^b *and* u^p) are linear but the rotation (θ_y^P) is quadratic in the axial (x) direction.

Even though this incompatibility error completely disappears as the mesh is refined, many studies have been proposed to eliminate this nonconforming error in the modeling of the eccentric beam model, which allow for the use of less refined meshes.

Miller (1980) solved this problem by using the same elements, but including an extra axial DOF at the middle of each element so that the axial displacements becomes quadratic. Each term of the transformation equation given in Eq. (2.2) is quadratic in the axial direction. Various researchers (Marx, 1985) (Khaleel and Itani, 1990) (Chan and Chan, 1999), have proposed higher order elements based on the Mindlin theory.

This theory automatically includes transverse shear deformation in element formulation and assumes that the normal to the midsurface remains straight after deformation, but not necessarily normal to the deformed midsurface.

The slab is modeled as eight-noded serendipity elements or nine-noded Lagrangian elements, as shown in Figure 2.4. Three-noded Timoshenko beam elements are used to model girders. The shape of the element is quadratic for rotations and displacements

separately. The elements used in modeling slab on girder bridge are completely compatible with the quadratic expression at the interface of the slab and beam elements.

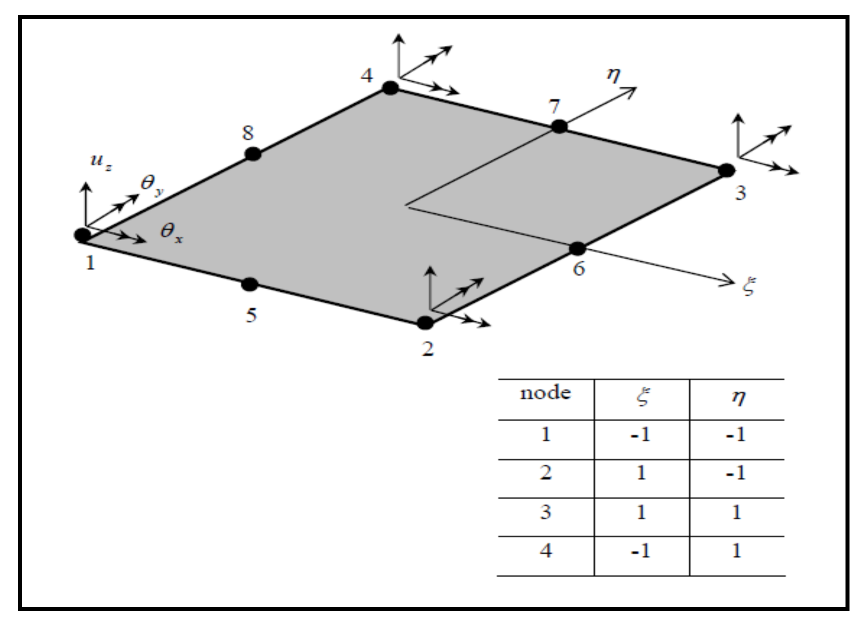

node	ξ	η
1	-1	-1
2	1	-1
3	1	1
4	-1	1

Figure 2.4 Typical Bending DOFs and Node Numbering of Shell Elements (Sotelino et al. 2004).

Bearings are mechanical systems that transfer the reaction of superstructure components to the substructure. Since the main purpose of this study is to analyze the bridge superstructure, it is assumed that substructures, such as piers and abutments, do not influence the behavior of the superstructure. Although bearings are typically located below the beam element, many previous models neglected this fact and assumed bearings to be located at the centroid of the beam element or at the bottom flange of the beam.

In this study, bearings are modeled by assigning boundary conditions to the zero-dimensional elements at their real location. For the simply supported beam, rotations in all directions are allowed in order to simulate the simply supported structure. Minimum restraints are assigned for longitudinal and transverse movement while vertical restraint is placed at the supports. Kinematic constraints are also supplied to nodes between the girders and the deck.

2.1.2 Finite Element Model of Vehicular Live Loads

The live load for bridge design is the AASHTO HS20 standard truck loading according to article 3.7.4 in AASHTO Standard Specification and shown in Figure 1.1, in previous chapter.

The applied loading on a bridge deck consists of pressure loads applied through a tire patch. The AASHTO bridge code specifies a “tire contact area” in order to ensure a more exact analysis. The contact area is based on the wheel of a standard HS design vehicle. The ratio of the length in the direction of traffic to the tire width is given as 1:2.5, and the wheel load is assumed to be a uniform pressure, as shown in Figure 2.5.

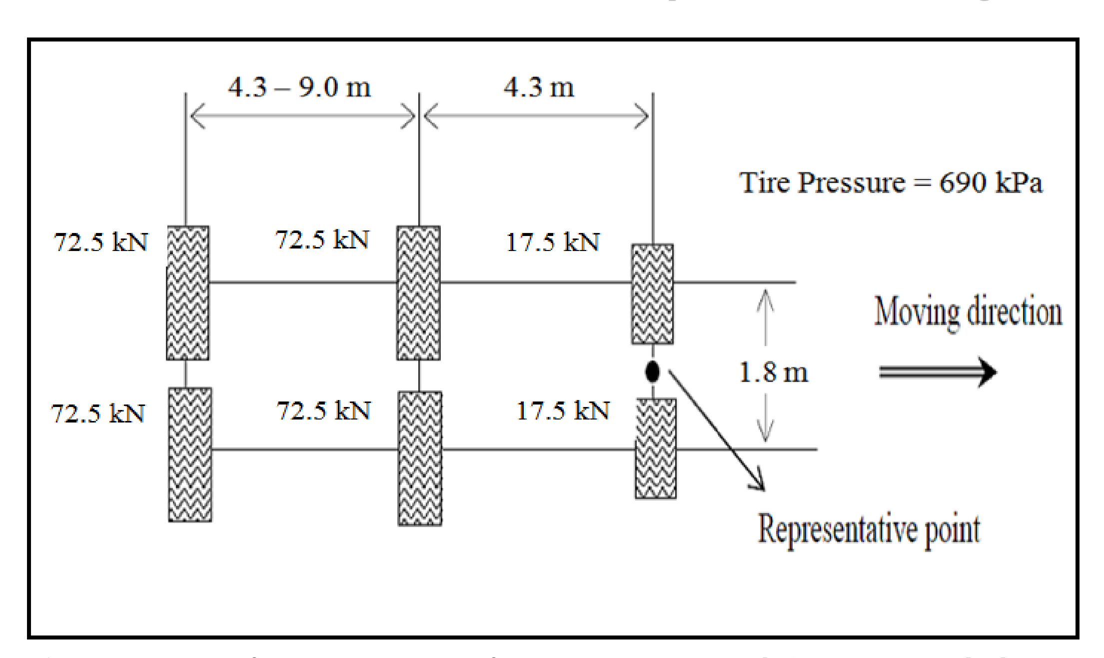

Figure 2.5 View of Tire Contact Area of AASHTO HS20 Truck (AASHTO Standard Specifications, 2002).

In finite element modeling, this requirement imposes the need for a fine mesh in the deck so that the element is fitted to the patch size. In order to uncouple the patch load from the mesh size, equivalent nodal loads are employed. Both Chen (1999) and Eamon and Nowak (2001) studies utilized the Mindlin shape functions for four-node shell elements in their equivalent nodal force calculation. Each wheel load is considered as a single concentrated load on the shell elements instead of the patch load. Kim (2000)

developed an algorithm that identifies the tire patch position and calculates equivalent nodal forces for the three-dimensional solid element in the application of FE analyses of pavement. The current FE model developed for this study requires 27-node shell element for modeling of the bridge deck and girders, were discussed in details in the next chapter.

The typical plate DOF of an eight-node shell element and the nodal numbering scheme are shown in the natural coordinate system, as in Figure 2.4. The equivalent nodal load of the patch load can be calculated by the surface integral as follow

$$\mathbf{R_e} = \int_S \mathbf{N}^T \mathbf{t} dS \tag{2.3}$$

where **t** is the surface traction vector and **N** is the shape function matrix. Using this method, one must identify the nodes and elements that lie on the patch load. The patch load is discretized as a number of uniformly distributed subpoint loads, as shown in Figure 2.6. This method considers each sub-point load as a single concentrated load.

If there are K sub-point loads applied to the tire patch on an element of an amount p, then the equivalent nodal forces are computed as

$$\mathbf{R_e} = \sum_{i=1}^{K} \mathbf{N}_i^T \mathrm{p}_i \tag{2.4}$$

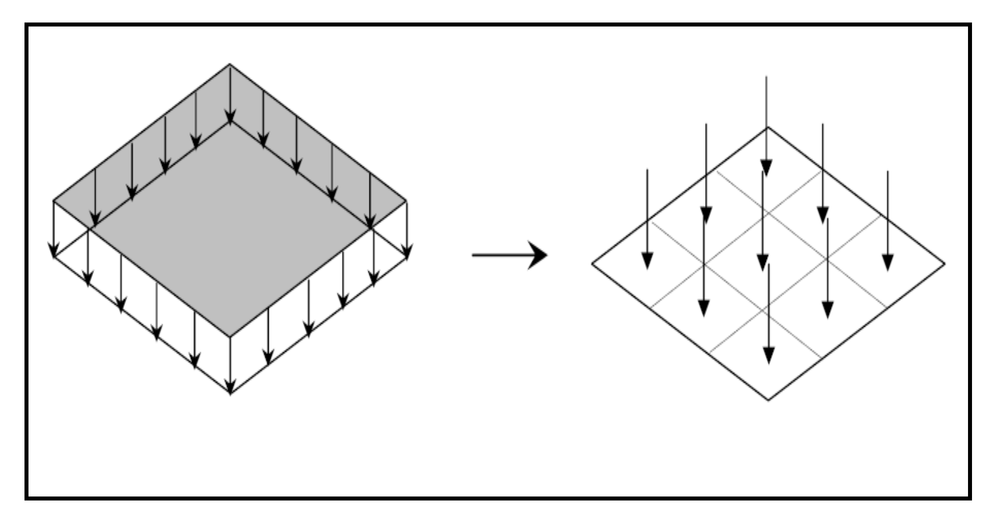

Figure 2.6 Discretization of Patch Load (Sotelino et al. 2004).

2.2 Method No. 2: Grillage Analysis

Grillage models became popular in the early 1960s with the advancement of the digital computer. As the methodologies for the stiffness method (or displacement analysis) of frames were well known. And it is probably the most popular computer-aided method for analyzing bridge decks, slab-on-girders bridges, and box girder bridges.

In practice, under extensive simplifying assumptions, grillage analysis has primarily been used to determine overall bridge behavior. This is because it is easy to comprehend and use, relatively inexpensive, and has been proved to be reliably accurate for a wide variety of bridge types. The method, pioneered for computer use by Lightfoot and Sawko represents the deck by an equivalent grillage of beams, as shown in Figure 2.7.

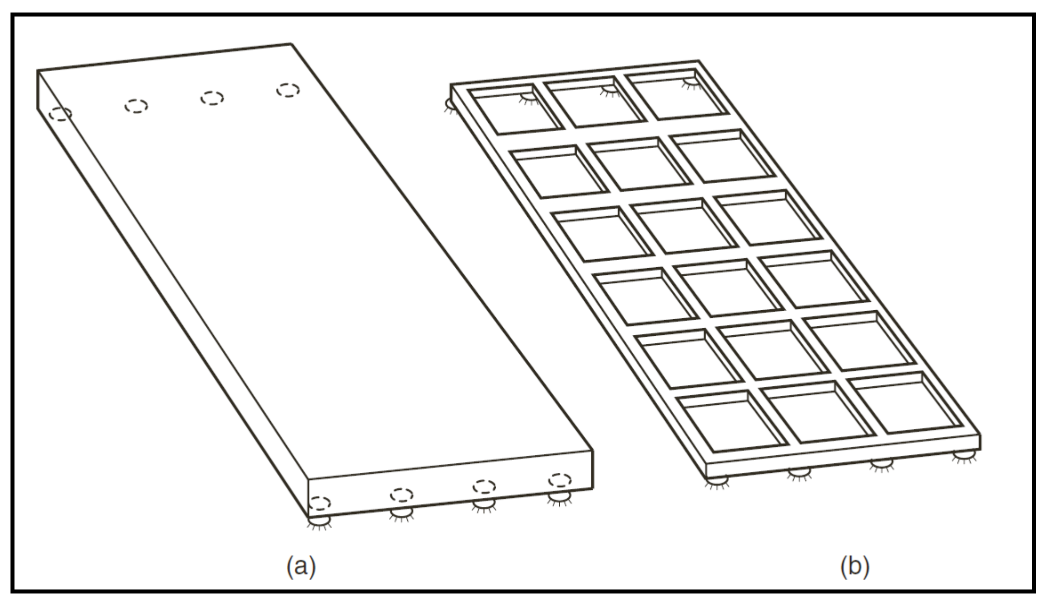

Figure 2.7 Grillage Model (a) Prototype Deck and (b) Equivalent Grillage (Hambly, 1991).

It should be noted that the Grillage method is not considered in this work, which is only another way of structural analysis, and finite element method are quick to discount the grillage method because it is non-rigorous as discussed next in details. But remember that such methods are used to obtain reasonable distribution of internal actions while accounting for equilibrium (lower bound theorem).

The dispersed bending and torsion stiffnesses in every region of the slab are assumed for purpose of analysis to be concentrated in the nearest equivalent grillage beam. The slabs longitudinal stiffnesses are concentrated in the longitudinal beams while the transverse stiffnesses are concentrated in the transverse beams

The properties of the longitudinal grillage members are determined from the properties of the girders and the portion of slab above them, about the neutral axis of the section. Similarly, the properties of the transverse grillage members are necessary to represent the transverse stiffness of the slab (Hambly 1991).

The section properties of a transverse grillage member, which solely represents slab, are calculated as for a slab. The moment of inertia and torsion constant as recommended by Hambly 1991 is

$$I = bd^3/12 \quad , \quad C = 2I = bd^3/6. \qquad (2.6)$$

In this way, grillage members represent the total stiffness of any portion of slab and girder. When the torsional inertia per unit width of the slab is computed, two points are to be noted, (a) the deck contributes to torsional stiffness in both the directions and hence the value of torsional inertia in each direction is to be taken as one-half of the combute value (i.e. torsional inertia equal to $(d^3/3) \times 0.5$) and (b) the lateral dimension is much larger than the depth.

This type of system would be similar to modeling a plate with a series of crossing beams where one element sits on top of the other as shown in Figures 2.8a and 2.8b. Note that at the intersection of the beams the only interaction force between the elements is a vertical force. This type of connection excessively simplifies the model of the deck, which is a continuum. In the continuum, a flexural rotation in one direction causes torsional rotation in an orthogonal direction. Consider the grillage joint shown in Figure 2.8c. Here the joint is continuous for rotation in all directions, that is, the

displacements of the joint is defined with the three displacements (degrees of freedom) shown in Figure 2.8d, which includes vertical translation and two rotations. This type of joint, in combination with elements that have both flexural and torsional stiffness, is more like the continuum and, therefore, models it more accurately. This type of numerical model is called a grillage.

Researchers looked for convenient ways to model continua with frame elements. The grillage model is such a technique. Ideally the element stiffnesses in the grillage model would be such that when the continuum deck is subjected to a series of loads, the displacement of the continuum and the grillage are identical.

In reality, the grillage can only approximate the behavior of the continuum, such as thin plate. The reason for this difference is twofold: (1) The displacement in the grillage tends to be more irregular (bumpy) than the continuum, and (2) the moment in the grillage is a function of the curvature along the beam. In the plate, the moment is a function of the curvatures in two orthogonal directions due to Poisson’s effect. Fortunately, these effects are small and the grillage method has been shown to be a viable method of analysis (Barker and Puckett, 2007).

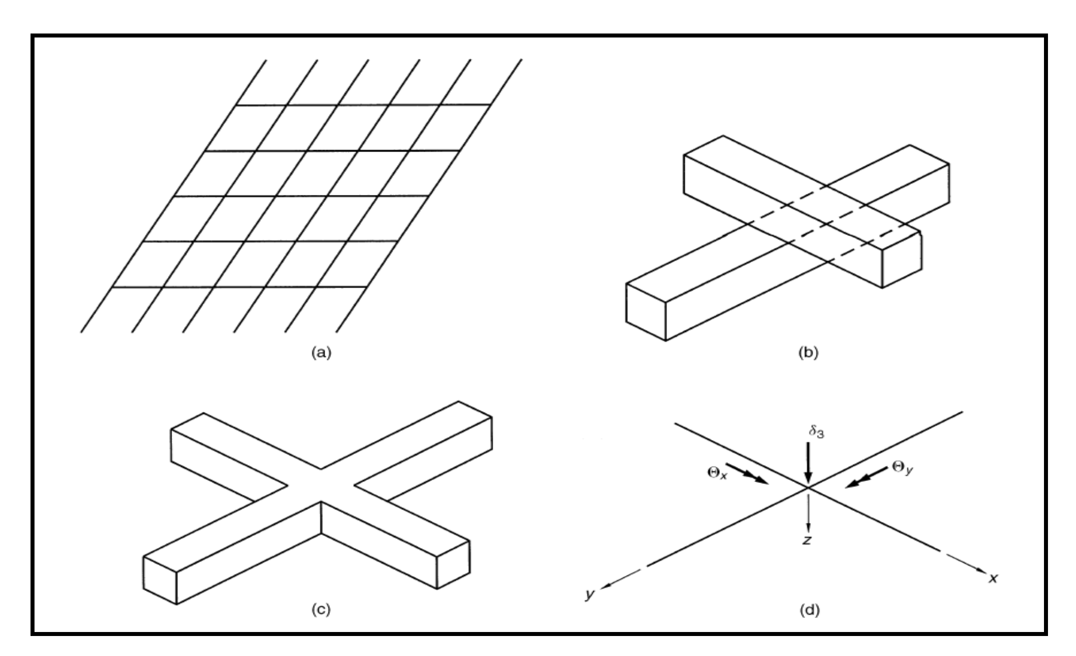

Figure 2.8 (a) Grillage Model, (b) Crossing with Translational Continuity, (c) Crossing with Translational and Rotational continuity, and (d) Degrees of Freedom in Grillage (Plane Grid) Modeling (Barker and Puckett, 2007).

2.2.1 Advantages and Disadvantages of Grillage Method

The Advantages of Grillage Method are listed below:

- The major advantage of plane grillage analysis is that shear and moment values for girders are directly obtained. Thus, the integration of stresses is not needed.
- Grillages can be used with any program that has plane grid or space frame capabilities.
- Results are easily interpreted and equilibrium is easily checked by free body diagrams of the elements and system as a whole.

The Disadvantages are several:

- It is impossible to model important physical phenomena, such as the interaction between girders and deck slab, support location, and shear lag. *This limitation comes from the fact that in grillage analysis structural members lie in one plane only*.
- Method is non-rigorous and does not exactly converge to the exact solution of the mathematical model.
- To obtain good solutions, the method requires experience and judgment. The mesh design and refinement can be somewhat of an art form.
- The assignment of the cross-sectional properties requires some discretion.
- Thin slabs on a girder can be considered as wide flange beams. When this structure is subjected to flexural loading, normal stresses are generated in the section. The compressive stresses in the girder flange and the slab are not uniform in the transverse direction.
- As a result, longitudinal shear is generated, in other words, some portions of the slab between girders do not receive the same amount of axial stress as those near the center of the bridge. This phenomenon, known as shear lag, is dependent both on the

geometric shape of the bridge deck and on the nature of the applied loading. Because of this, the neutral axis location in the bridge deck varies and moves towards the centroid of the wide flange section.

- The moments in two longitudinal and two transverse grillage members meeting end-to-end are not necessarily the same. The discontinuity between moments is balanced as a discontinuity of torques in the beams in the opposite direction to keep the moment in equilibrium at the node, the moment discontinuity may be exaggerated in the case of the edge of the grillage, and
- The torque in the transverse beam, which has no other transverse beam to balance it, introduces discontinuity in the longitudinal beams.

2.3 Nonlinear Analysis of Bridges under Plastic Stages

Structural nonlinearity can be grouped into three major types. The first one is geometric nonlinearity, the second type is material nonlinearity, which occurs in most materials at different levels of importance, being evident in concrete, and the third type is contact nonlinearity, which discussed in details in the next chapters.

In nonlinear analysis the total load applied to the model is divided into smaller load increments or load steps. At the end of each load step the stiffness matrix of the model is adjusted to reflect nonlinear changes in the structural stiffness before proceeding to the next load step.

Live loads have been a focal concern in bridge design for a long time, with their regulation appearing in the form of empirical distribution factors in the first edition of the AASHTO code in 1931 (Senders, 1984).

They play a key role in the structural degradation of bridges as crack initiators and propagators. Although significant progress has been made since then, much is yet to be accomplished in this area.

The knowledge of how live loads are distributed beyond the elastic range will increase engineer's ability to evaluate the condition of both existing and new bridges using predictive analysis. These methods will enable engineers to design bridge systems which will perform as expected at minimum maintenance costs by withstanding deterioration in a more effective way.

Nonlinear live load distribution analyses up to ultimate strength are tools needed to assure that these predictive methods are structurally sound. Load distribution factors calculated according to AASHTO (2010) LRFD Specifications, *yield linear elastic results only, which, theoretically, correspond to service loadings.*

Load distribution is determined by distribution factors which were reported to be within 5% of the distribution factors calculated with detailed finite element models (Zokaie, 1991). Zokaie's study is the basis for LDF regulations in the current AASHTO LRFD Specifications. These distribution factors are based on linear elastic analysis of simply supported bridges using HS20 trucks.

Load distribution factors at the ultimate stage have not been extensively studied and may be significantly different from that in the service stage. The main objectives of this study is to understand bridge systems performance in plastic stages, and to demonstrate how the load distribution affects the behavior of PC girder as the live load is increased to higher values in order to cause cracking of the concrete, yielding of prestressing tendons, and a consequent, nonlinear response.

This information will help engineers evaluate bridge capacity more accurately, thus avoiding unnecessary and costly bridge postings as well as identifying unsafe bridges from the transportation network. Particularly, a nonlinear analysis would help researchers understand the real capacity of the prestressed concrete bridges, especially if the diaphragms are eliminated.

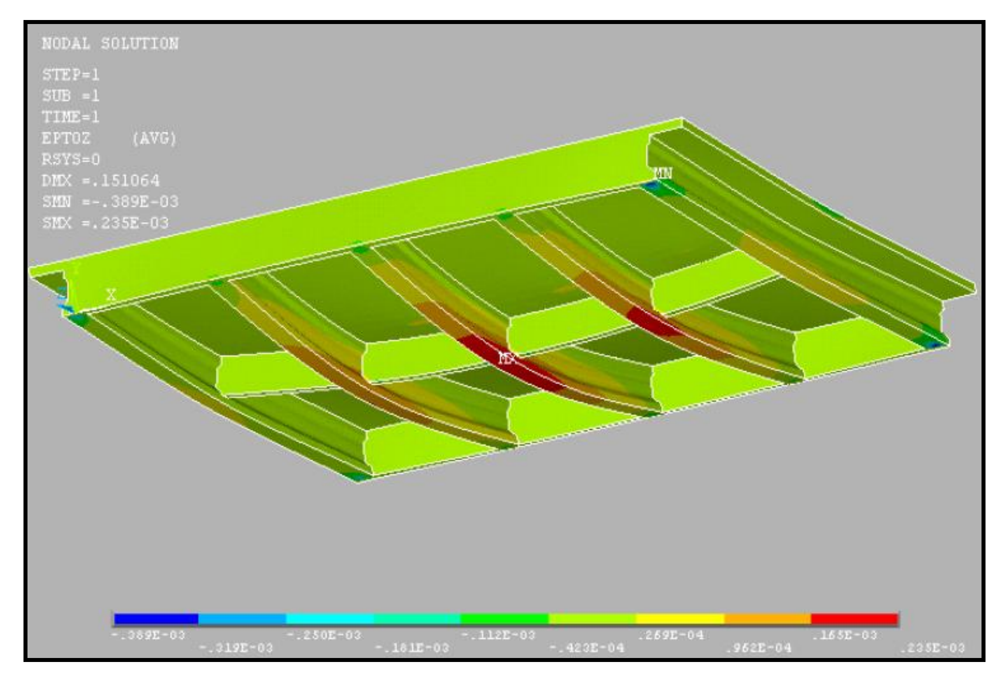

Figure 2.9 Stress Contour for Bridge Model under Live Load, (Araujo, 2009).

Finite element modeling of concrete as mentioned before is difficult because of its non-homogeneous and anisotropic properties. According to Nilson (1968), early simulations were widely based on predefined cracking patterns, which were very limited due to the need for frequent adjustments to the input files.

Isoparametric formulations were later introduced to represent cracking in concrete. The first method to use these formulations was the smeared cracking, which considers cracked concrete an orthotropic material (Rashid, 1968).

According to this approach, cracking takes place whenever the principal stress in any direction exceeds the ultimate tensile stress. The elastic modulus is then assumed to be zero in the direction perpendicular to the crack (Suidan and Schnobrich, 1973).

CHAPTER ③: FINITE ELEMENT MODEL OF PC BRIDGES

CHAPTER 3
FINITE ELEMENT MODEL OF PC BRIDGES

3.1 Description of Bridge Models

The modeled bridges are 15 m long simply supported Slab-on-Girder Posttensioned Prestressed Concrete (PC) non-skewed bridges; the first model is slab on six AASHTO-PCI bulb tee girders BT54 as shown in Figure 3.1 spaced 2.40 m from center to center, and the second model is slab on six AASHTO spread box girders BIV36 as shown in Figure 3.2 spaced 2.60 m from center to center.

The roadway widths are 13 m and 14 m curb to curb for bridge model one and two, respectively. The cross-sectional dimensions of the analyzed bridge are presented in Figure 3.3 and 3.4. The concrete compressive strength (f_c') for prestressed girders was modeled as 55 MPa, and 30 MPa for cast-in-place deck slab and diaphragms.

The reinforced concrete diaphragms for bridge model No.1 are 300 mm thick and 914 mm deep, and for bridge model No.2 are 300 mm thick and 700 mm deep. A seven-wire, low-relaxation strands with yield strength of 1860 MPa, were used as the reinforcement.

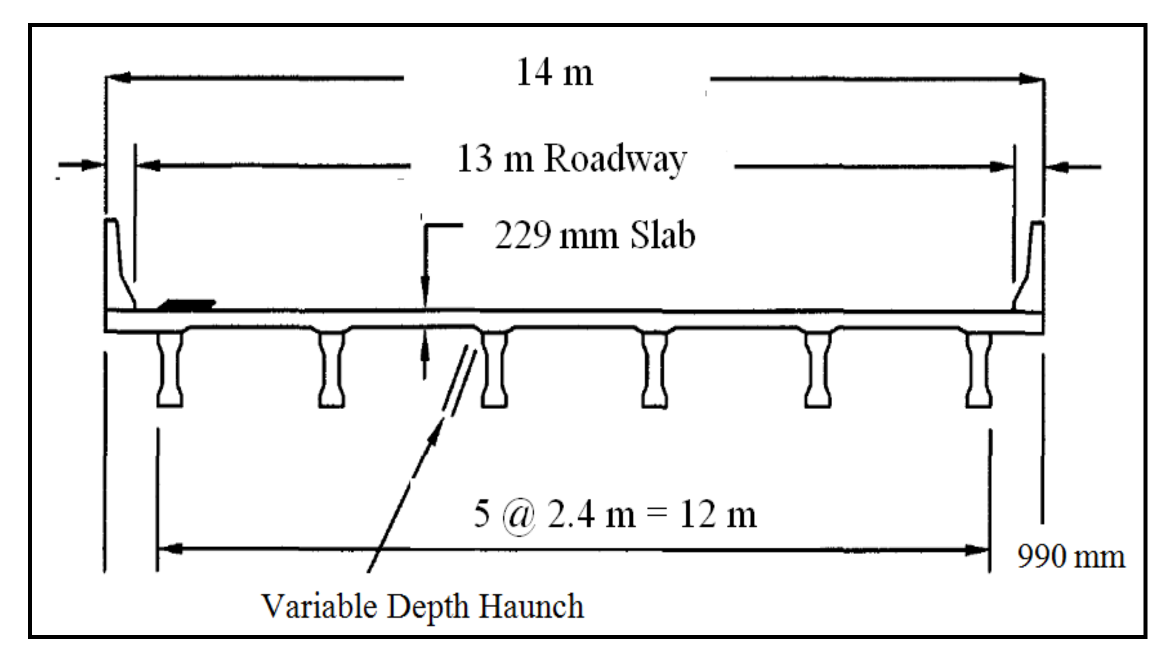

Figure 3.1 Cross-Section of Bridge Model No. 1: Slab on BT54 Girders Bridge.

The unit weight of concrete and steel were modeled as 25 kN/m^3 and 76 kN/m^3, respectively, Young`s modulus of concrete and steel is 35.5 GPa and 197 GPa, respectively, and the poisson`s ratio for concrete and steel was 0.2 and 0.3, respectively (AASHTO A5.4.2.4 A5.4.2.5, and A5.4.4.2).

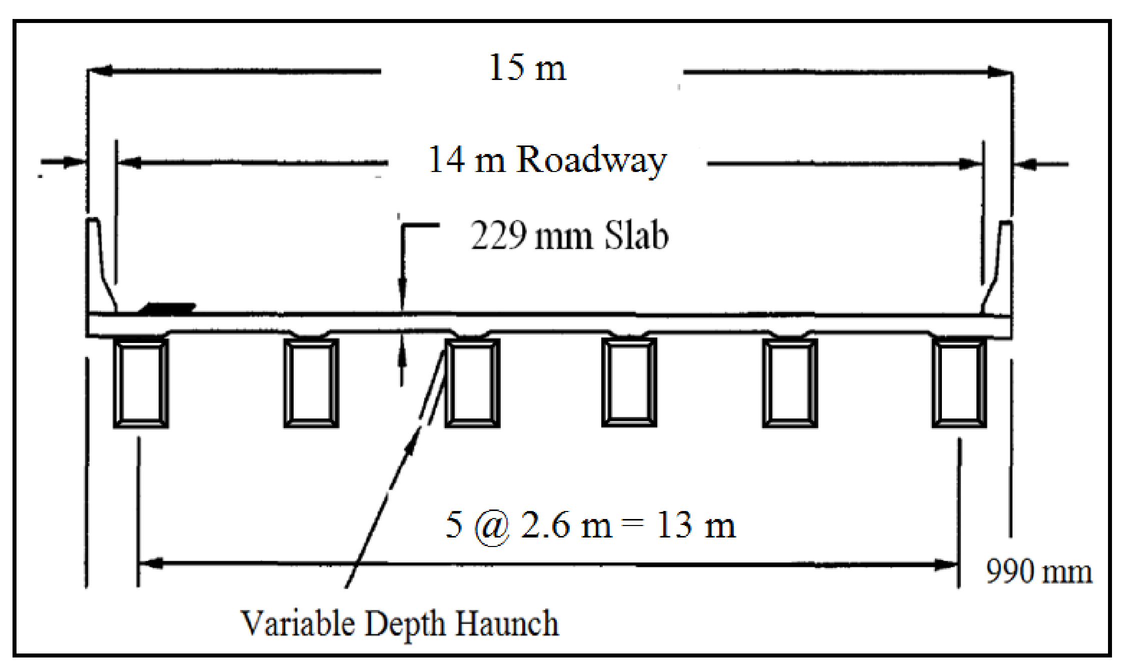

Figure 3.2 Cross-Section of Bridge Model No. 2: Slab on BIV36 Girders Bridge.

The models were further verified while investigating the effects of Intermediate Diaphragms, and End Diaphragms on Load Distribution Factor (LDF). LDF comparisons were made between the full 3D Finite Element model predictions and the LDF calculated according to AASHTO Standard Specifications and AASHTO LRFD Specifications.

Two different bridge configurations were studied, investigation are made for exterior and interior loading of each bridge configurations:

- Configuration No.1, modeling according to the assumptions made in the AASHTO codes, which do not take into account the effects of diaphragms.
- Configuration No.2, modeling with end diaphragms and one intermediate diaphragm located at the mid-span.

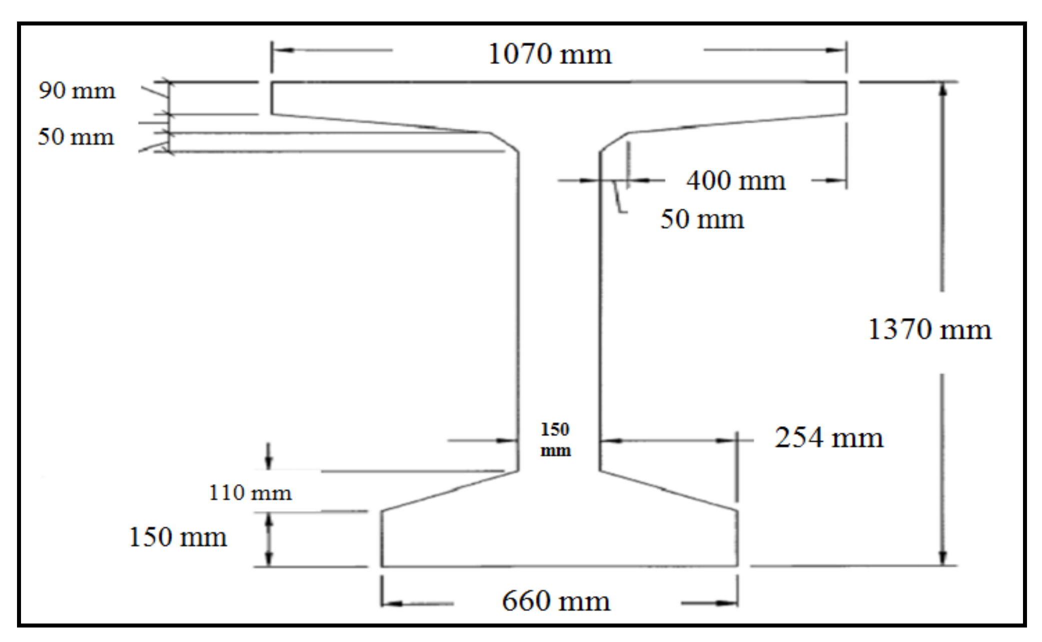

Figure 3.3 Postensioned AASHTO-PCI Girder BT54, A_g = 425000 mm^2.

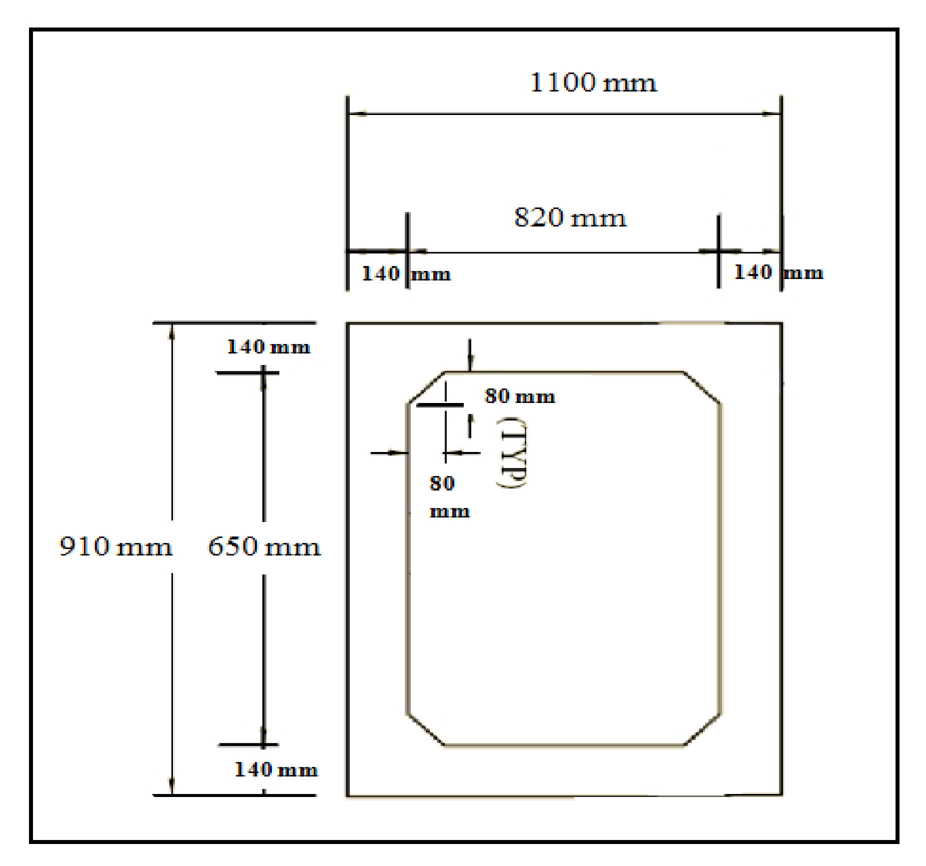

Figure 3.4 Postensioned AASHTO Box Girder BIV36, A_g = 458000 mm^2.

3.2 Finite Element Modeling by ADINA

3.2.1 An Overview

The response of a bridge under live load is important for both design and evaluation purposes. This is because; this knowledge enables the engineer to find the strength and serviceability of a given superstructure. However, determining an accurate load distribution is difficult because of the complexity of bridge structures.

The objective of this chapter is to present a new 3D Nonlinear Finite Element Plastic Modeling (NFEPM). This model involves detailed modeling of the bridge superstructure. As mentioned earlier, the exact load distribution factor may not often be found analytically or experimentally because of the complexity of bridge structures. However, since the actual behavior of a bridge structure is three dimensional in nature, 3D Finite Element discretization scheme is the most appropriate analytical model to analyze this behavior.

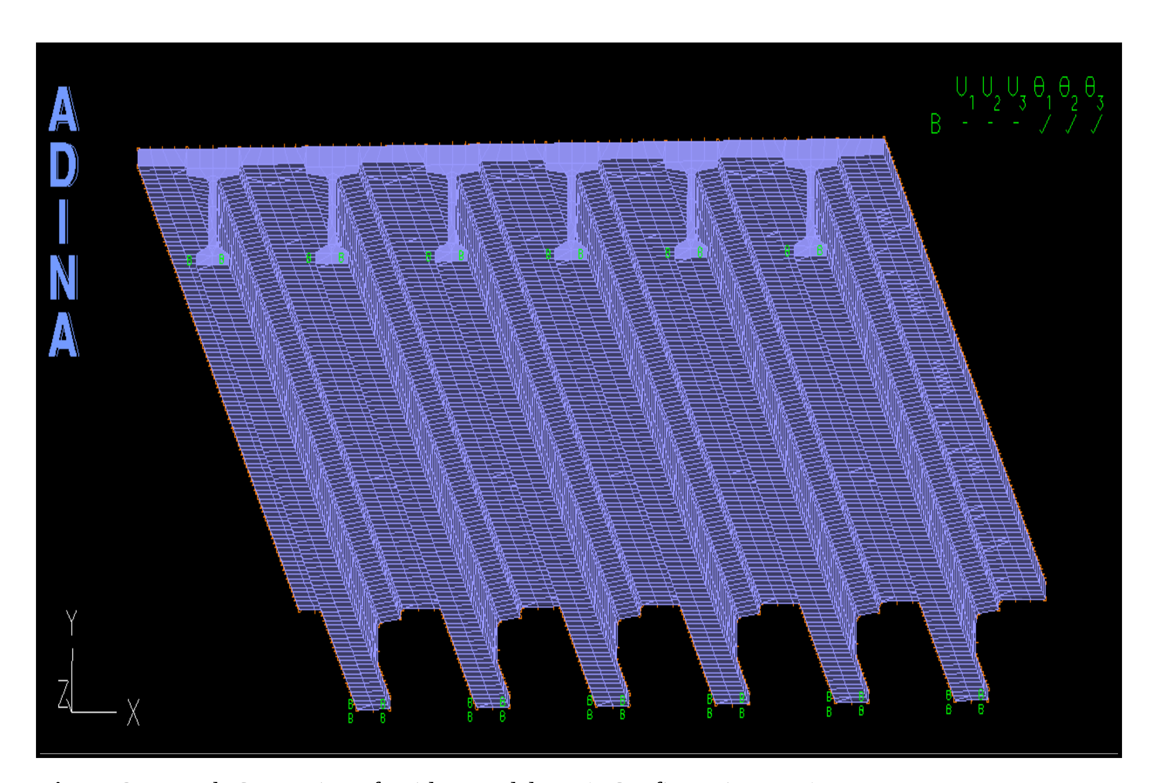

Figure 3.5 Mesh Generation of Bridge Model No.1_Configuration No.1.

In order to facilitate repeated modeling, Excel spread sheets were used to generate the ADINA 3D solid finite element models, key point coordinates were defined to build the bridge geometry, which was then joined to generate the solid elements.

After 3D model was built, it was then meshed, loaded, and analyzed. The vehicular traffic orientation on the bridge indicates the z-axis of the full 3D model, the y-axis indicates the vertical direction and x-axis is along the transverse direction.

The reference point (0,0,0) indicates the model`s origin and is located at the mid-point of the bottom flange at one end of one of the exterior girder. All other point were within the model were located in relation to the origin.

It should be noted that some of the FE bridge models available in the literature introduce geometric errors and/or compatibility errors. This can potentially result in incorrect representation of flexural behavior. In this study, several FE modeling techniques were thoroughly investigated in order to avoid modeling errors by employing displacement transformation and a proper selection of Finite Elements.

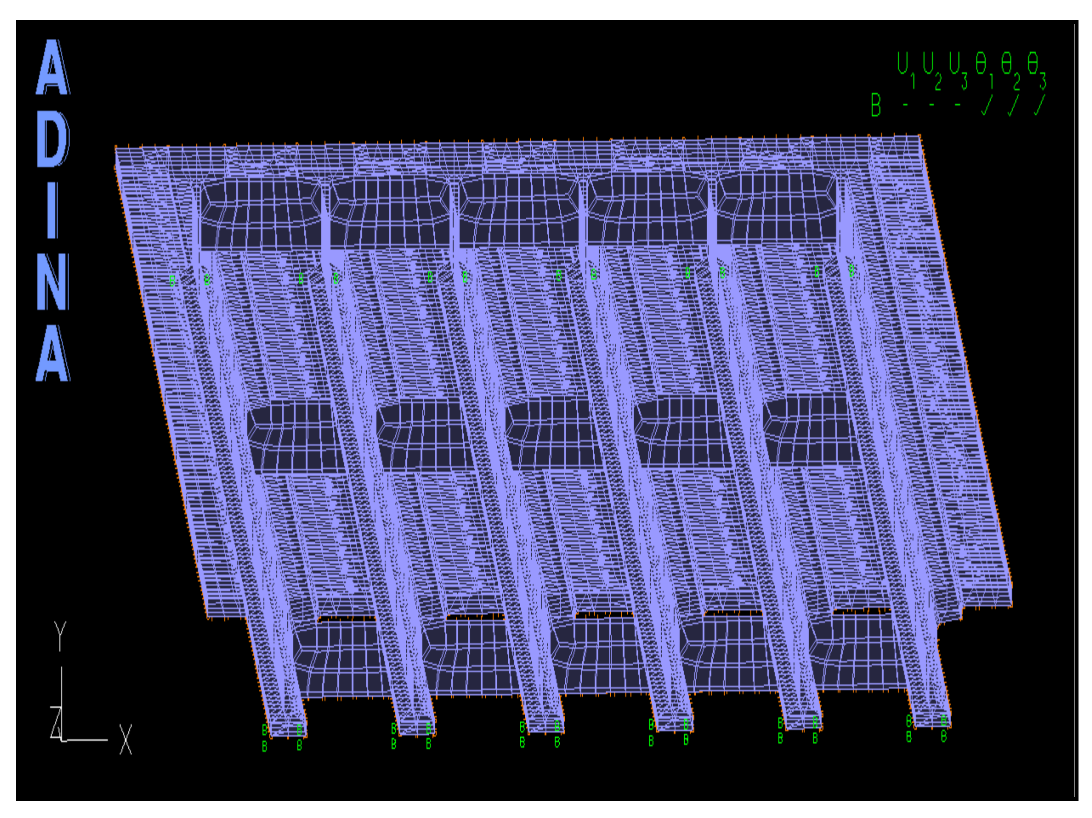

Figure 3.6 Mesh Generation of Bridge Model No.1_Configuration No.2.

The FE model chosen for this study was developed based on 3D discretization; this model is capable of including physical behavior, such as composite action and the eccentricity effect between the deck slab and the girder. Using this model, it is also possible to capture shear lag, which is important in order to understand bridge deck behavior. Boundary conditions are carefully evaluated in order to avoid unwanted constraints to the nodes and, consequently, to the model. The number of constraints required to provide stability to the bridge models is kept to the minimum possible, keeping in sight that actual bridge behavior and performance had to be achieved. Unnecessary constraints would generate secondary stresses, thus altering the stresses distribution in certain elements. Girder supports are simulated by applying proper boundary conditions to nodes at both ends, as shown in Figure 3.5. Since the analyzed bridge was simply supported, it's required to restrict all translational degree of freedom, while allowing rotational degree of freedom. (B) Notation, indicate the boundary conditions in ADINA Program, as shown in Figure 3.5.

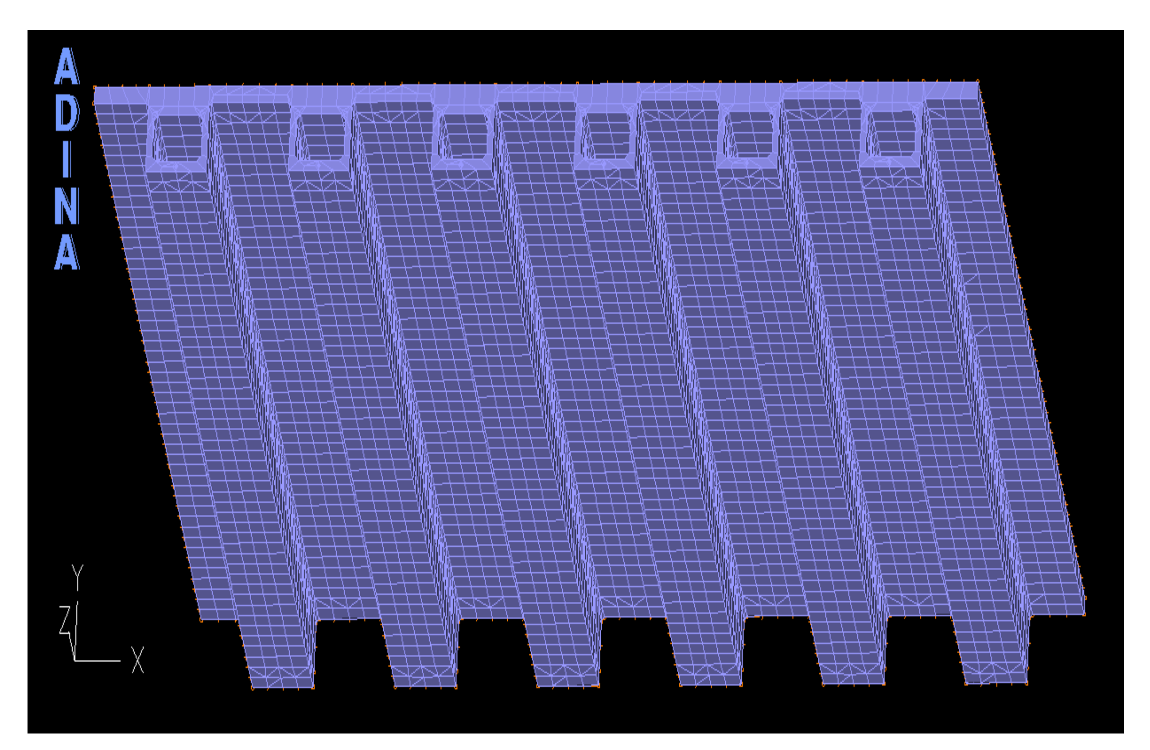

Figure 3.7 Mesh Generation of Bridge Model No.2_Configuration No.1.

In this study, the concrete deck slab and girders were modeled as 3D solid elements with 27-node element, which is the most accurate among all available elements in ADINA Program. However, the use of this element can be costly, and required a high computer “horse power” for nonlinear plastic analysis.

The 8-node element as recommended for 3D solids by literatures such as Araujo (2009) cannot be used in ADINA Program, since it should only be used in analysis when bending effects are not significant.

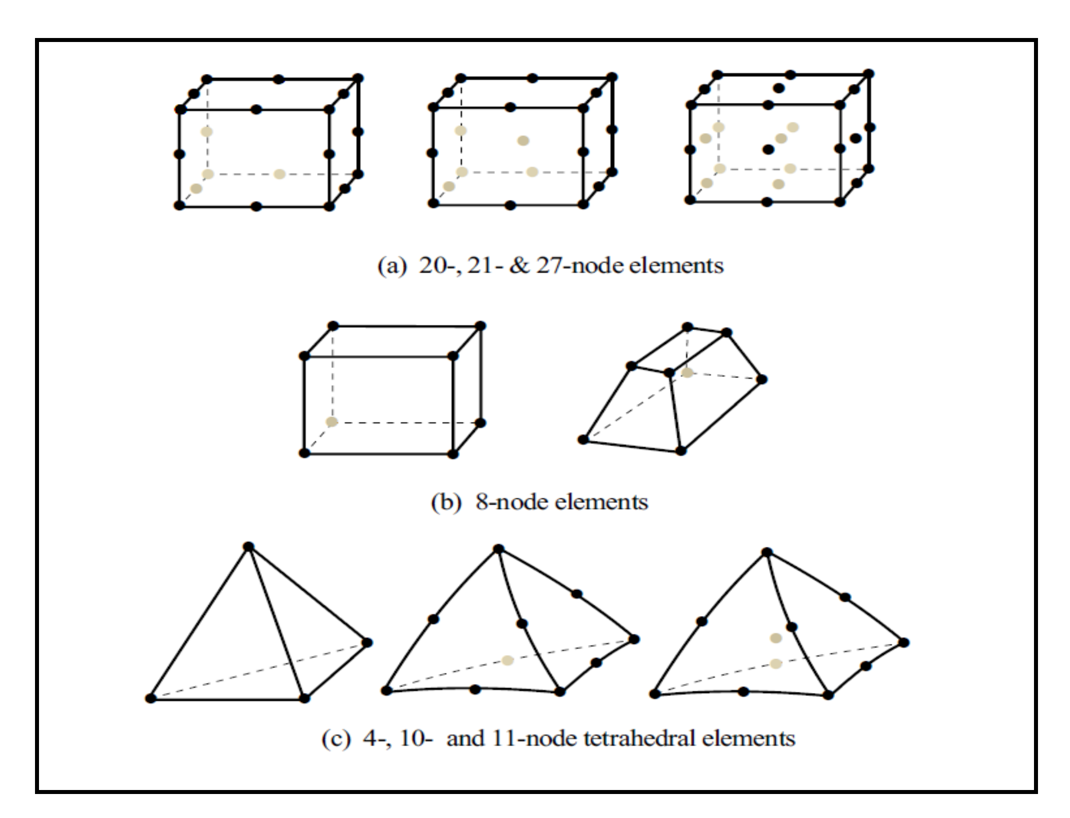

Figure 3.8 Some 3D Solid Elements (ADINA Manual, 2005).

Gupta and Ma (1977) and Balmer (1978) investigated the incompatibility between the beam element and the shell element in the eccentric beam model. The commonly used four-node thin shell element assumes that the shape functions are such that in axial and flexural modes of deformations are uncoupled.

The axial mode is interpolated using linear shape functions, and the flexural mode is characterized by a Hermitian cubic for transverse displacement shape function. These

researchers pointed out that the quadratic expression of the rotation in the linear constraint equation of axial displacement leads to inconsistencies.

Miller (1980) eliminated this incompatibility by adding internal degrees of freedom at the middle of element edges so that axial displacements were compatible with quadratic shapes. Marx (1985) and Sadek and Tawfik (2000) used nine-node Lagrangian elements based on Mindlin plate theory in the shell formulation and three-node Timoshenko beam elements with shear deformation.

Since all shape functions are quadratic the compatibility of the axial displacement field between the shell and the beam elements are ensured, Khaleel and Itani (1990), Chan and Chan (1999), and Prusty and Satsangi (2001) idealized the deck slab using an eight-node serendipity shell element, but the approach was basically similar to the one in Marx's study.

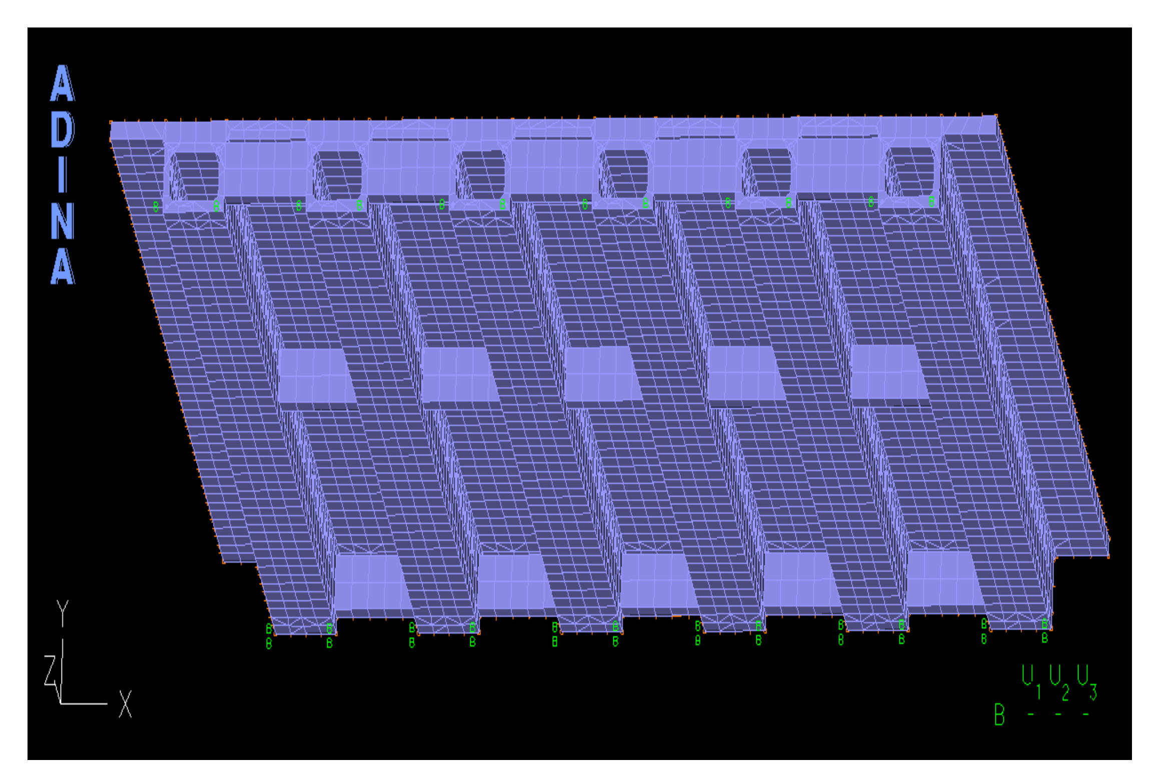

Figure 3.9 Mesh Generation of Bridge Model No.2_Configuration No.2.

The 3D Finite Element modeling of bridges is generally divided into three categories, Eccentric beam model, detailed beam model, and solid deck model. The primary structural members for the distribution of live load are deck slab and girders.

The modeling techniques of primary members are considered even though a number of studies also include secondary member modeling. A majority of studies (Barr et al. 2001; Chen 1999; Ebeido and Kennedy 1996; Shaway and Huang 2001; Zokaie 1991; Marx 1985) utilized the eccentric beam model to idealize the bridge superstructures as shown in Figure 3.10.

Tarhini and Frederick (1992), Mabsout et al. (1997), and Eamon and Nowak (2001) used the three-dimensional solid elements with three degrees of freedom at each node, which have linear shape functions, to model deck slab as shown in Figure 3.10. The steel girder flanges and web were modeled by quadrilateral shell elements. By imposing no releases between the shell elements and beam elements, the composite behavior between concrete deck and steel girder was simulated.

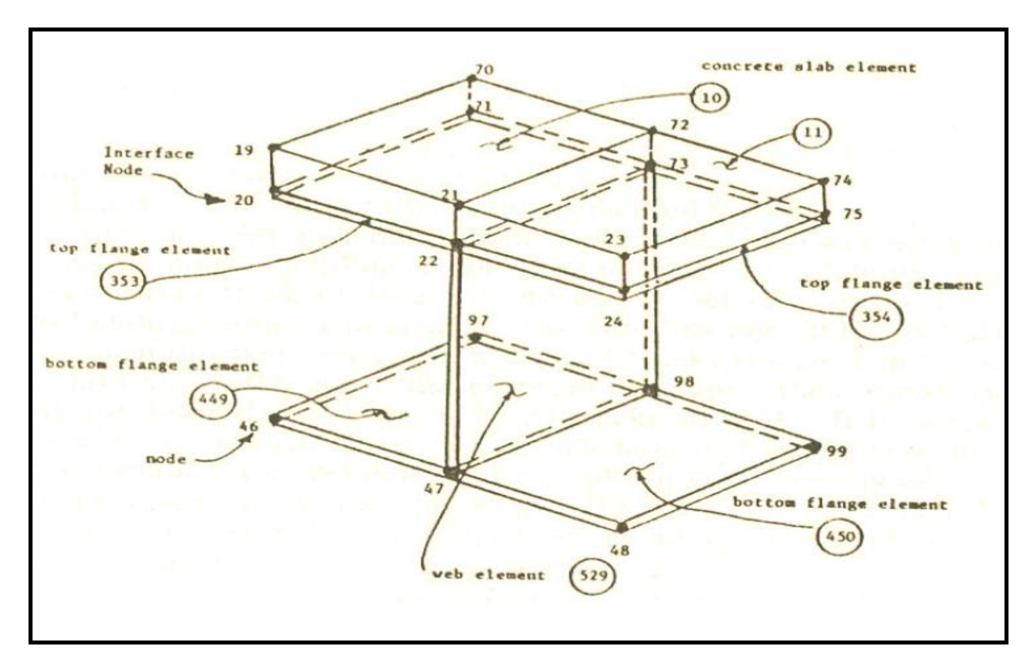

Figure 3.10 Solid Deck Model (Tarhini and Frederic, 1992).

3.2.2 Modeling of Prestressing Tendons

In the finite element modeling of prestressed concrete girder bridges, eccentric truss elements are added in the framework of the eccentric beam model to idealize the prestressing tendons. Since the tendon profile varies along the length of the girder, the eccentricity between the centroid of the composite section and the prestressing tendon varies from node to node as shown in Figure 3.11.

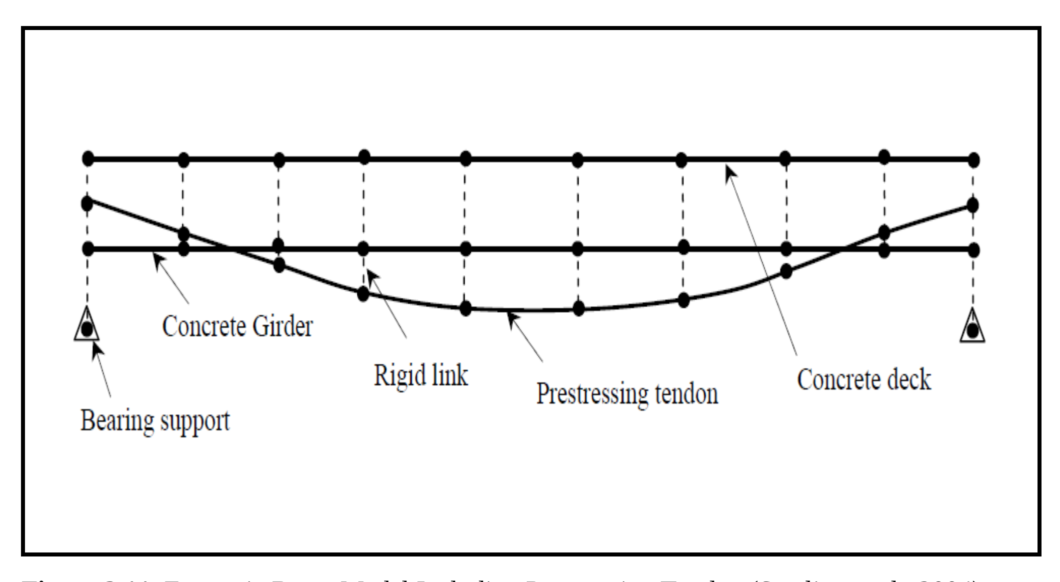

Figure 3.11 Eccentric Beam Model Including Prestressing Tendon (Sotelino et al., 2004).

In addition to modeling the profile of the prestressing tendons, the prestressing force must also be represented appropriately. Prestressing forces are specified through the initial strain of each truss element representing prestressing tendons. The magnitude of the initial strain *at final stages* can be determined by (f_{py}/E_p) × (initial jacking × losses), which is equal to 0.006 (Lins T.Y. 1981).

After the girders, slab, and prestressing tendons are all effective, live load cases are applied to the final configuration of PC girder bridges as shown in Figure 3.10, and this is the most accurate and most rigorous model, which referred to as a full load analysis (Hays et al. 1994).

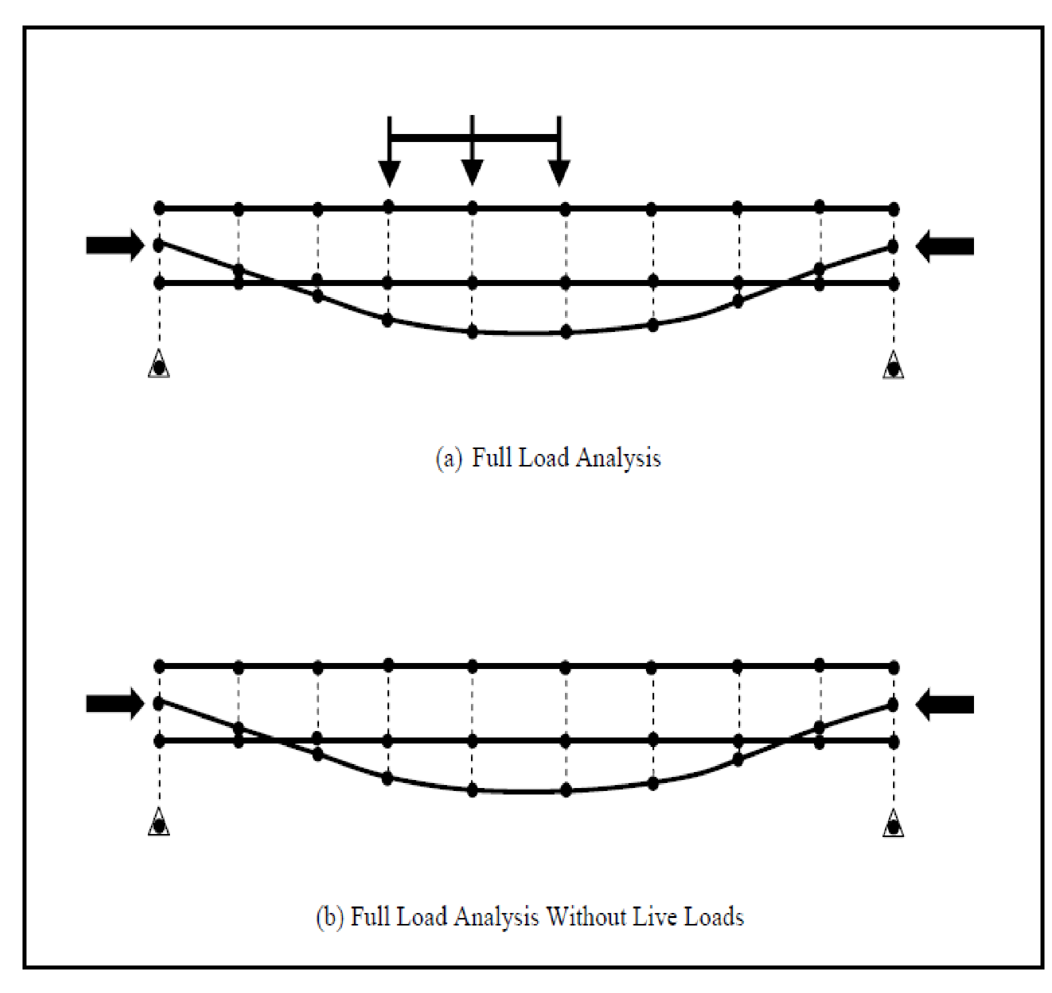

Figure 3.12 Prestressed Concrete Bridge Model (Sotelino et al., 2004).

In this study, however, only the effect of live loads is of interest since the load distribution factor (LDF) is due to live loads such as AASHTO HS20 trucks or lane loading.

Figure 3.13, shows the prestressing harped tendons in Bridge Model No.1, where cgc line act at 670 mm from top flange, end eccentricity (e_{end}) and mid eccentricity (e_{mid}) act at 305 mm and 550 mm, respectively from cgc line.

Figure 3.14, shows the prestressing straight tendons in Bridge Model No.2, where cgc line act at 383 mm from top flange, and the end eccentricity (e_{end}) and mid eccentricity act at 70 mm. Note that, harped tendons in Bridge Model No. 2, required a high computer “horse power” for nonlinear plastic analysis.

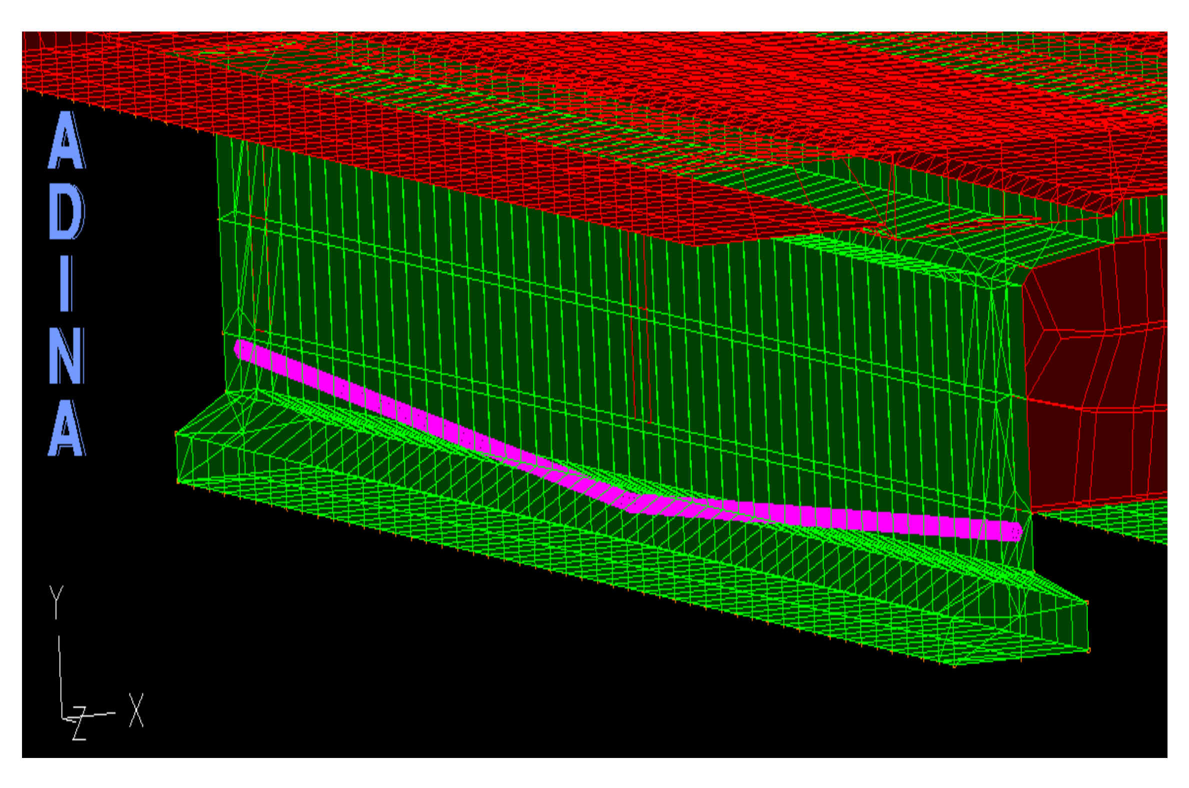

Figure 3.13 Profile of Harped Tendons, Defined as Truss Element in Bridge Model No.1.

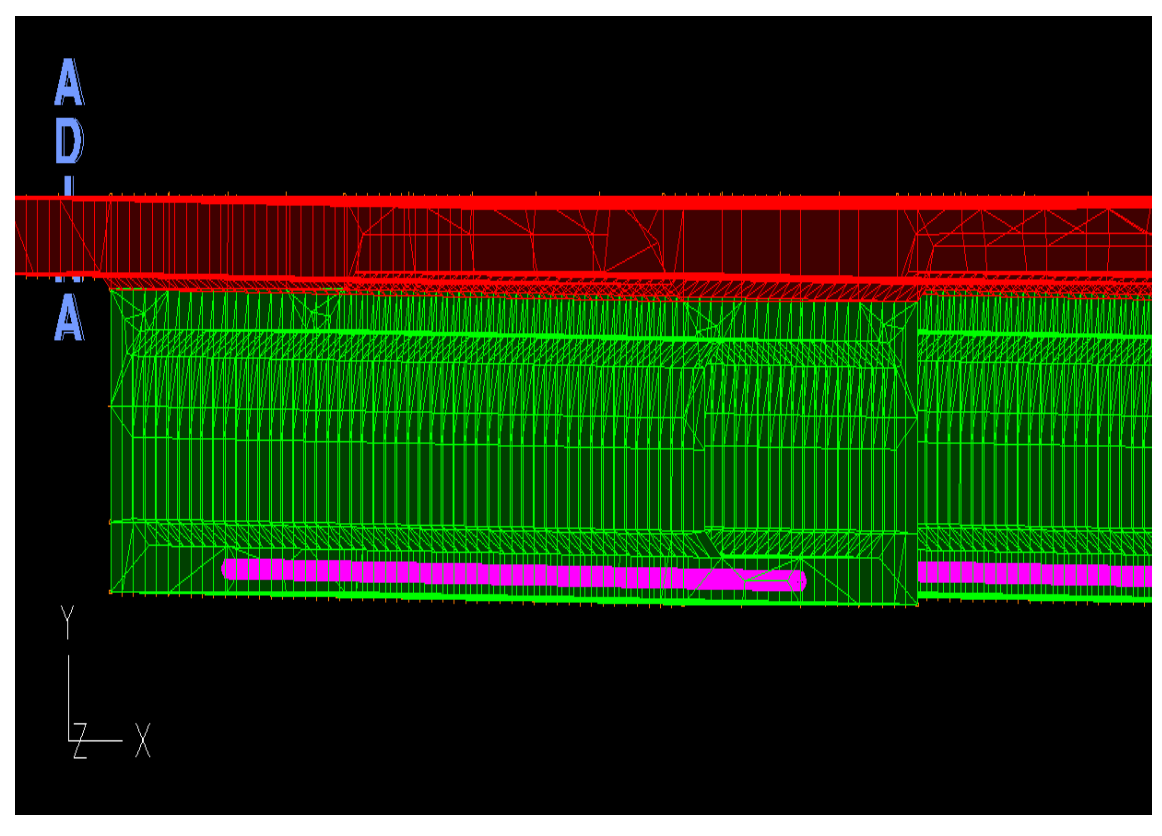

Figure 3.14 Profile of Straight Tendons, Defined as Truss Element in Bridge Model No.2.

3.2.3 Modeling of Vehicular Loads

The Load Distribution Factors (LDF) may be used for bridges with fairly regular geometry, as stated in AASHTO articles [A4.6.1.2–A4.6.2.2], the method is limited to systems with a constant cross section, number of beams is four or more, beams are parallel and have approximately the same stiffness, roadway part of the cantilever overhang does not exceed 910 mm, and plan curvature is small.

The provisions for LDF are contained in several AASHTO articles and only a few are discussed here. These articles represent some of the most important provisions in Section 4 of the AASHTO (2010) LRFD Specifications, and because of the many algebraically complex equations, these are not presented in the body of this discussion, and the distribution factors formulas for slab-girder bridges are discussed in chapter 1. The lever rule is a method of analysis; it involves a statical distribution of load based on the assumption that each deck panel is simply supported over the girder, except at the exterior girder that is continuous with the cantilever.

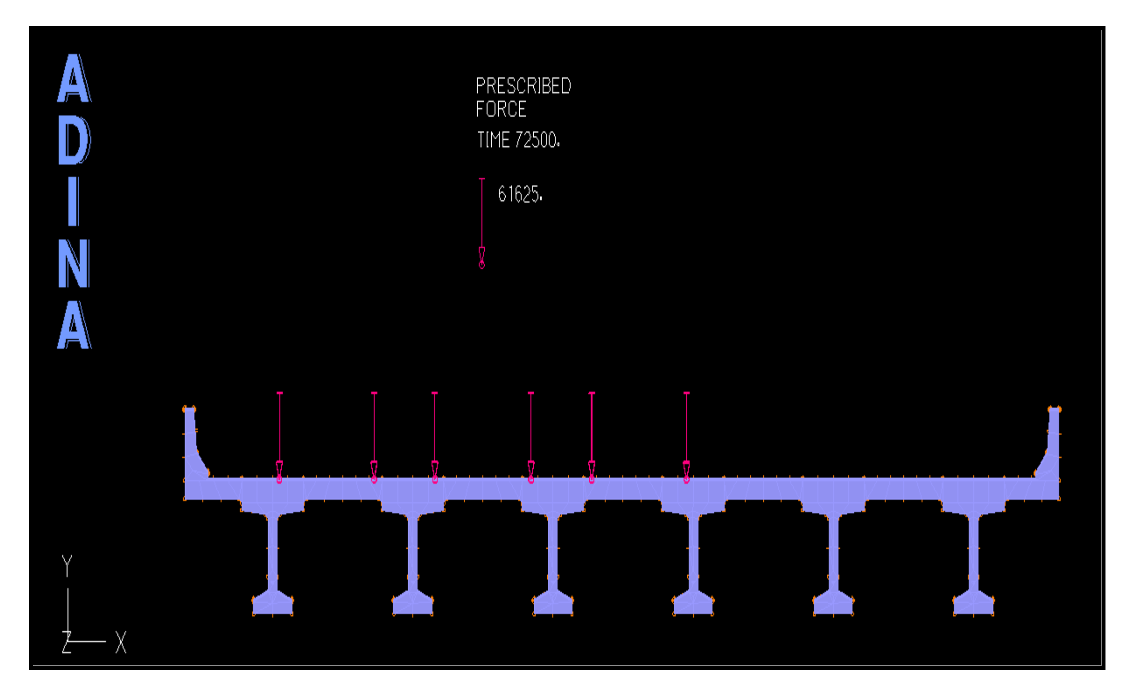

Figure 3.15 Exterior Girder Loading in Bridge Model No.1_Configuration No.1.

Because the load distribution to any girder other than one directly next to the point of load application is neglected, the lever rule is a conservative method of analysis.

Zokaie et al. (1991) performed hundreds of analyses on bridges of different types, geometrics, and stiffness. Many of these structures were actual bridges that were taken from the inventories nationwide. Various computer programs were used for analysis and compared to experimental results. The programs that yielded the most accurate results were selected for further analysis in developing the AASHTO formulas, which based on linear elastic analysis.

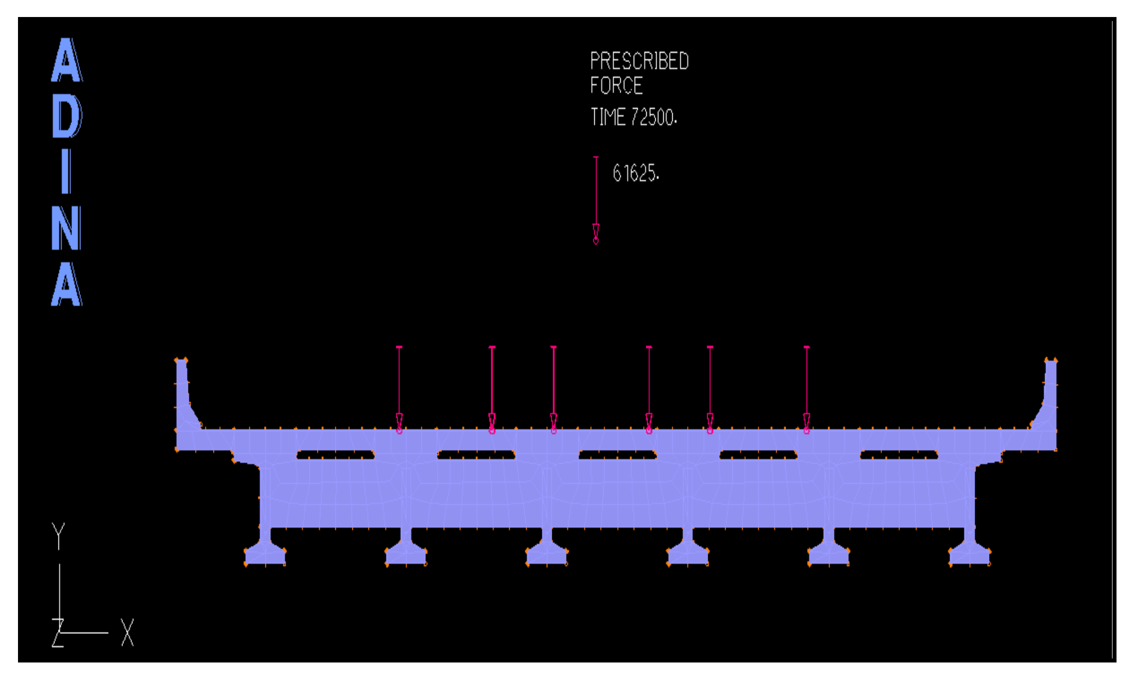

Figure 3.16 Interior Girder Loading in Bridge Model No.1_Configuration No.2.

The database of actual bridges was used to determine “an average bridge” for each type. Within each type, the parametric studies were made to establish the distribution factor equations, and the most sensitive parameter for this type of bridge is the girder spacing. It is important to note that the span length and girder stiffness affect the load distribution but to a lesser extent. This effect is reflected in the LDF equations.

Unlike the previous AASHTO equations, the important parametric properties of the bridge were used to develop prediction models based on a power law.

Each parameter was assumed to be independent of others in its effect on the distribution model. Although this is probably not strictly true, the resulting equations seem to work well, (Cai et al, 2004).

The single design lane formulas were developed with a single design truck, and the multilane loaded formulas were developed with two or more trucks. Therefore, the most critical situation for two, three, or more vehicles was used in the development.

Traditionally, an older edition of AASHTO Standard Specifications has based analysis on the wheel line or half the axle weight. In the present AASHTO (2002) Standard Specifications the analysis is assumed to be based on the entire vehicle weight.

Thus, if one compares the distribution factors historically used by AASHTO to those presently used, then the traditional factors must be divided by 2, or the present factor must be multiplied by 2, as discussed in Chapter one.

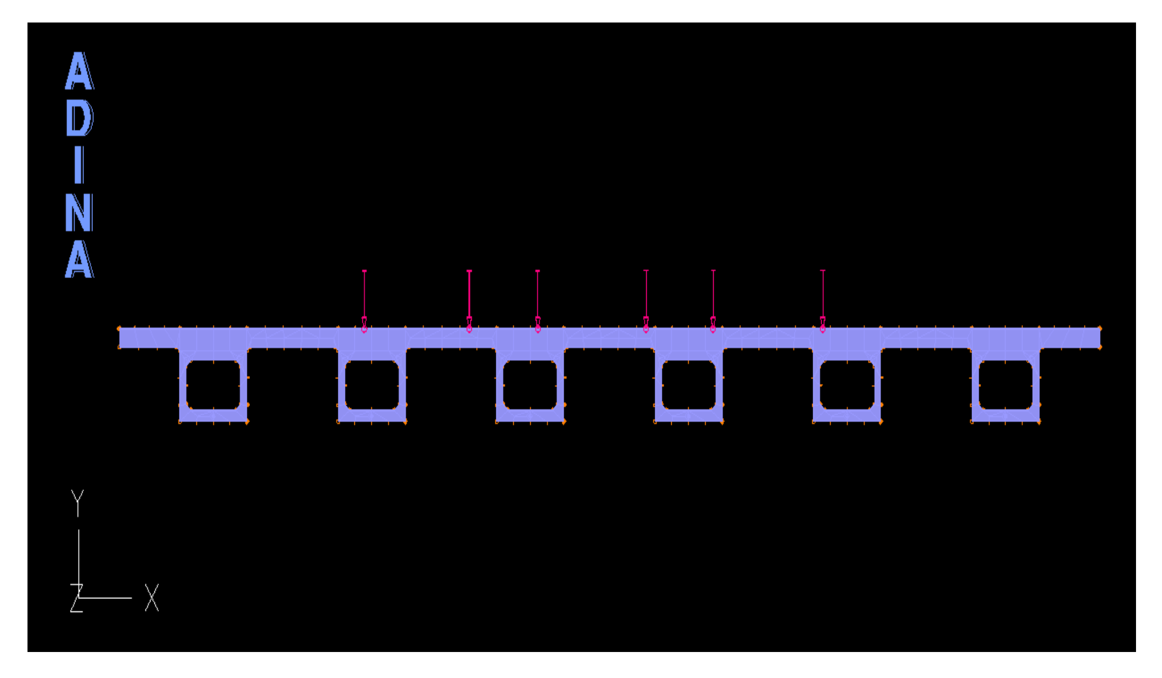

Figure 3.17 Interior Girder Loading in Bridge Model No.2_Configuration No.1.

The multiple presence factor, 0.85 for three loaded lanes were included in the analytical results upon which the formulas are based, Figure 3.15 shown, 0.85×72500 N which is

equal to 61625 N. Thus, the multiple presence factors are not to be used in conjunction with the factors, but rather the multiple presence is implicitly included in these factors.

The development of the present AASHTO (2010) LRFD Specifications, distribution factor was based on simply supported bridges, as linearly elastic approach. The investigators also studied systems to quantify the effect of continuity. Given the relative insensitivity of girder stiffness to the distribution factors, it is expected that continuity does not significantly affect the distribution factors, (Barr et. al, 2001).

In this study, two preprocessors are developed for the Finite Element analysis of slab-on-girder bridges in order to expedite the analyses. They are the maximum longitudinal position generator; first, the truck position that produces the maximum moment or shear should be determined in the longitudinal direction. The transverse truck position is then positioned manually.

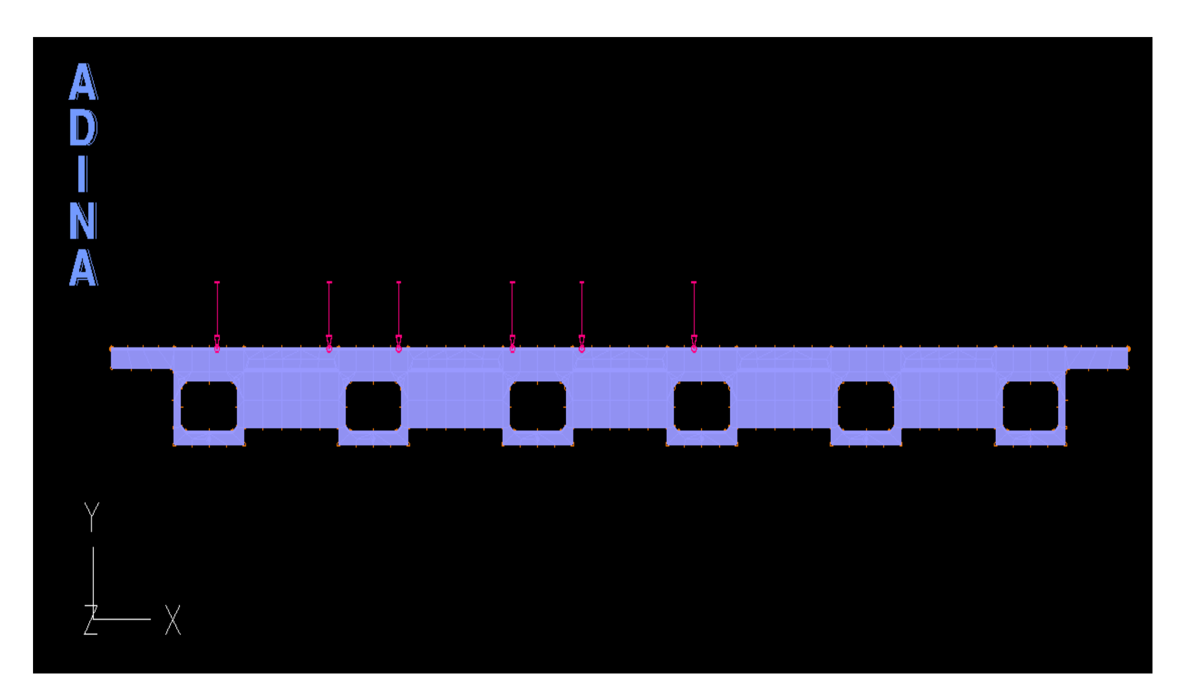

Figure 3.18 Exterior Girder Loading in Bridge Model No.2_Configuration No.2.

In this procedure, it is required that a number of load cases be tested to determine the maximum effect to the specific girder. Three design lanes were loaded at a time, with

one HS20 truck each at three transverse loading positions, causing maximum moments in internal and external girders for each loading position. Longitudinally they were positioned with their middle axles 600 mm from the midspan of the bridge, as shown in Figures 3.15 to 3.18.

These trucks do not represent actual vehicles, but can be considered umbrella loads, as discussed in chapter 2. The wheels attached to each of these three axles carry same load, the front axle weighs 35 kN and other two axles weighs 145 kN each. The spacing between the first and second axles is 4.3 m, and the spacing between the second and third axles, was taken as 4.3 m for all cases, since this configuration of truck generates the maximum load effect for all bridge configurations. The width of each of these three axles is 1.8 m, wheels of adjacent trucks are never closer than 1.2 m, and the curb edge distance is never less than 0.6 m, as in Figure 1.1.

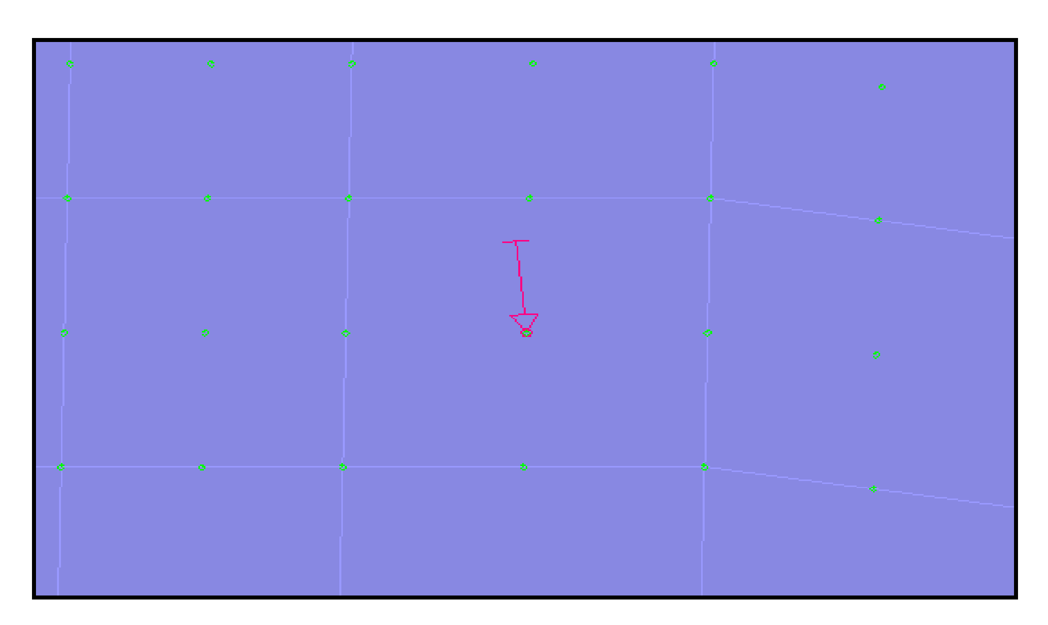

Figure 3.19 Single Concentrated Wheel Load on Shell Element.

The lane loading was not considered in this study, since the difference between the load distribution of lane and truck loading is insignificant, as observed by previous researchers (Chen 1995, Chen and Aswad, 1996). Meanwhile, Barr et al. (2001)

concluded that using truck load distribution for lane load is more conservative. Thereafter, only the effect of truck loading on the analyzed bridge was studied.

This is also consistent with the methodology used in developing the AASHTO (2010) LRFD Specifications, where only truck loads were considered in determining the load distribution factors.

3.2.4 Modeling of RC Diaphragms

Formulas of the AASHTO (2010) LRFD Specifications has been developed using sophisticated finite element analysis of hundreds of bridges, and LDF equation does not include some important features of bridges, such as cross bracing, diaphragms, and parapets in bridges, which may affect lateral load distribution. These elements are not considered in the development of the AASHTO LRFD LDF equation. Previous parametric studies (Eamon and Nowak 2002; Eamon and Nowak 2004; Mabsout et al. 1997) have shown that consideration of secondary elements, which are typically present in steel girder bridges, has a significant effect on the lateral load distribution. Consequently, the AASHTO LRFD equation provides overly conservative results.

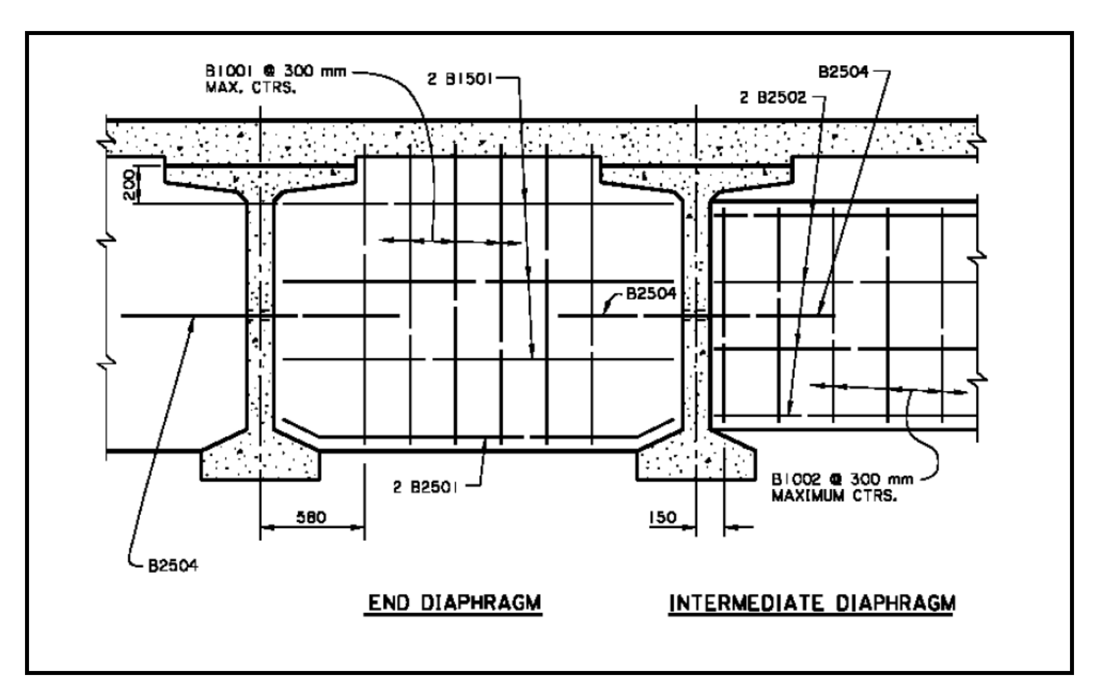

Figure 3.20 Typical Diaphragm Details (Bridge Design Manual, 2002).

The objective of this study is to investigate the influence of end diaphragms and intermediate diaphragms on the lateral load distribution of prestressed concrete girder bridges through the 3D nonlinear finite element analysis in plastic range, where diaphragms are connected at the intersection of the flanges and the web.

For simply supported conditions, rotations in all directions are allowed. Minimum restraints are assigned for longitudinal and transverse movement while vertical restraint is placed at the supports.

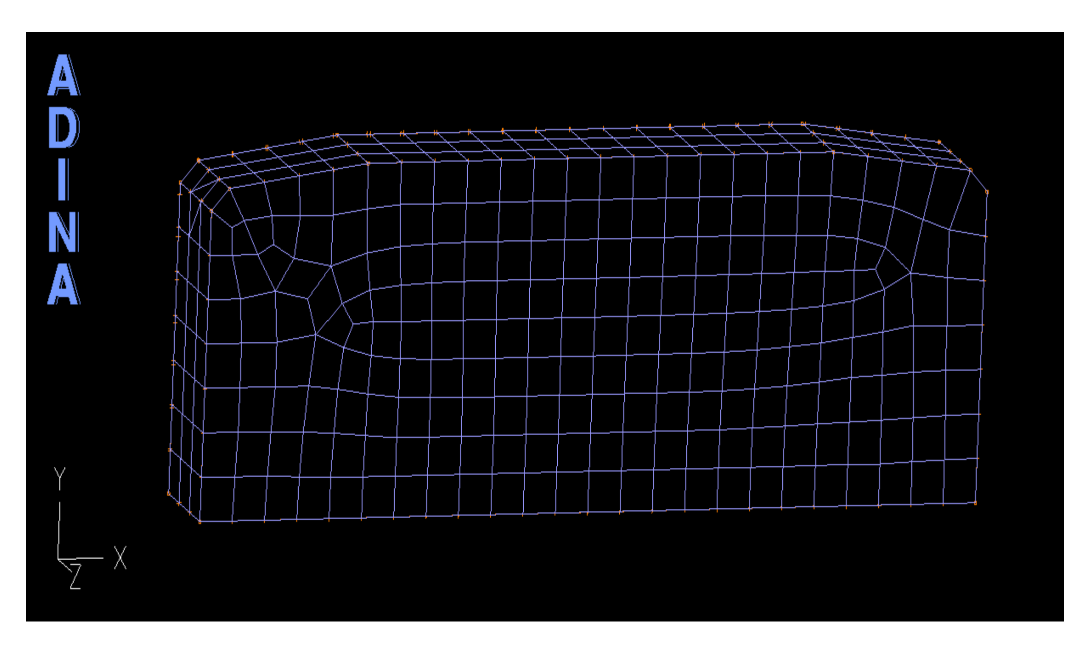

Figure 3.21 Mesh Generation of RC Diaphragm in Bridge Model No.1.

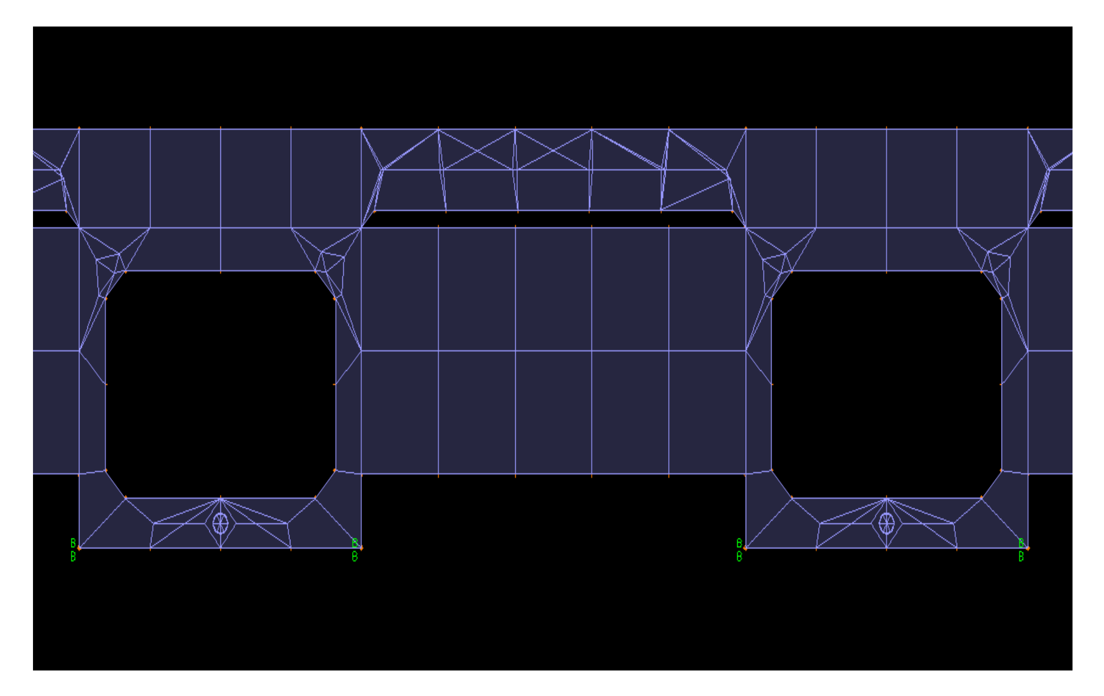

Figure 3.22 RC Diaphragm in Bridge Model No 2.

3.3 Structural Nonlinearity of PC Bridges

3.3.1 An Overview

A nonlinear analysis is complex and involves many simplifying assumptions. Engineers must be familiar with those complexities and assumptions to design bridges that are safe and economical. Many factors contribute to the nonlinear behavior of a bridge. These include factors such as material inelasticity, geometric effects, abutment locations, time-dependent effects due to concrete creep and shrinkage, etc.

Structural Nonlinearity can be grouped into three major types. The first one is Geometric Nonlinearity, in which deformation is large enough that equilibrium equations must be written with respect to the deformed structural geometry, also loads may change direction as they increase, as when pressure inflates a membrane (Cook, R. et al. 2002).

The second type is Material Nonlinearity, in which material properties are functions of the state of stress or strain; examples include nonlinear elasticity, plasticity, and creep. Material nonlinearity occurs in most materials at different levels of importance, being evident in concrete.

The Third type is Contact Nonlinearity, in which a gap between adjacent parts may open or close, the contact area between parts changes as the contact force changes, or there is sliding contact with frictional forces. *In this study the prestressing tendons and concrete girder were modeled using the contact nonlinearity approach*.

Problems in these categories are nonlinear because stiffness and perhaps loads as well, become functions of displacement or deformation. Thus, in structural equations [K].{D}={R}, coefficient matrix [K] and perhaps load vector {R} become functions of {D}.

We cannot immediately solve for {D} because information needed to construct [K] and {R} is not known in advance. An iteration process is required to obtain {D} and its associated [K] and {R} such that the product [K].{D} is in equilibrium with {R}. When equations [K].{D}={R} are nonlinear the principle of superposition does not apply (Cook, R. et al. 2002).

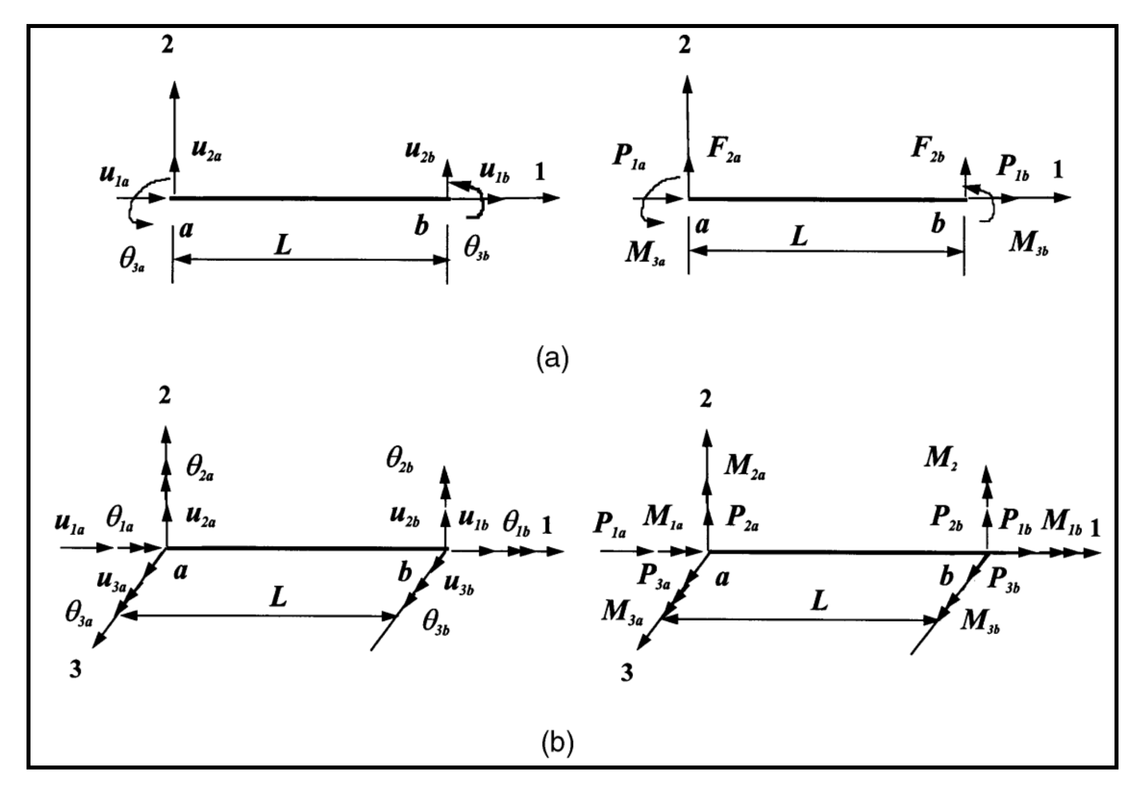

Figure 3.23 Degrees of Freedom and Nodal Forces for a Framed Member, (a) 2D Member, (b) 3D Member (Chen, W.F. and Duan, L., 2000).

3.3.2 Material Nonlinearity – Plastic Models

These material models are based on; the von Mises yield condition, an associated flow rule using the von Mises yield function, an isotropic or kinematic, bilinear or multilinear, and hardening rule.

For many practical applications, reasonable results are obtained by assuming an elastic-plastic stress-strain behavior. Initially, the behavior is elastic until the yield stress σ_Y is reached. The elastic modulus is denoted by E. after yielding, the plastic phase begins with a slope of E_t. If the load is reduced after the material goes into plastic state, the resulting unloading is elastic and follows the initial slope.

If the loading is continued in the opposite direction, the material will eventually yield in that direction.

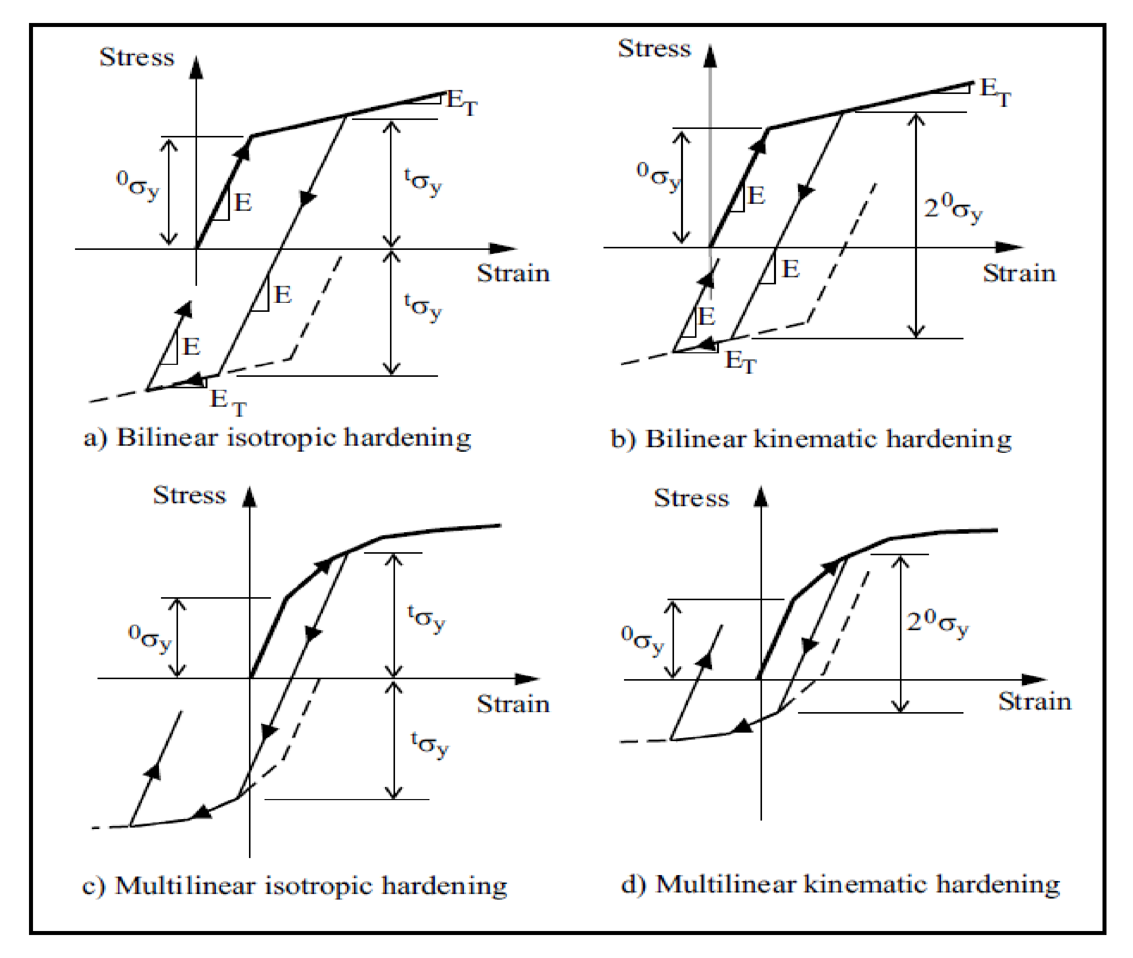

Figure 3.24 Isotropic and Kinematic Hardening (ADINA Manual, 2005).

The yield stress during subsequent loading and unloading cycles depends on the type of strain hardening model. Two commonly used strain hardening models are shown in Figure 3.24. The kinematic hardening model assumes that the elastic range remains constant. Thus, the elastic lines have the same length and are equal to each other. In the isotropic hardening model, one assumes that the yields stress for the reversed loading is equal to the previous yield stress, thus the elastic region keeps growing in this model (Bhatti, M.A., 2005).

3.3.4 Material Nonlinearity – Concrete Models

The analysis of structural concrete is very complex and time-consuming due to the highly complex behavior of concrete structures. Such structures are, by their nature, non-homogeneous and anisotropic. This is due to the composition of plain concrete, which is a non-homogeneous mixture of coarse aggregate, sand, and hydrated cement paste. Concrete has different behavior in tension and compression, such that it is much more resistant to compression than to tension.

In general, its tensile strength is in the order of 8% to 15% of its compressive strength. When subjected to compression concrete behaves linearly until approximately 30% to 50% of compressive strength.

After this point the compressive stress increases gradually to a maximum, reaching the concrete compressive strength. After reaching the maximum stress, the stress strain curve descends into a softening region, eventually crushing and failing at an ultimate strain, as illustrated in Figures 3.25.

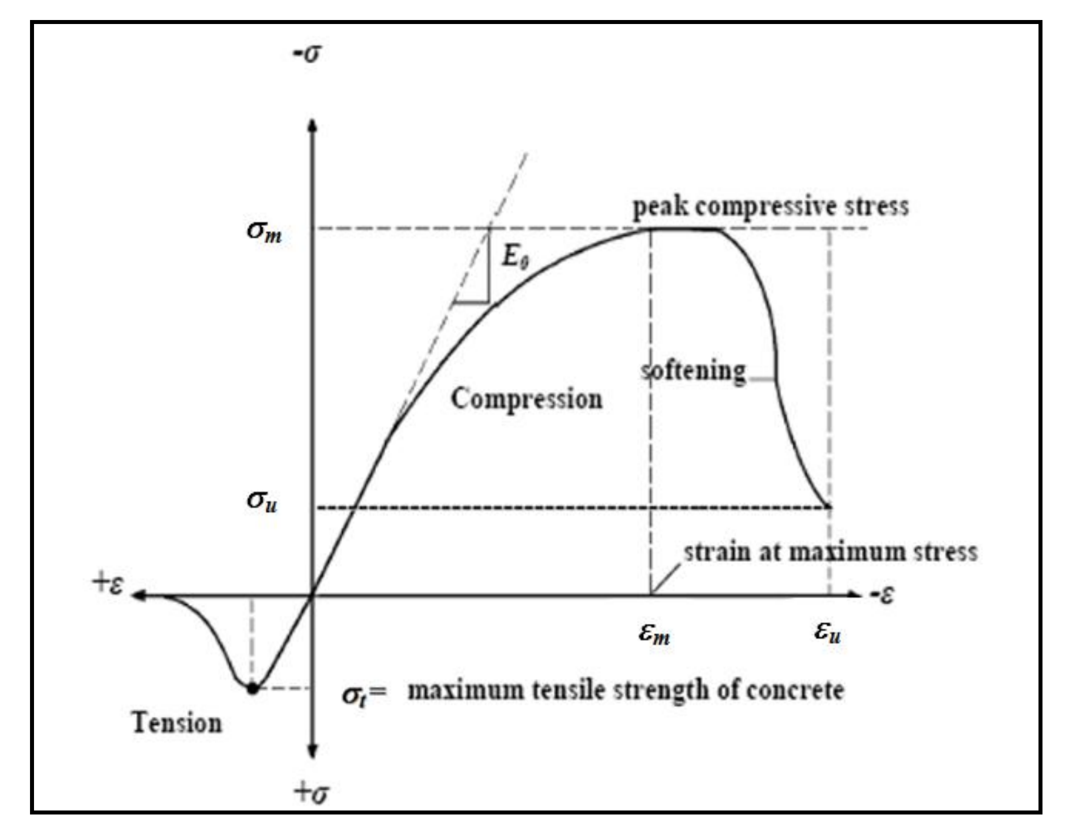

Figure 3.25 Uniaxial Compressive and Tensile Stress-Strain Curve of Concrete.

In this study the concrete model employed with the 3D solid elements in ADINA Program, and can be used with the small and large displacement formulations, in all cases small strains are assumed. When used with the small displacement formulation, a materially nonlinear only formulation is employed.

Although the model is entitled “Concrete Model” in ADINA Program, the basic material characteristics are tensile failure at a maximum, relatively small principal tensile stress, compression crushing failure at high compression, and strain softening from compression crushing failure to an ultimate strain, at which the material totally fails.

The tensile and compression crushing failures are governed by tensile failure and compression crushing failure envelopes. These material characteristics pertain, for example, to a variety of rocks (ADINA Manual, 2005).

3.3.5 Contact Nonlinearity

The contact problem is a kind of geometrically nonlinear problem that arises when different structures or different surfaces of a single structure come into contact (Cook, R. et al. 2002).

Several practical problems involve situations in which one or more bodies may come in contact during loading. An example is the determination of load transmission between rotating components such as vehicle tire forces on the pavement.

In this study the contact problems lie between the prestressing tendons and concrete girder which is built monolithically. These types of contact problems are formulated in a variety of ways. The simplest situation is the frictionless, small-displacement, elastic contact problem. The other extreme is the contact problem involving friction and large strain inelastic behavior.

From the finite element point of view, all formulations use some form of constrains equations. Because of highly nonlinear and discontinuous nature of contact problems, great care and trial and error are necessary to obtain solutions to practical problems.

It should be noted that the contact problems are always *nonlinear* even when the finite element model itself is based on small-displacement linear elastic assumptions (Bhatti, M.A., 2005). Also, the solution of contact problems involves inequalities.

A solution of such system must be obtained by using optimization techniques for constrained problems. For simple cases the contact function idea can be used to avoid dealing with inequalities. Contact conditions can be specified in ADINA to model contact involving solid elements, 3D solid and structural elements such as truss element or other elements.

Contact in ADINA is modeled using contact groups; each contact group is composed of one or more contact surfaces. The presence of contact groups renders the analysis nonlinear even when no nonlinear element groups are defined. Contact pairs are then defined between contact surfaces, contact pair consists of the two contact surfaces that may come into contact during the solution. One of the contact surfaces in the pair is selected to be the contactor (slave) surface and the other contact surface to be the target (master) surface. The direction of a contact surface is marked by a normal vector pointing towards the interior of the contact surface as shown in Figure 3.26 and 3.27.

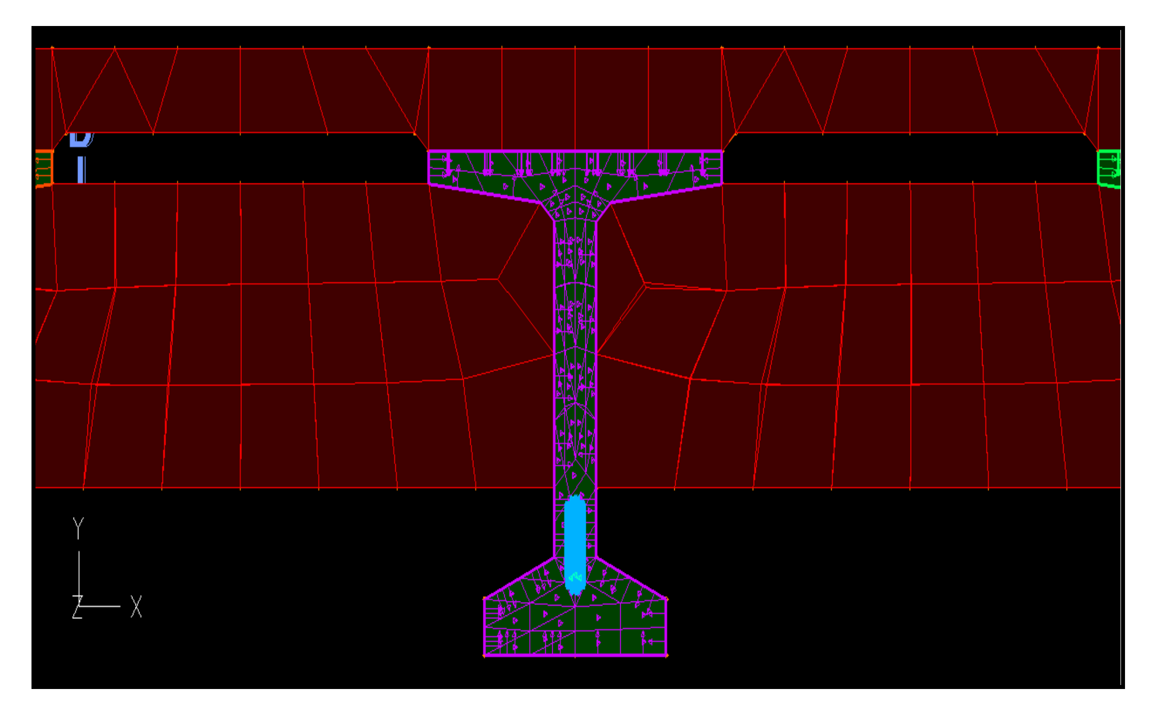

Figure 3.26 Normal Vectors in Contact Conditions between BT54 Girder and Prestressing Tendons in Bridge Model No.1

The double-sided contact is required to model Prestressing tendons and concrete girder, the contactor surface nodes in this case are prevented from crossing from one side of the target contact surface to the other during solution. This option is more common for shell based contact surfaces.

ADINA offers three contact solution algorithms; constraint function method, Lagrange multiplier (segment) method, and Rigid target method. Each contact group must belong

to one of these three contact algorithms. It's recommended by ADINA Manual, 2005 to use the constraint function method, which is the most frictionless contact problem and more effective than the Lagrange (segment) method.

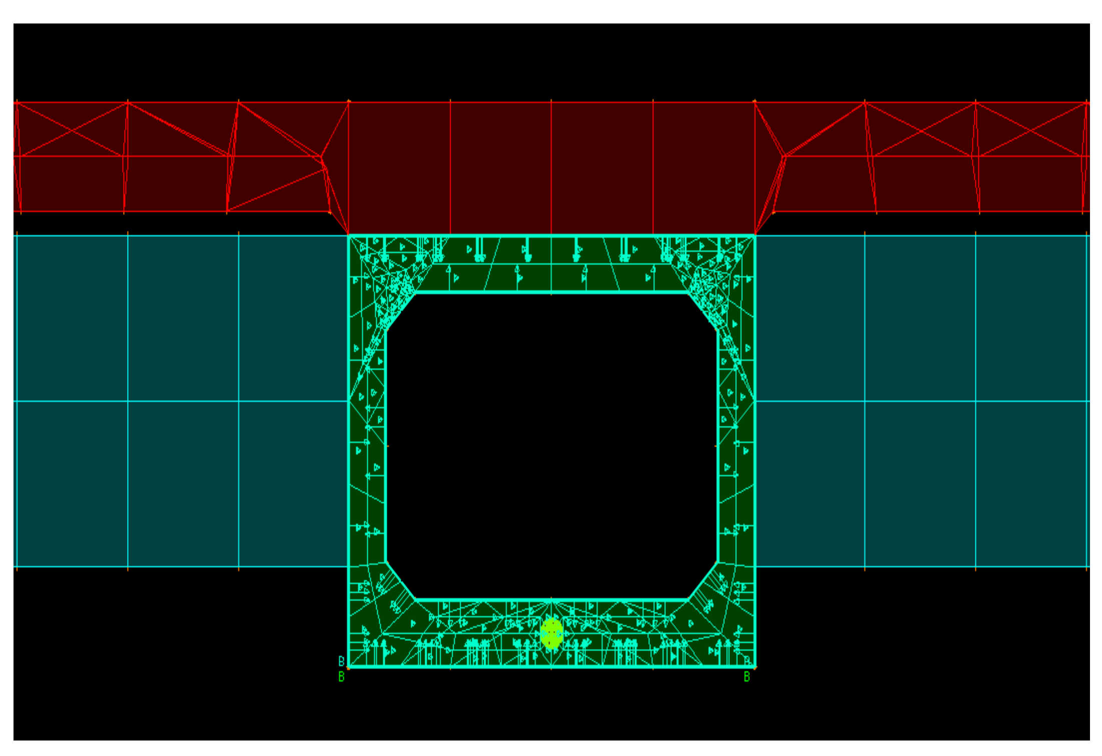

Figure 3.27 Normal Vectors in Contact Conditions between BIV36 Girder and Prestressing Tendons in Bridge Model No.2

3.4 Nonlinear Analysis of PC Bridge

In nonlinear static analysis the equilibrium equations to be solved are:

$$ {}^{t+\Delta t}\mathbf{R} - {}^{t+\Delta t}\mathbf{F} = \mathbf{0} \tag{3.1} $$

where ${}^{t+\Delta t}\mathbf{R}$ is the vector of externally applied nodal loads at time (load) step $t + \Delta t$, and ${}^{t+\Delta t}\mathbf{F}$ is the force vector equivalent (in the virtual work sense) to the element stresses at time $t + \Delta t$.

The nonlinearity may come from the material properties, the kinematic assumptions, the use of contact conditions, or the use of special features. The solution to the static equilibrium equations can be obtained in ADINA using; Modified Newton iterations, The Broyden-Fletcher-Goldfarb-Shanno (BFGS) method, Full Newton iterations, and Automatic Step incrementation [Automatic Time Stepping (ATS)].

In this study, the Full Newton iterations, which is the most powerful method, were used for PC Bridge. However, the ATS algorithms can be used with all iteration methods provided by ADINA program, and do not require the stiffness matrix to be positive definite, thus allowing for the solving of bifurcation problems.

If a reasonable number of time (or load) steps are used for the nonlinear response, then the use of the ATS method will result in almost the same iteration path as when not using the method. Namely, no step subdividing will be performed if convergence is always directly reached at the user specified load levels (ADINA Manual, 2005).

The use of the Full Newton iteration method and a reasonable load incrementation is frequently sufficient to ensure that an accurate solution of the response of the model will be obtained. However, the Modified Newton iteration is less expensive (per iteration) than the BFGS method, which is, in turn, less expensive per iteration than the

Full Newton iteration, and the more expensive method (per iteration) may require less iterations to achieve convergence.

Every nonlinear analysis should be preceded by a linear analysis, if only to check that the model has been set up correctly. The linear analysis results will tell whether proper boundary conditions are imposed, all degrees of freedom without stiffness have been deleted, and so on, and the finite element mesh is adequate.

In practice, it is recommended by ADINA Manual, 2005 to set up the complete nonlinear model, but only perform a one load step analysis without equilibrium iterations. The displacement results obtained from this solution are linear analysis results and can frequently be used to establish a reasonable load incrementation for the nonlinear solution.

If the use of a sufficient number of load steps and equilibrium iterations with tight convergence tolerances at each load step is considered to yield an accurate solution of the model, then the basic aim is to obtain a response prediction close to this accurate one at as small a solution cost as possible.

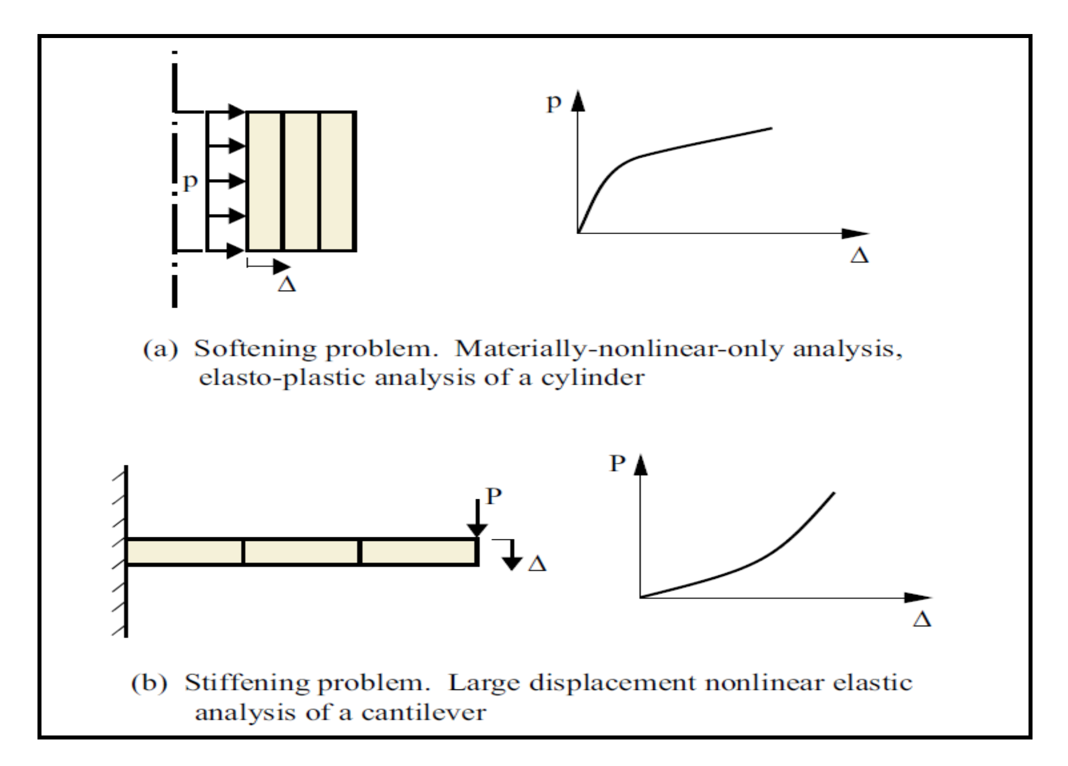

Figure 3.28 Different Types of Nonlinear Analysis (ADINA Manual, 2005).

CHAPTER ④:

DISCUSSION OF MODELING & RESULTS

CHAPTER 4. DISCUSSION OF MODELING AND RESULTS

4.1 An Overview

The ADINA system program generates a wide variety of results, for example, stresses, displacements, reactions, etc. The results computed by ADINA are made available to the user when the corresponding porthole file is loaded, results control are available when model was defined during preprocessing.

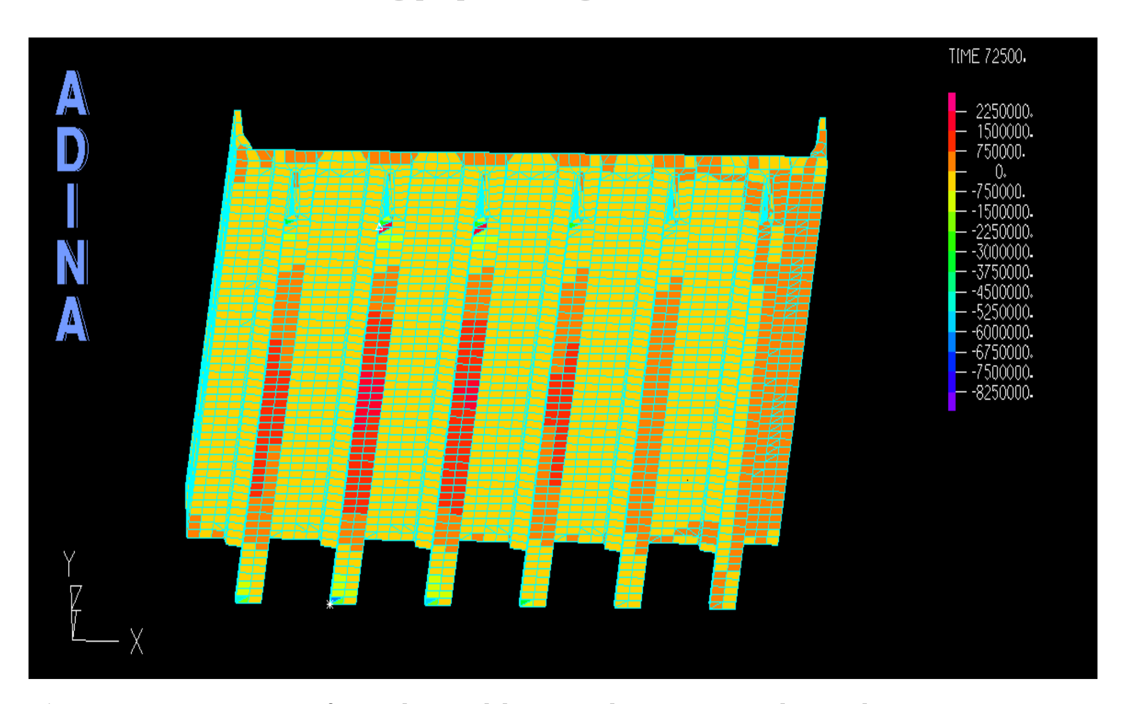

Figure 4.1 Stress Contour for Bridge Model No.1 under Exterior Girder Loading.

In general, regarding results output along with the elements, either output stresses or forces, but not both as shown in Figure 4.1. The actual results of output stresses depend upon the material model and upon the stress reference.

Results can be evaluated at various types of locations within the model, for example locations within elements or element layers; these can be the integration points, the element local nodes or other locations within the element.

If the element is an ADINA multilayer shell element, its need to enter the layer number, otherwise used a layer number of 1. There are several conventions to specify the point

within the element (or element layer), in ADINA system elements, there are two subtypes of element points: integration points and local nodes.

The results are computed by the solution program at only one of these subtypes, and can be evaluated at the element points where they were computed by the solution program, or can be extrapolated to other element points.

3D Solid elements can be extrapolated from -1.0 to 1.0, and for isoparametric coordinates parameters can be extrapolated from 0.0 to 1.0 (ADINA Manual, 2005).

If an element/layer variable is requested within an element at a point, the variable is interpolated or extrapolated using four methods in ADINA program as follows: Linear interpolation, Face interpolation, Centroid interpolation, and Integration point interpolation.

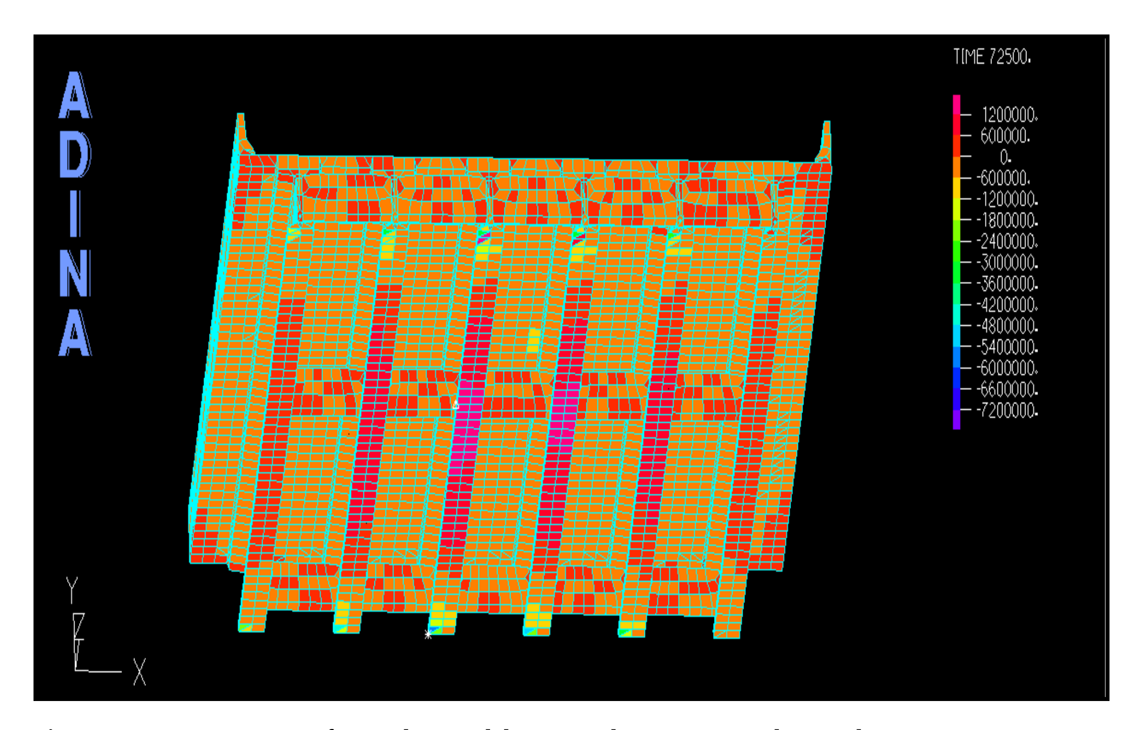

Figure 4.2 Stress Contour for Bridge Model No.1 under Interior Girder Loading.

4.2 Behavior of Concrete and Plastic Material Models

Prestressing tendons defined as a Multilinear Plastic material model with kinematic strain hardening for which the stress-strain relationship is defined using the following parabolic equation:

$$f_p = E_s \, \varepsilon_p \left[0.0165 + \frac{0.9835}{\left[1 + \left(118 \, \varepsilon_p \right)^5 \right]^{0.2}} \right] \tag{4.1}$$

Figure 4.3; illustrate the definition of the stress-strain law. Note that the stress is uniquely defined as a function of the strain only; hence for a specific strain, reached in loading or unloading, a unique stress is obtained from the curve in Figure 4.3.

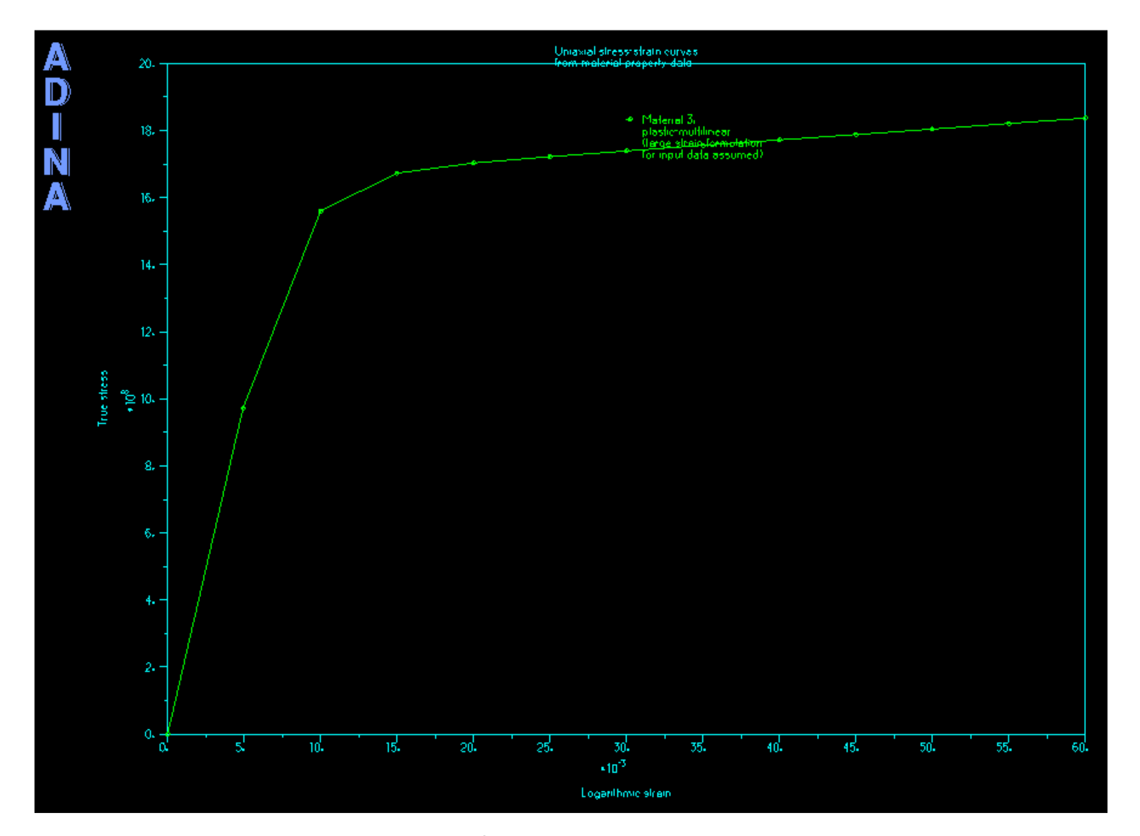

Figure 4.3 Uniaxial Stress-Strain Curve for Prestressing Tendons, by ADINA Program .

There is no restriction on the number of stress-strain points in the stress-strain curve in multilinear plasticity (ADINA Manual, 2005).

In Concrete Models, the tensile and compression crushing failures are governed by tensile failure and compression crushing failure envelopes. These material characteristics pertain, for example, to a variety of rocks (ADINA Manual, 2005).

The uniaxial compressive and tensile stress-strain relationship was obtained through the following parapolic equation by Lins (1981):

$$f_c = f_c' \left[\frac{2\varepsilon}{0.002} - \left(\frac{\varepsilon}{0.002} \right)^2 \right] \tag{4.2}$$

For PC girders as illustrated in Figure 4.4, σ_m is the uniaxial maximum compressive stress = -55 MPa, ε_m is the uniaxial maximum compressive strain = -0.002, σ_u is the uniaxial ultimate compressive stress = -41.25 MPa, ε_u is the uniaxial maximum compressive strain = -0.003, and σ_t is the uniaxial cut-off tensile stress = +3.71 MPa.

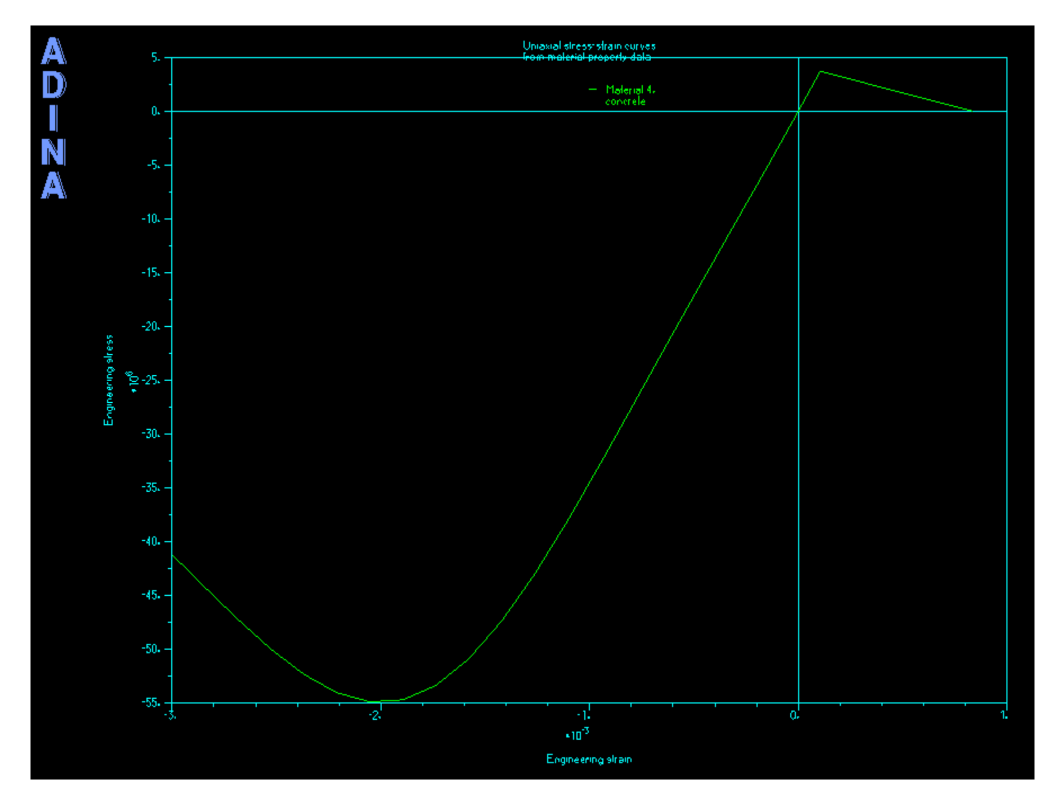

Figure 4.4 Uniaxial Compressive and Tensile Stress-Strain Curve of PC Girder, by ADINA Program.

The basic features were used in the concrete model; a nonlinear stress-strain relation to allow for the weakening of the material under increasing compressive stresses.

It is accepted that concrete is a very complex material; the model provided in ADINA Program may not contain all the detailed material characteristics that may look at for.

However, considering the variability of concrete materials that need to be described in practice, and recognizing that the model may also be useful in the modeling of rock materials, the objective of this study is to provide an effective model with sufficient flexibility to model most of the commonly used material behaviors.

For deck slab and diaphragms as illustrated in Figure 3.28, σ_m is the uniaxial maximum compressive stress = -30 MPa, ε_m is the uniaxial maximum compressive strain = -0.002, σ_u is the uniaxial ultimate compressive stress = -22.5 MPa, ε_u is the uniaxial maximum compressive strain = -0.003, and σ_t is the uniaxial cut-off tensile stress = +2.8 MPa.

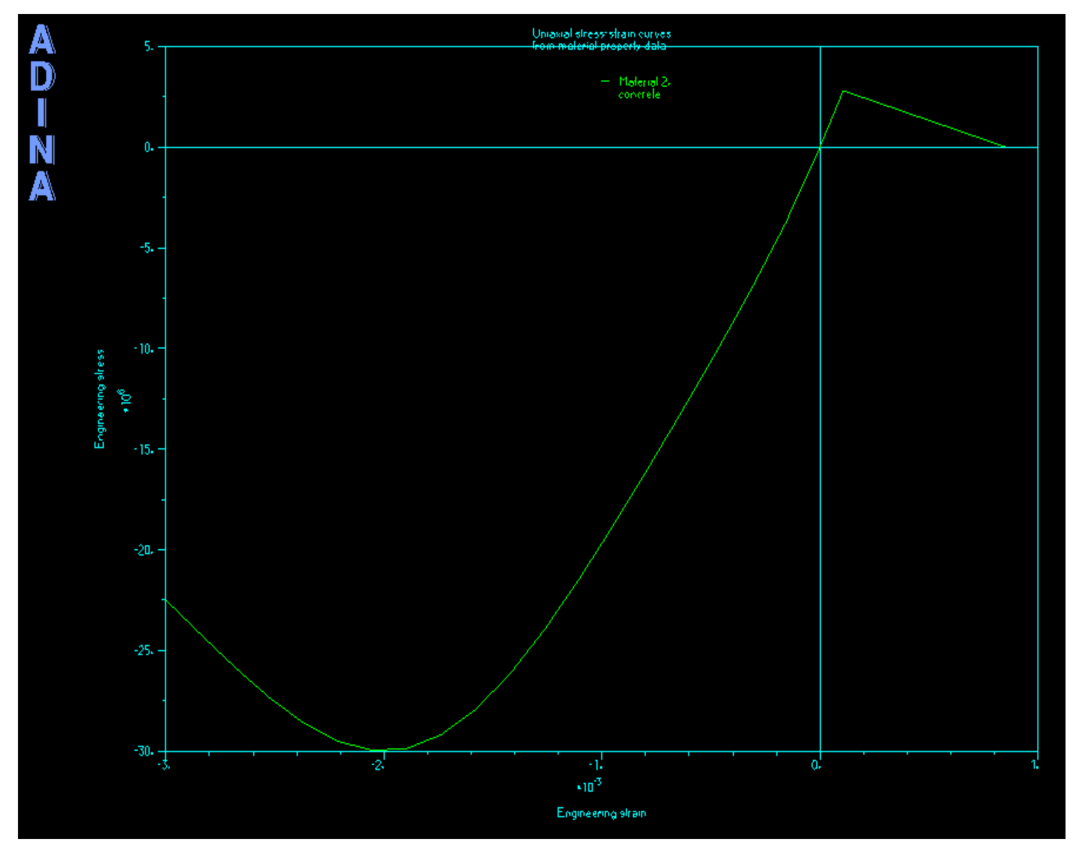

Figure 4.5 Uniaxial Compressive and Tensile Stress-Strain Curve of Deck Slab and Diaphragms, by ADINA Program.

4.3 Calculation of Load Distribution Factors

4.3.1 An Overview

In order to obtain the load distribution factor (LDF), the postprocessing ADINA-PLOT of the finite element results is required; the computation of stress resultants, forces, moments and other can be requested in ADINA.

Stress resultants (forces and moments) can be calculated as recommended by ADINA manual, 2005 for isoparametric coordinates as follows

$$R = \int_0^1 \sigma \; dz$$
$$M = \int_0^1 \sigma . z \; dz \tag{4.3}$$

These moments were used to calculate the distribution factors as follows. Considered the one-dimensional beam analysis, which is analogous to the bridge configuration as illustrated in Figure 4.6; the length of beam is the same as the bridge span length. However, the loading on the beam analysis is one line of wheel loads or more, depending on the number of loaded lanes, placed at the position that produces the maximum moment.

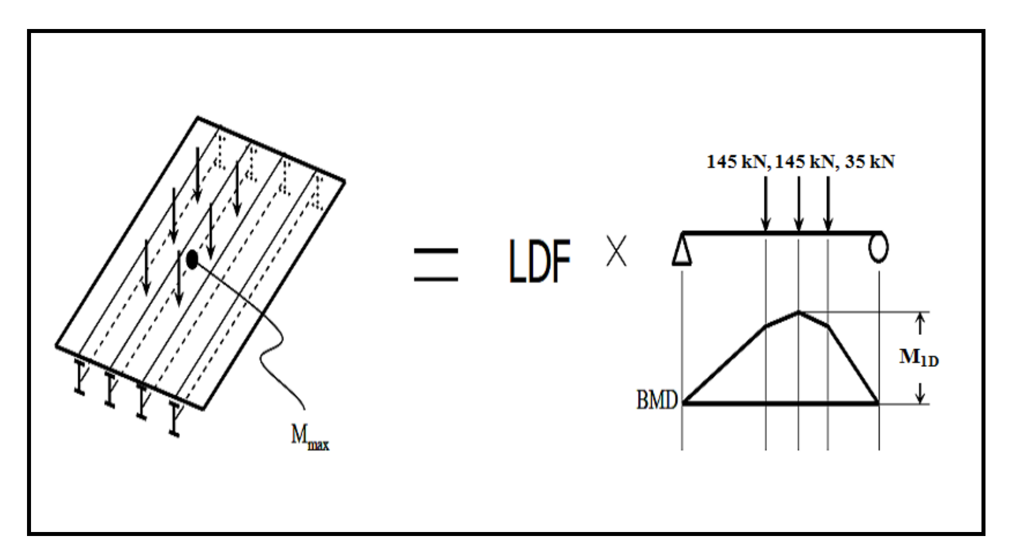

Figure 4.6 Determination of Load Distribution Factors (LDF).

4.3.2 FEA Results of Analyzed Bridges

Table 4.1 Max. Stresses and Moments for Bridge Model No.1: BT54 Girders Bridge.

Bridge Cases	Maximum Stresses (N/m^2)	Maximum Moments (N-m), by Eq. (4.3)
Interior Girder Loading		
FEA Non-Diaphragms	3284064	1642032
FEA Diaphragms	3042144	1521072
Exterior Girder Loading		
FEA Non-Diaphragms	3024000	1512000
FEA Diaphragms	3265920	1632960

From the maximum mid-span moments on girder, the maximum exterior and interior moments were selected. Multiple presence factors (live load intensity reduction factors) of 0.85 are applied to all the moments calculated with three loaded lanes condition, as shown in Figure 3.13 in previous chapter.

Finally, the distribution factors for the interior and exterior girders are found by dividing the maximum interior and exterior girder moments (M_{max}) by the static moment (M_{1D}) calculated for HS20 truck, placed on the one-dimensional beam, as shown in Figure 4.6, and using the principles of statics, we can obtain M_{1D} = 3024 kN-m.

Tables 4.5 to 4.8 and Figures 4.9 to 4.12 show the calculated load distribution factors for all bridge configurations using the LDF calculation methods discussed above.

Table 4.2 Max. Stresses and Moments for Bridge Model No.2: BIV36 Girders Bridge.

Bridge Cases	Maximum Stresses (N/m^2)	Maximum Moments (N-m), by Eq. (4.3)
Interior Girder Loading		
FEA Non-Diaphragms	2994127	1497063.5
FEA Diaphragms	2744091	1372045.5
Exterior Girder Loading		
FEA Non-Diaphragms	3127465	1563732.5
FEA Diaphragms	3109357	1554678.5

Table 4.3 Max. Shears for Bridge Model No.1: BT54 Girders Bridge.

Bridge Cases	Maximum Shear (N)
Interior Girder Loading	
FEA Non-Diaphragms	173738
FEA Diaphragms	159924
Exterior Girder Loading	
FEA Non-Diaphragms	173808
FEA Diaphragms	164346

Table 4.4 Max. Shears for Bridge Model No.2: BIV36 Girders Bridge.

Bridge Cases	Maximum Shear (N)
Interior Girder Loading	
FEA Non-Diaphragms	158654
FEA Diaphragms	152997
Exterior Girder Loading	
FEA Non-Diaphragms	167748
FEA Diaphragms	160990

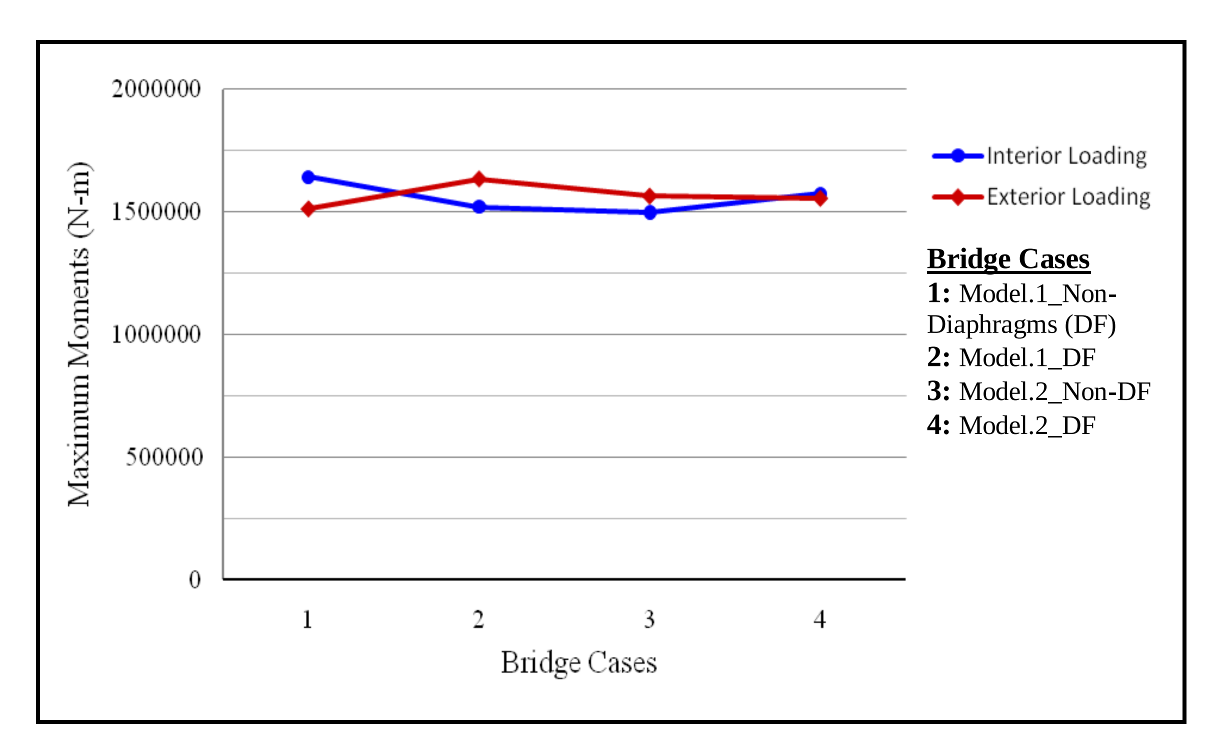

Figure 4.7 Comparison of FEA Max. Moments between All Bridge Models.

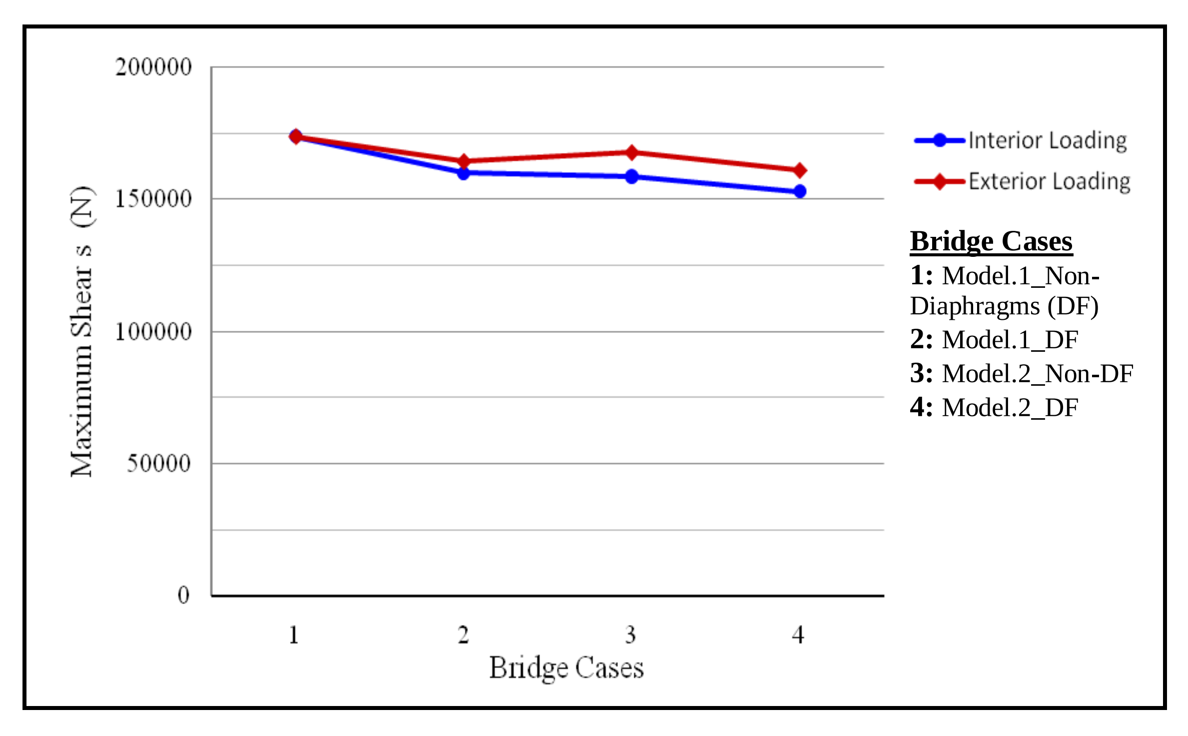

Figure 4.8 Comparison of FEA Max. Shears between All Bridge Models.

Table 4.5 Comparisons of Moments LDF in Bridge Model No.1.

Bridge Cases	AASHTO LRFD[a] (A)	AASHTO Standard[b] (B)	FEA (C)	(A) – (C) ÷ (A) (%)	(B) – (C) ÷ (B) (%)
Interior Girder Loading					
FEA Non-Diaphragms	0.780	1.456	0.543	30 %	63 %
FEA Diaphragms	0.780	1.456	0.503	35.5 %	65.5 %
Exterior Girder Loading					
FEA Non-Diaphragms	0.780	1.456	0.500	36 %	66 %
FEA Diaphragms	0.780	1.456	0.540	31 %	63 %

[a] AASHTO LRFD LDF is the number of design lanes per girder.
[b] AASHTO Standard LDF is the number of wheel lines per girder.

Table 4.6 Comparisons of Moments LDF in Bridge Model No.2.

Bridge Cases	AASHTO LRFD[a] (A)	AASHTO Standard[b] (B)	FEA (C)	(A) – (C) ÷ (A) (%)	(B) – (C) ÷ (B) (%)
Interior Girder Loading					
FEA Non-Diaphragms	0.683	1.220	0.495	27.5 %	59.4 %
FEA Diaphragms	0.683	1.220	0.454	33.5 %	62.8 %
Exterior Girder Loading					
FEA Non-Diaphragms	0.740	1.220	0.517	30 %	57.6 %
FEA Diaphragms	0.740	1.220	0.514	30.5 %	57.9 %

[a] AASHTO LRFD LDF is the number of design lanes per girder.
[b] AASHTO Standard LDF is the number of wheel lines per girder.

Table 4.7 Comparisons of Shears LDF in Bridge Model No.1.

Bridge Cases	AASHTO LRFD[a] (A)	AASHTO Standard[b] (B)	FEA (C)	(A) – (C) ÷ (A) (%)	(B) – (C) ÷ (B) (%)
Interior Girder Loading					
FEA Non-Diaphragms	0.826	1.456	0.660	20 %	55 %
FEA Diaphragms	0.826	1.456	0.607	26.5 %	58.3 %
Exterior Girder Loading					
FEA Non-Diaphragms	0.826	1.456	0.660	20 %	55 %
FEA Diaphragms	0.826	1.456	0.624	24.5 %	57 %

[a] AASHTO LRFD LDF is the number of design lanes per girder.
[b] AASHTO Standard LDF is the number of wheel lines per girder.

Table 4.8 Comparisons of Shears LDF in Bridge Model No.2.

Bridge Cases	AASHTO LRFD[a] (A)	AASHTO Standard[b] (B)	FEA (C)	(A) – (C) ÷ (A) (%)	(B) – (C) ÷ (B) (%)
Interior Girder Loading					
FEA Non-Diaphragms	0.848	1.220	0.602	29 %	51 %
FEA Diaphragms	0.848	1.220	0.581	31.5 %	52.4 %
Exterior Girder Loading					
FEA Non-Diaphragms	0.848	1.220	0.637	25 %	48%
FEA Diaphragms	0.848	1.220	0.611	28 %	50 %

[a] AASHTO LRFD LDF is the number of design lanes per girder.
[b] AASHTO Standard LDF is the number of wheel lines per girder.

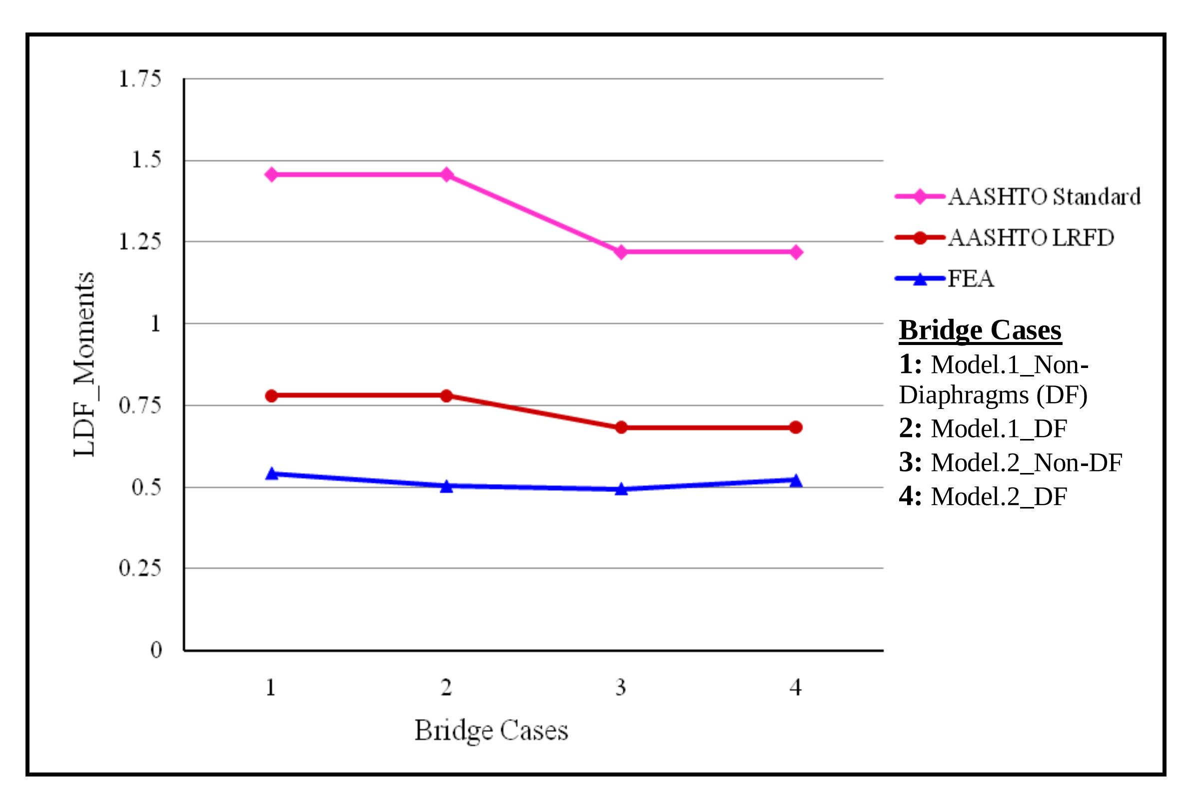

Figure 4.9 Comparison of FEA Moments LDFs to AASHTO Moments LDFs between All Bridge Models for Interior Loading.

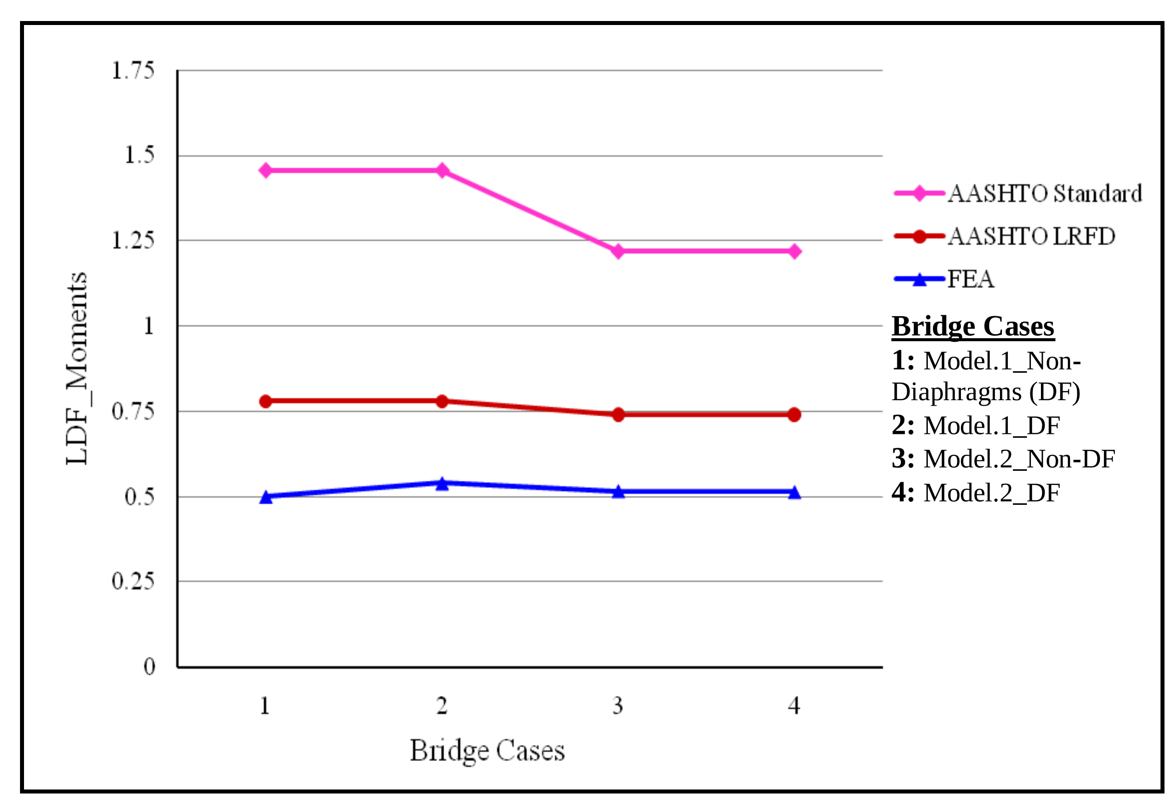

Figure 4.10 Comparison of FEA Moments LDFs to AASHTO Moments LDFs between All Bridge Models for Exterior Loading.

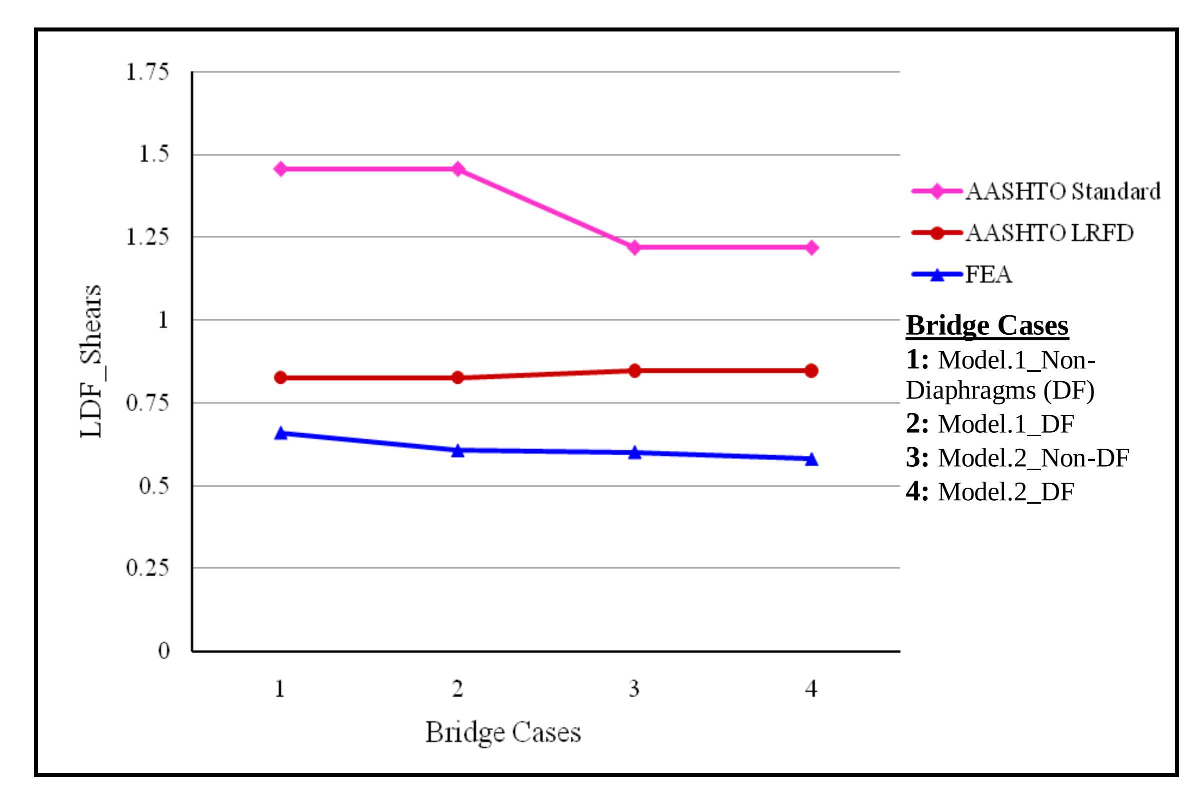

Figure 4.11 Comparison of FEA Shears LDFs to AASHTO Shears LDFs between All Bridge Models for Interior Loading.

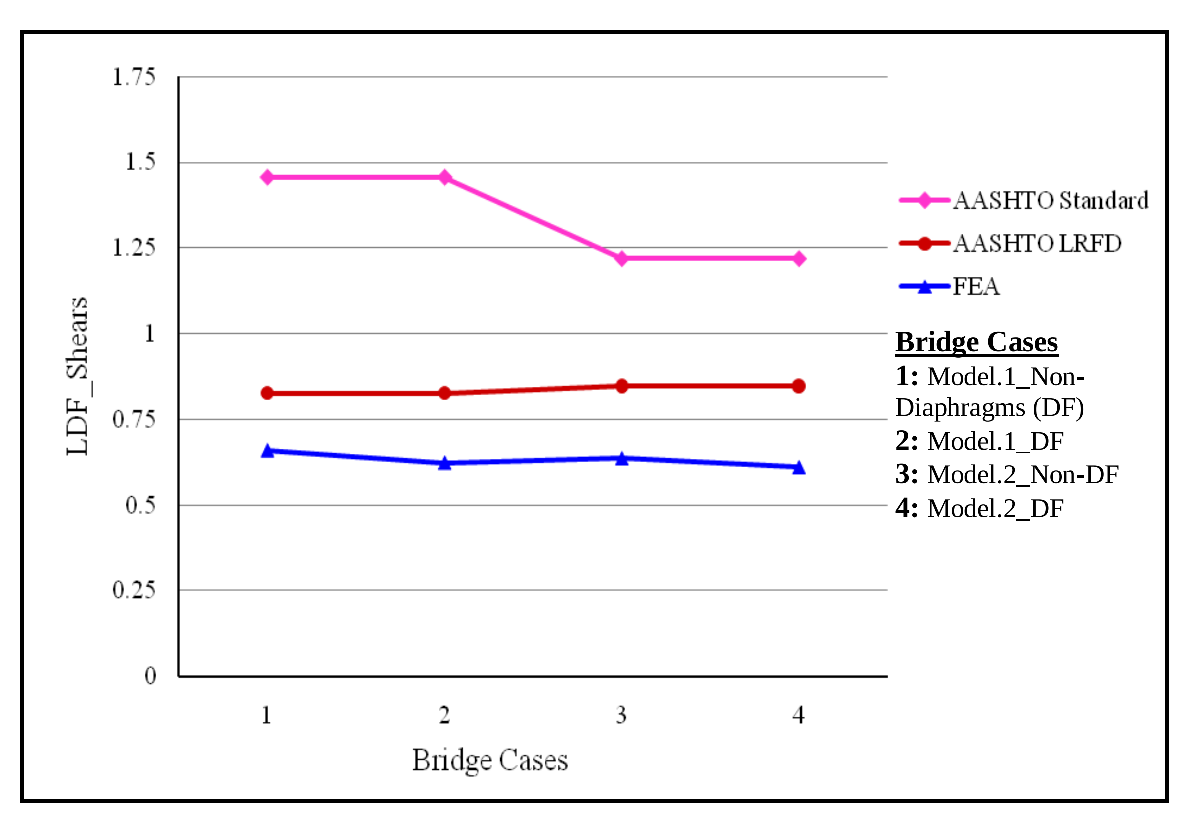

Figure 4.12 Comparison of FEA Shears LDFs to AASHTO Shears LDFs between All Bridge Models for Exterior Loading.

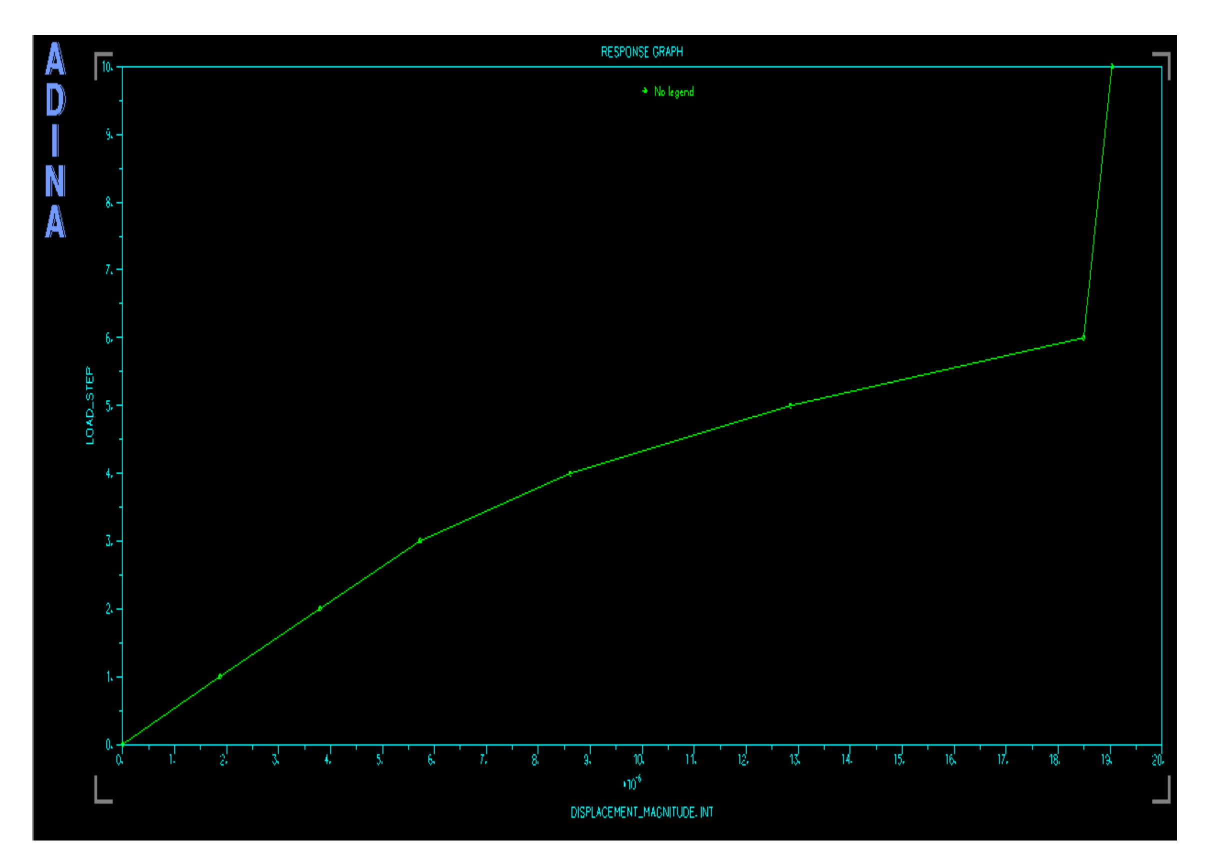

Figure 4.13 Nonlinear Curve (Load Steps Vs Displacement) at Midspan, by ADINA Program. The Jump at the Final Point Indicates the Failure Point of Bridge Model.

Table 4.9 Comparisons of Moments LDFs at Elastic and Ultimate Stages for Diaphragms Models in Bridge Model No.1.

	Elastic Stages	**Ultimate Stages**
FEA Diaphragms/Interior Loading		
Load Values (N)	32625	72500
Maximum Moments (N-m)	583014.5	1521072
LDF	0.193	0.503
FEA Diaphragms/Exterior Loading		
Load Values (N)	32625	72500
Maximum Moments (N-m)	580856.5	1632960
LDF	0.192	0.540

Table 4.10 Comparisons of Moments LDFs at Elastic and Ultimate Stages for Non-Diaphragms Models in Bridge Model No.1.

	Elastic Stages	**Ultimate Stages**
FEA Non-Diaphragms/Interior Loading		
Load Values (N)	32625	72500
Maximum Moments (N-m)	605511.5	1642032
LDF	0.200	0.543
FEA Non-Diaphragms/Exterior Loading		
Load Values (N)	32625	72500
Maximum Moments (N-m)	641657	1512000
LDF	0.212	0.500

Table 4.11 Comparisons of Moments LDFs at Elastic and Ultimate Stages for Diaphragms Models in Bridge Model No.2.

	Elastic Stages	**Ultimate Stages**
FEA Diaphragms/Interior Loading		
Load Values (N)	36250	72500
Maximum Moments (N-m)	652310	1574031
LDF	0.220	0.521
FEA Diaphragms/Exterior Loading		
Load Values (N)	36250	72500
Maximum Moments (N-m)	740648	1554678.5
LDF	0.245	0.514

Table 4.12 Comparisons of Moments LDFs at Elastic and Ultimate Stages for Non-Diaphragms Models in Bridge Model No.2.

	Elastic Stages	**Ultimate Stages**
FEA Non-Diaphragms/Interior Loading		
Load Values (N)	24167	72500
Maximum Moments (N-m)	494425	1497063.5
LDF	0.164	0.495
FEA Non-Diaphragms/Exterior Loading		
Load Values (N)	24167	72500
Maximum Moments (N-m)	524771	1563732.5
LDF	0.174	0.517

Table 4.13 Comparisons of Shears LDFs at Elastic and Ultimate Stages for Diaphragms Models in Bridge Model No.1.

	Elastic Stages	**Ultimate Stages**
FEA Diaphragms/Interior Loading		
Load Values (N)	32625	72500
Maximum Shears (N)	74840	159924
LDF	0.284	0.607
FEA Diaphragms/Exterior Loading		
Load Values (N)	32625	72500
Maximum Shears (N)	76646	164346
LDF	0.291	0.624

Table 4.14 Comparisons of Shears LDFs at Elastic and Ultimate Stages for Non-Diaphragms Models in Bridge Model No.1.

	Elastic Stages	**Ultimate Stages**
FEA Non-Diaphragms/Interior Loading		
Load Values (N)	32625	72500
Maximum Shears (N)	81249	173738
LDF	0.308	0.660
FEA Non-Diaphragms/Exterior Loading		
Load Values (N)	32625	72500
Maximum Shears (N)	81165	173808
LDF	0.308	0.660

Table 4.15 Comparisons of Shears LDFs at Elastic and Ultimate Stages for Diaphragms Models in Bridge Model No.2.

	Elastic Stages	**Ultimate Stages**
FEA Diaphragms/Interior Loading		
Load Values (N)	36250	72500
Maximum Shears (N)	80120	152997
LDF	0.304	0.581
FEA Diaphragms/Exterior Loading		
Load Values (N)	36250	72500
Maximum Shears (N)	81510	160990
LDF	0.309	0.611

Table 4.16 Comparisons of Shears LDFs at Elastic and Ultimate Stages for Non-Diaphragms Models in Bridge Model No.2.

	Elastic Stages	**Ultimate Stages**
FEA Non-Diaphragms/Interior Loading		
Load Values (N)	24167	72500
Maximum Moments (N-m)	56622	107374
LDF	0.215	0.602
FEA Non-Diaphragms/Exterior Loading		
Load Values (N)	24167	72500
Maximum Moments (N-m)	57126	112100
LDF	0.217	0.637

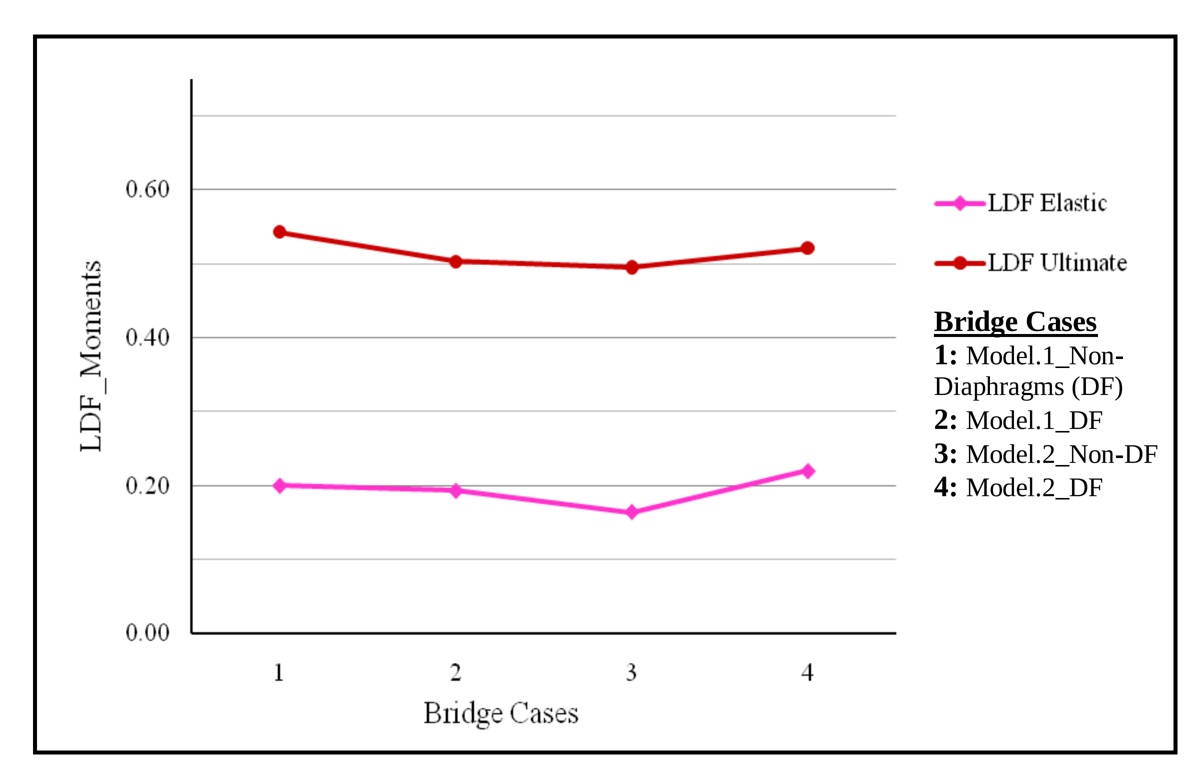

Figure 4.14 Comparison of Moments LDFs at Elastic and Ultimate Stages between All Bridge Models for Interior Loading.

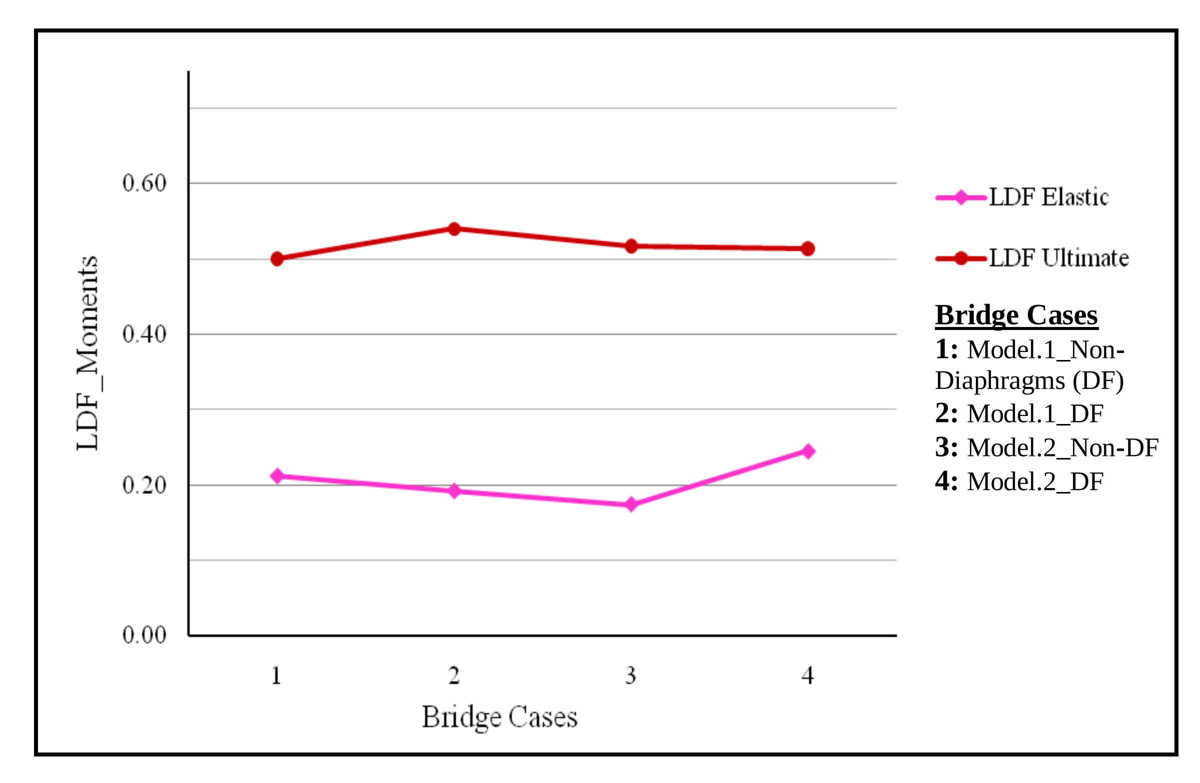

Figure 4.15 Comparison of Moments LDFs at Elastic and Ultimate Stages between All Bridge Models for Exterior Loading.

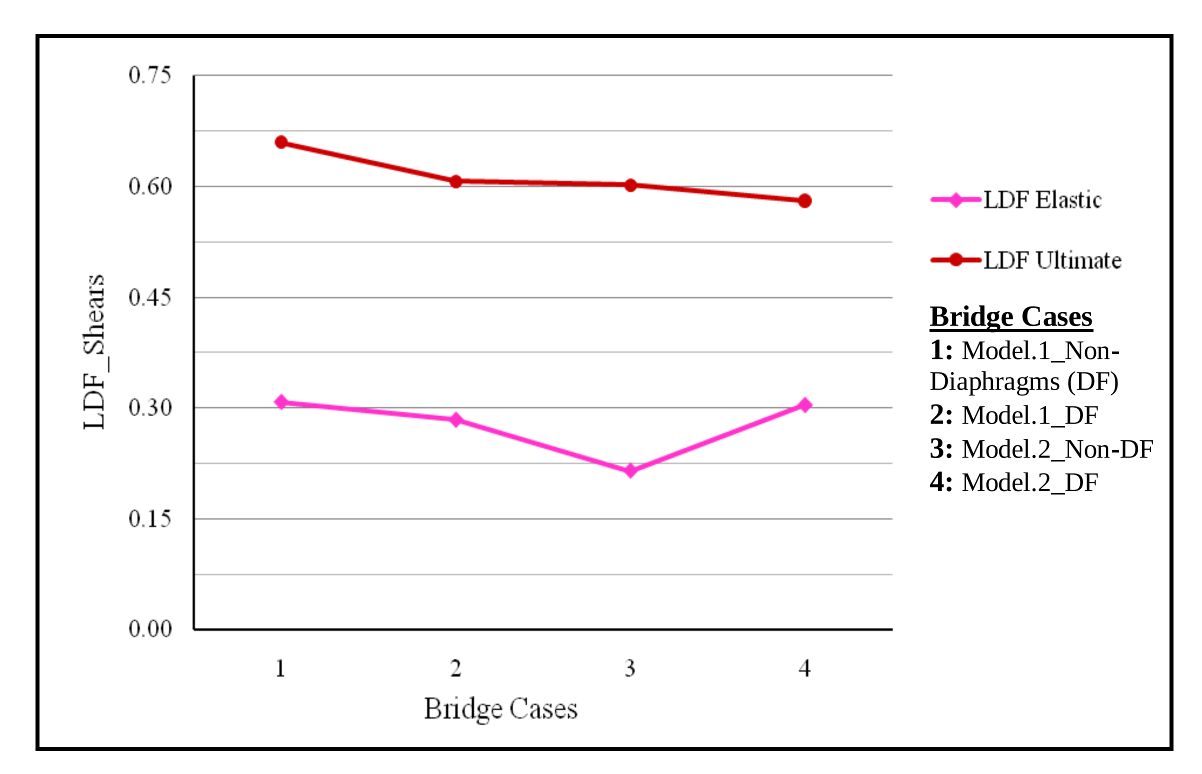

Figure 4.16 Comparison of Shears LDFs at Elastic and Ultimate Stages between All Bridge Models for Interior Loading.

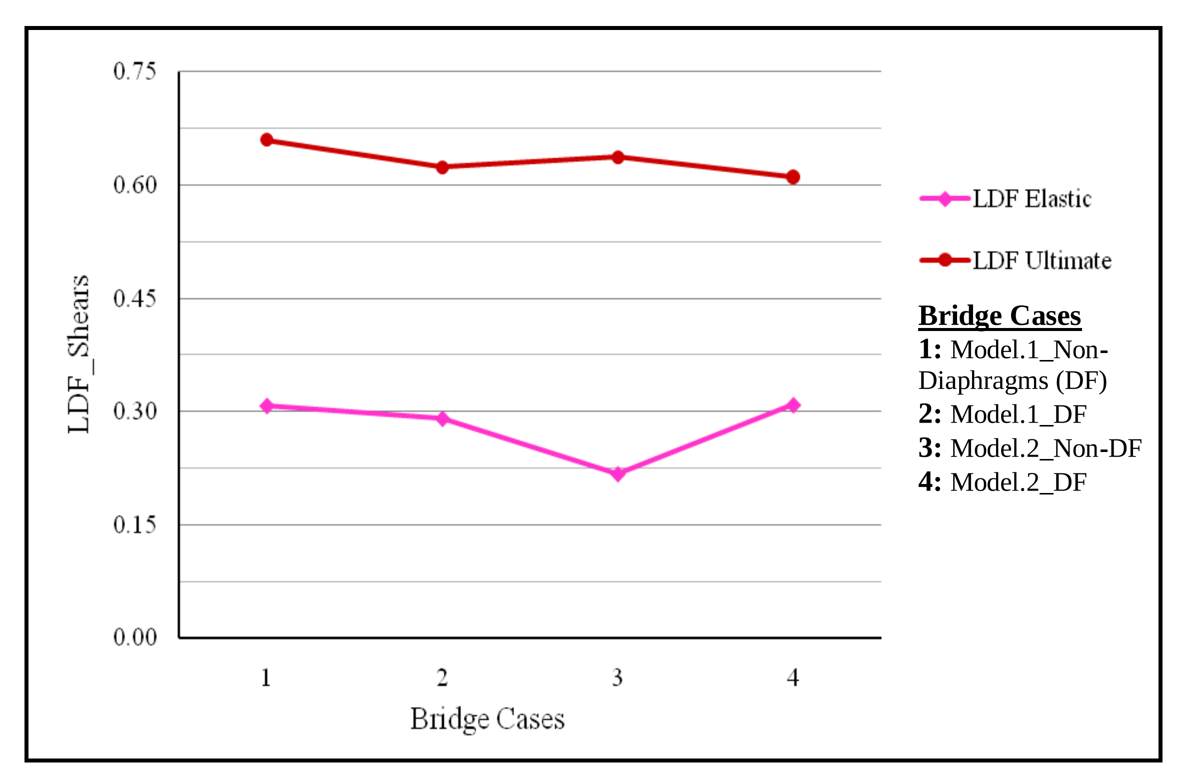

Figure 4.17 Comparison of Shears LDFs at Elastic and Ultimate Stages between All Bridge Models for Exterior Loading.

4.4 Discussion of Results

Load distribution factors were calculated using AASHTO LRFD (2010), AASHTO Standard (2002) and Finite Element Analysis (FEA). The calculation of LDFs from the FEA results can be obtained based on stresses, strains, and deflections at the midspan with the respective equations presented above.

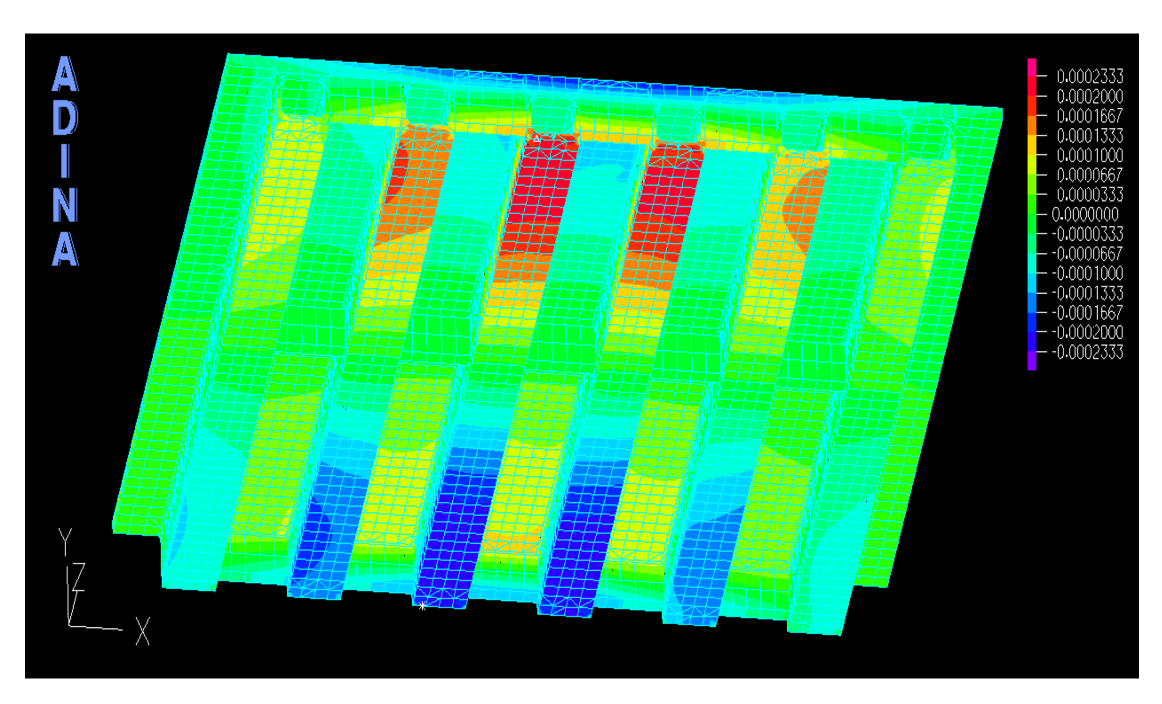

Figure 4.18 Displacement Contour for Bridge Model No.2 under Interior Loading.

Once the results produced by model were verified in service ranges, the truck loads were increased to higher values in order to cause cracking of the concrete, yielding of prestressing tendons, and a consequent, nonlinear response, Figures 4.19 and 4.20 show the bridge models at its ultimate strength, where cracks have propagated throughout the whole cross-section causing the model to fail as shown in Figure 4.13.

This Figure shows the midspan deflection, nonlinear curve produced by the finite element model as a function of the applied load. Jump at the final point of the nonlinear curves indicates the failure point of bridge model.

For each model and load case, the mid-span moment and maximum shear forces in each model is calculated according to equations discussed above, and shown in Tables 4.1 to 4.4 and Figures 4.7 and 4.8.

The moment in the girder section is the resultant of three components from the finite element results, these three components are noncomposite moments, composite moments, and prestressing moments. It was observed that for interior girder loading in non-diaphragms configurations; the maximum moment and shear values increased in model no.1 and decreased in model no.2.

For exterior girder loading, the maximum moment values decreased, and increased for shear values in model no.1, while the maximum moment values increased, and decreased for shear values in model no.2.

Also, in diaphragms configurations, the maximum moment values decreased for interior girder loading, and increased for shear values in model no.1, and in model no.2 the maximum moment values increased, while decreased for shear values.

For exterior girder loading in model no.1, the maximum moment and shear values increased, and these values were decreased in model no.2.

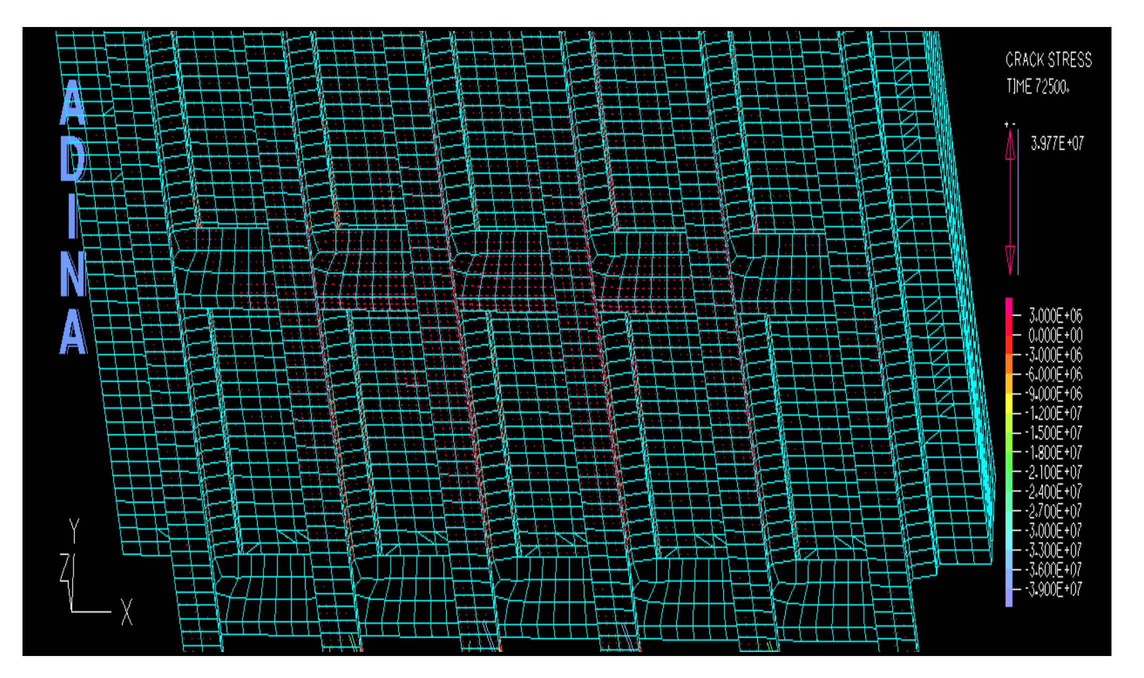

Figure 4.19 Crack Stress for Bridge Model No.1 under Interior Girder Loading.

Depending on the girder arrangement, outside or exterior girders are often subjected to heavier loads than interior girders. Superimposed dead loads such as curbs, sidewalks, railings, barriers, etc., which are placed on an exterior girder after the deck has cured, can be distributed equally among all primary members (AASHTO A3.23.2.3.1.1). If an exterior girder under sidewalk, the girder should be designed for truck load on the sidewalk.

According to the results obtained, it was verified that the use of strains to calculate the LDF are acceptable only in the elastic range, however, using strains to calculate LDFs at ultimate stages, led to unpredictability; this is expected due to plasticity, where superposition is not valid.

This is explained by large strains which develop at crack locations at the bottom of the girders. Similarly, the use of deflections to calculate LDFs was consistently acceptable in the linear range only. Therefore, the use of strains and deflections to obtain LDFs should be limited to linear elastic ranges in computational analyses, since strains are not reliable after cracking (Cai et al, 2004).

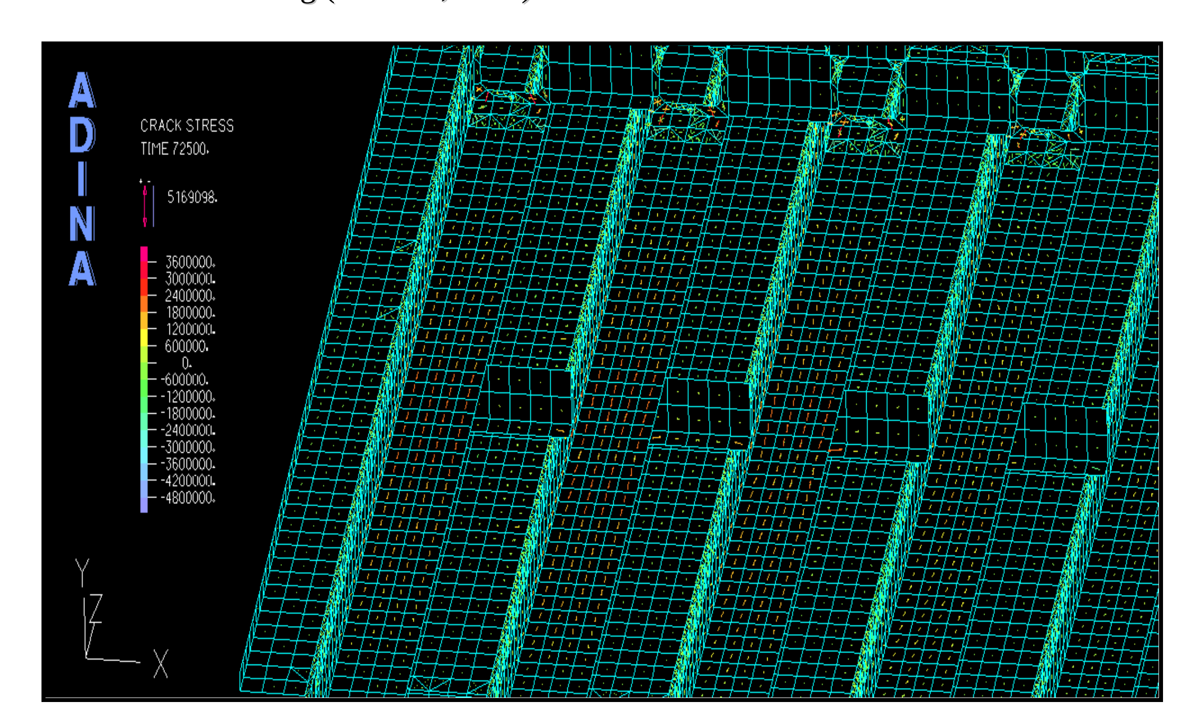

Figure 4.20 Crack Stress for Bridge Model No.2 under Exterior Girder Loading**.**

Based on the linear and nonlinear simulations, it is verified that stresses conveyed the best live load distribution results at ultimate loads.

In this work, LDF calculations based on stresses produced the most realistic results, which were consistently accurate in both linear ranges and ultimate stages. When cracking occurs, the load being carried by a girder is redistributed primarily to the adjacent ones. The stresses contour diagrams in Figure 4.2, which were obtained from solid model analysis in ADINA, shows that there is significant stress concentration at the diaphragms-girder interface; this stress is alleviated by concrete cracking after the rupture stress is reached as shown in Figures 4.19 and 4.20.

A tensile stresses due to live loads in diaphragms may exceed or reach a value close to the rapture modulus. In reality, heavy loads create the possibility of cracks at the diaphragm-girder connection, and only a part of the diaphragm stiffness effectively contributes to load distributions.

It has been observed that the connection between the girder and the diaphragm is essentially a cold joint and is structurally weak, with usually one or two reinforcement bars connecting these elements. The stiffness at the connection is variable and is based on the load levels. At low loads, the connection is close to full moment connection. As loads increase up to the ultimate stage, the cold joint may crack and open, leaving only the steel reinforcement effective in the tension region of the diaphragm-girder interface. Therefore, it is necessary to model diaphragms rationally to simulate its actual behavior and to appropriately estimate its effectiveness (Cai et al, 2004).

Plots of the LDFs for moments and shears calculated in this full 3D Finite Element Analysis of two bridge models are presented in Tables 4.5 to 4.8.

The calculated results were then compared considering LDFs for moments and shears calculated according to AASHTO LRFD and AASHTO Standard Specifications, as

shown in Figures 4.9 to 4.12. These LDF values are presented as percentages relative to AASHTO LRFD and AASHTO Standard Specifications results and are made for exterior and interior girder loading cases. AASHTO Standard (2002) LDF values were consistently higher than the AASHTO LRFD (2010) value.

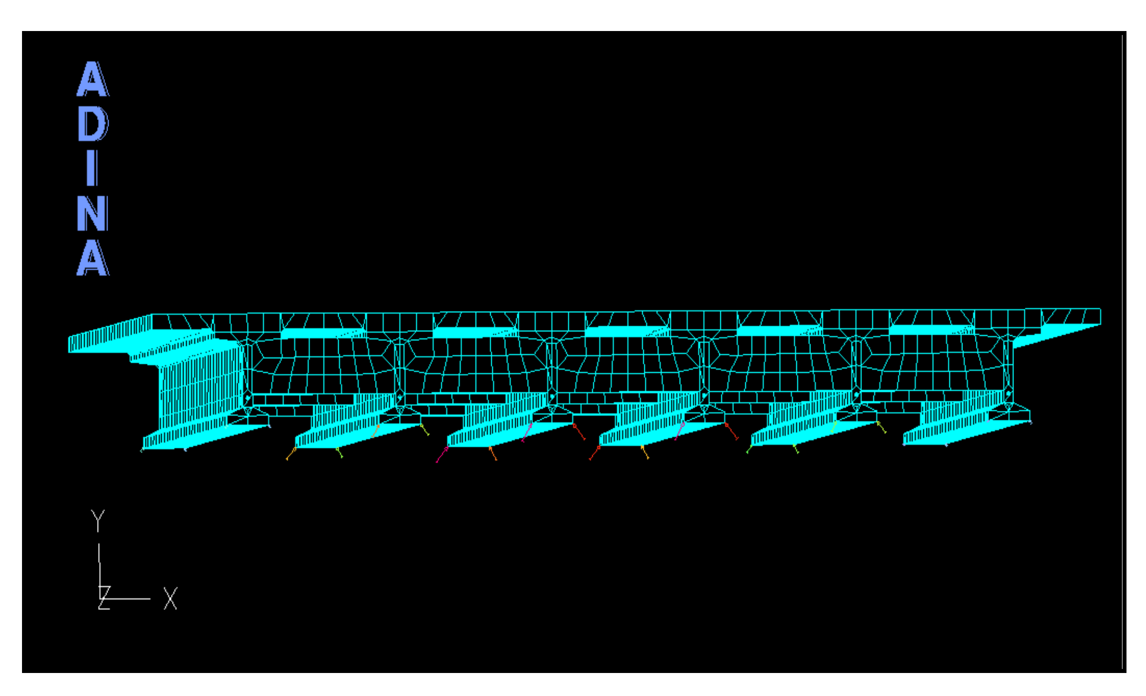

Figure 4.21 Reactions Plots for Bridge Model No.1 under Interior Loading.

4.4.1 Effect of Diaphragms on LDF

The only difference between the bridge configurations I and II were the addition of end and intermediate diaphragms. For interior girder loading it was observed that, the presence of diaphragms decreased the moments LDFs in model no.1 about 7.4% and increased about 5.0% in model no.2. Also, the presence of diaphragms in exterior girder loading increased the moments LDFs in model no.1 about 7.4% and slightly decreased about 0.6% in model no.2.

Diaphragms decreased the shears LDFs for interior girder loading about 8.0% and 3.5% for model no.1 and model no.2, respectively. While, decreased the shears LDFs for exterior girder loading about 5.5% and 4.1% for model no.1 and model no.2, respectively.

For both interior and exterior girders loading, the addition of diaphragms in non-skewed bridge models were investigated in this work had a significant effect on the live load distribution factors. It's required to study more bridge models with skew angle larger than 40^o, and different bridge parameters, to provide more investigation of the effects of diaphragms on load distribution factors.

It is clear from the previous observation that the effect of secondary elements such as diaphragms on the load distribution factor can be significant. In general, it is found that the presence of secondary elements helps the lateral load distribution of girder bridges.

Diaphragms influence the midspan moment in a loaded girders, if the diaphragms are torsionally stiff, they inhibit end rotation of the loaded girder at the expense of causing some end rotation in the adjacent unloaded girders, and this behavior affects the live load distribution factors.

4.4.2 Effect of Girder Types on LDF

The percentage difference in LDFs due to different girder types as in Figures 4.9 and 4.10; indicate that a significant difference exists between the diaphragms effects on load distributions for different girder types. It could occur because of the existing difference in the stiffness of the girder and the diaphragms due to the sections geometry, and BT54 girders require greater diaphragms stiffness than BIV36 girder.

Tables 4.5 to 4.8 show the effects of girder types in non-diaphragms models were decreasing the interior moments LDFs about 8.84% and slightly increasing about 3.5% in diaphragms models. The exterior moments LDFs increasing in non-diaphragms models about 3.3% and decreasing in diaphragms models about 4.8%.

For the Shears LDFs; the effects of girders types in diaphragms models were decreasing the interior LDFs values about 4.3% and decreasing about 8.8% in non-diaphragms

models. While, slightly decreasing the exterior LDFs values in diaphragms models about 2.1% and decreasing about 3.5% in non-diaphragms models.

The LRFD Specifications produce a reasonable and conservative estimate at lower depth and stiffness values, but multi-lane estimates tend to get increasingly conservative for larger girders. Note that the formulas show more conservatism for deeper sections 2.44 m and deeper.

Also, it should be noted that the deepest section (3 m) has a Kg (Stiffness parameter) value that is outside the range of applicability; however, although these results are more conservative, they are considerably less conservative than the lever rule.

The AASHTO Standards Specifications in this case produce highly conservative results (up 50%). Both specifications ignore this effect. However, the LRFD Specifications remain slightly conservative, even at larger sizes (higher depth and stiffness), while AASHTO Standards is unconservative for both single lane and multiple lane cases.

In general, the girder types with wider flange will increase the vertical deflection of the deck due to the enhanced coupling between the girders and the deck, and increasing the web height of girders will increase the girder stiffness as well as the total bridge stiffness; however, the local displacement at the loading point is also increased due to the increase of web height (McLean et al, 2008).

For all bridge configurations, the live load distribution factors calculated from the AASHTO LRFD Specifications were conservative. However, the degree of conservatism varied greatly among the configurations as shown in Tables 4.5 to 4.8 and Figures 4.9 to 4.12.

4.4.3 Effect of Structural Nonlinearity on LDF

The distribution factors calculated within the codes procedures were up to 23% and 50% for AASHTO LRFD and AASHTO Standard, respectively larger than the factors calculated with the FEA models. The load distribution factor by AASHTO LRFD is the number of design lanes per girder, while other load distribution factors are in terms of the number of wheel lines per girder.

In comparison of the FEA Moments LDFs to AASHTO Moments LDFs, it was observed that in the presence of diaphragms in model no.1, the Nonlinear Finite Element Plastic Modeling (NFEPM), decreasing the maximum interior LDFs values about 35.5% and 65.5% for AASHTO LRFD and AASHTO Standard, respectively, and for model no.2 decreasing the maximum interior LDFs values about 23.7% and 57.3% for AASHTO LRFD and AASHTO Standard, respectively.

For maximum exterior LDFs, the NFEPM decreasing these values in model no.1 about 31% and 63% for AASHTO LRFD and AASHTO Standard, respectively and decreasing the maximum exterior LDFs values in model no.2 about 30.5% and 57.9% for AASHTO LRFD and AASHTO Standard, respectively.

While, for the FEA Shears LDFs to AASHTO Shears LDFs it was observed that in model no.1, the NFEPM decreasing the maximum interior LDFs values about 26.5% and 58.3% for AASHTO LRFD and AASHTO Standard, respectively, and for model no.2 decreasing the maximum interior LDFs values about 31.5% and 52.4% for AASHTO LRFD and AASHTO Standard, respectively.

For maximum exterior LDFs, the NFEPM decreasing these values in model no.1 about 24.5% and 57% for AASHTO LRFD and AASHTO Standard, respectively, and decreasing the maximum exterior LDFs values in model no.2 about 28% and 50% for AASHTO LRFD and AASHTO Standard, respectively.

Estimation of shear distribution according to AASHTO Standard tends to be unconservative when they are based on formulas for moment distribution. Furthermore, both AASHTO LRFD and AASHTO Standard formulas always produce conservative results when all secondary elements are considered.

Nonlinear Finite Element Plastic Modeling (NFEPM) shows that the live load distribution factors (LDF) calculated according to AASHTO LRFD (2010) Specifications is conservative, underestimating the strength of the bridge.

The theoretical ultimate LDF values was calculated by dividing the number of lanes loaded by the number of girders, assuming that all girders take the same amount of load at the ultimate stage due to ideal load redistribution.

In this study, one of the ultimate LDFs was 0.495, which means that the live load taken by each girder should converge to this value under ideal circumstances.

Tables 4.9 to 4.16, and Figures 4.14 to 4.17, gives a comparison of LDFs at elastic and ultimate stages, it was observed that for all bridge configurations the difference ranges from 52.3% to 67%, and from 48% to 66%, for Moments LDFs and Shears LDFs respectively.

Also, the LDFs derived from the NFEPM results are the lowest for all study cases, as compared to those obtained from the code specified empirical formulae.

The LDFs derived from elastic finite element results; produced a little effect, values close to each other in all study cases, and gives small values as compared to those derived from ultimate stages, this phenomena is due to the large displacement and large strain energy assumptions in ADINA Program. In general, the LDFs derived from ultimate stages are not valid yet, and only plastic analysis is valid in this case, it’s also being function of many other factors.

If the distribution factors from the finite element model of the bridge had been used to design the girders, instead of the conservative factors from the LRFD Specifications, the required release strength could have been reduced from 50 MPa to 40 MPa. Alternatively, the bridge could have been designed for a 39% higher live load (Barr et al, 2001).

This implies a significant cost saving in girder construction if the FEA method is employed; the cost for the FEA is merely a fraction of the total project cost, and AASHTO method is conservative, underestimating the strength of the bridge.

4.5 General Checks on ADINA

Finite element programs are notorious for generating stacks of printout and a multitude of results. It is essential that the designer conduct some checks by independent means to detect any gross errors that may be introduced into the analysis through incorrect input data. To achieve this objective, using the beam formula *as recommended by Chen Y., 1999*, to predict the average tensile stress (σ_{avg}) in the bottom fiber as follows

$$\sigma_{avg} = \frac{\begin{pmatrix} No.of\ loaded \\ lanes \end{pmatrix} \begin{pmatrix} Midspan\ moment \\ per\ lane \end{pmatrix}}{(No.of\ beams)(S_b)} \qquad (4.4)$$

where S_b is the noncomposite elastic modulus of girder = 0.159 m^3 (PCI Handbook, 2010).

And from equation 4.4, the average tensile stress (σ_{avg}) = 3.17 MPa, this value is close to the one derived from ADINA program results (i.e., 3.20 MPa).

CHAPTER ⑤: CONCLUSIONS AND RECOMMENDATIONS

CHAPTER 5. CONCLUSIONS AND RECOMMENDATIONS

Finite Element Analysis (FEA) enables bridge engineers to determine the distribution of live loads more accurately than using empirical of restricted code formulas.

The AASHTO LRFD (2010) load distribution factors equations were developed based on linear elastic finite element analysis and probability theory, considering only primary members, i.e., the effects of secondary elements such as diaphragms were not considered. The load distribution factor by AASHTO LRFD is the number of design lanes per girder, while other load distribution factors are in terms of the number of wheel lines per girder.

The purpose of this study was to investigate the effect of secondary elements on the live load distribution of girder bridges. The secondary elements such as diaphragms were modeled using detailed 3D Nonlinear Finite Element Plastic Models (NFEPM), and the calculated load distribution factors for moments and shears were compared with the code-specified values.

From previous observation, the effect of secondary elements such as diaphragms on the load distribution factor can be significant. In general, it is found that the presence of secondary elements helps the lateral load distribution of girder bridges.

Live loads have been a focal concern in bridge design for a long time, with their regulation appearing in the form of empirical distribution factors in the first edition of the AASHTO code in 1931.

Load distribution factors at the ultimate stage have not been extensively studied and may be significantly different from that in the service stage. The main objectives of this study is to understand bridge systems performance in plastic stages, and to demonstrate how the load distribution affects the behavior of prestressed concrete girders as the live

load is increased to higher values in order to cause cracking of the concrete, yielding of prestressing tendons, and a consequent, nonlinear response.

This information will help engineers evaluate bridge capacity more accurately, thus avoiding unnecessary and costly bridge postings as well as identifying unsafe bridges from the transportation network. Particularly, a nonlinear analysis would help researchers understand the real capacity of the prestressed concrete bridges, especially if the diaphragms are eliminated.

In general, the LDF derived from ultimate stages is not valid yet, and only plastic analysis is valid in this case, it's also being function of many other factors.

Nonlinear Finite Element Plastic Models (NFEPM), showed that the ultimate strength calculated according to AASHTO LRFD (2010) Specifications is conservative, underestimating the strength of the bridge.

Some recommendations are presented below in order to further investigate and apply the findings of this study.

1) Bridge vibrations due to moving loads have gained importance due to the accelerated deterioration they can cause in bridge structures if not within acceptable ranges. The intense vibration caused by heavy trucks at high speeds may result in cracks at the cold joint in the diaphragm-girder interface, thus influencing diaphragms effectiveness. More experimental full-scale test is recommended in order to verify the need to increase impact values (IM) for future design.

2) More bridge models must be investigated, a database models containing at least 15 bridge models or more with different parameters such as; girder types, number of girders, span length, girders spacing, continuous girders, location of diaphragms, and a skew angle larger than 40^{o}, to gives a deep investigation of the effects of different parameters on load distribution factors.

3) Effect of high strength concrete girders on load distribution factors, AASHTO standard (2002) don't take into account the influence of the compressive strength of concrete in girders, while AASHTO LRFD (2010) takes this factor into account through the inclusion of modular ratio (n) in load distribution formulas, and recognized these effects as stated in the commentary. However, this effect is not included in the formulas of load distributions. It is necessary to provide an option when designers choose to consider this effect.

4) Steel diaphragms are another option, and can be used to replace reinforced concrete diaphragms.

5) Effects of bridge deck cracking into load distribution factors; many bridges have been identified as having significant cracking in the concrete deck. Even though deck cracking is a well-known phenomenon, the significance of pre-existing cracks on the load distribution has not yet been assessed.

6) Nonlinear Finite Element Plastic Modeling, for bridge span more than 20 meter might not be a possibility yet due to the high computer "horse power" demand. A typical Finite Element Analysis using Mainframe would take less than 10 minutes of CPU time for a 50 meter long bridge with 6 girder lines. In a previous study, a microcomputer was used, and its CPU time would be under three hours.

7) The described Finite Element technique can be used to analyze any bridge configurations and girders, not just simply-supported straight bridges with I-shaped or box girders.

8) Load ratings of bridges are necessary to ensure the safety of general public because some bridges have aged and deteriorated over the course of their life, and are used to determine the safe live load carrying capacity of a highway structure. Nonlinear finite element load rating of bridges has not been extensively studied yet, however, when

implemented; this method can predict the safe load carrying capacity of bridges more accurately, possibly avoiding unnecessary bridge postings and replacement.

REFERENCES

AASHTO (2002), **Standard Specification for Highway Bridges,** (17th ed.), American Association of State Highway and Transportation Officials, Washington, DC, USA.

AASHTO (2010), **LRFD Bridge Design Specification, Customary US units**, (5th ed.), American Association of State Highway and Transportation Officials, Washington, DC, USA.

AASHTO (2007), **LRFD Bridge Design Specification, SI units**, (4th ed.), American Association of State Highway and Transportation Officials, Washington, DC, USA.

ADINA (2005), **Theory and Modeling Guide**, Volume I: ADINA Solid and Structures, ADINA R & D, Inc., Watertown, MA, USA.

Barker, R.M and Puckett, J.A. (2007), **Design of Highway Bridges, An LRFD Approach**, (2nd ed.), Wiley, USA.

Barr, P.J., Eberhard, M.O., and Stanton, J.F. (2001), **Live-Load Distribution Factors in Prestressed Concrete Girder Bridges**. Journal of Bridge Engineering, Vol. 6, No. 5, September/October, pp 298-306.

Bhatti, M.A. (2005), **Advanced Finite Element Analysis of Structures**, Wiley, USA.

Bhatti, M.A. (2005), **Fundamental Finite Element Analysis and Application**, Wiley, USA.

Cai, C.S., Avent, R.R., Araujo, M.C., Chandolu, A. (2006), **Assessing the needs for intermediate diaphragms in prestressed concrete bridges**. LTRC Project No. 03-3ST, State Project No.736-99-1134.

Chen, W.F and Duan. L. (2000), **Bridge Engineering Handbook**, CRC Press, USA.

Chen, Y. (1995), **Prediction of lateral distribution of wheel loads on bridges with unequal girders**. Computers and structures, Vol. 54, No. 4, pp. 609-620.

Chen, Y. (1995), **Refined and simplified lateral load distribution for bridges with unequally spaced girders**: 2. Applications. Computers and structures, Vol. 55, No. 1, pp. 17-32.

Cook, R., Malkus, D., Plesha, M. and Witt, R. (2002), **Concept and Application of Finite Element Analysis**, (4th ed.), Wiley, USA.

Eamon, C. D. and Nowak, A. S. (2002), **Effects of edge-stiffening elements and diaphragms on bridge resistance and load distribution**. Journal of Bridge Engineering, ASCE, Vol. 7, No.5, pp. 258-266.

Garcia, T. M. (1999), **IDs for precast prestressed concrete bridges**. Western Bridge Engineer's Seminar, Seattle, Washington.

Griffin, J.J. (1997), **Influence of Diaphragms on Load Distribution in P/C I-girder Bridges**. PhD Dissertation, University of Kentucky.

Gupta, A.K. and Ma, P.S. (1977), **Error in Eccentric Beam Formulation**. **International Journal for Numerical Methods in Engineering**. Vol. 11, No. 9, pp 1473-1477.

Hambly, E.C. (1991), **Bridge Deck Behaviour**, (2nd ed.), Chapman & Hall, London.

Keogh, D.L. and O'Brien, E.J. (1996), **Recommendations on the Use of a 3-D Grillage Model for Bridge Deck Analysis. Structural Engineering Review**, Vol. 8, No. 4, pp 357-366.

Khaloo. R. and Mirzabozorg. H. (2003), **Load distribution factors in simply supported skew bridges**, Journal of Bridge Engineering, ASCE 8 (4), 241-244.

Kim, S. and Nowak, A.S. (1997), **Load Distribution and Impact Factors for I-Girder Bridges**. Journal of Bridge Engineering, Vol. 2, No. 3, August, pp 97-104.

Mabsout, M. E., Tarhini, K. M., Frederick, G. R., and Tayar, C. (1997), **Finite-element analysis of steel girder highway bridges**. J. Bridge Engrg., ASCE, 2(3), 83–87.

Nawy, E.G. (2005), **Prestressed Concrete, A Fundamental Approach**, (5th ed.), Prentice Hall, USA.

PCI (2010), **PCI Design Handbook**, (7th ed.), Precast/Prestressed Concrete Institute, USA.

Tonias, D.E. & Zhao, J.J. (2006), **Bridge Engineering**, (2nd ed.), McGraw Hill, USA.

Troitsky. (1994), **Planning and Design of Bridges**, Wiley, USA.

Xanthakos, P. (1993), **Theory and Design of Bridges**, Wiley, USA.

Zienkiewicz, O.C. (2005), **The Finite Element Method, Its Basis and Fundamentals**, (6th ed.), Elsevier, USA.

Zokaie, T., Osterkamp, T. A., and Imbsen, R. A. (1991), **Distribution of wheel loads on highway bridges**. National Cooperative Highway Research Program, Project 12-26, Imbsen and Associates, Inc.

Zokaie,T. (2001), **AASHTO-LRFD live load distribution specifications. Journal of Bridge Engineering**, ASCE, Vol. 6, No. 2, pp. 131-138.

تـأثيـر مـكونــات الجسـور على تـوزيــع الحـمل الحــي فـي الجسـور الخـرسـانيـة سـابقـة الإجـهـاد

إعــداد
مـعـــاذ عـلـي الأمـيـــن

المشـرف
الدكتـور نزال صالح العرموطي

المـلخــــــــــــص

لقد تم التحقق من عوامل توزيع الحِمل (LDFs) لقوى العزم والقص في الجسور المتعددة العوارض لمختلف الحالات. وتمت دراسة تأثير أنواع العوارض (Girders) و وجود الحُجب (Diaphragms) على عوامل توزيع الحِمل. وأُخذ بالإعتبار في هذا العمل نوعين للعوارض، وهما الجسور الخرسانية السابقة الإجهاد للعوارض (Bulb Tee Girder) و (Spread Box Girder).

تم استحداث نموذج العنصر المحدود للجسور بإستخدام برنامج (ADINA). ونُمذج سقف الجسر كعناصر صلبة ثلاثية الأبعاد، بينما تم نمذجة العوارض والحُجب كعناصر قشرية لاخطية. وتم تنفيذ التحليل من خلال النطاق اللدن (Plastic).

وقد وجد كما هو متوقع، إن معادلات توزيع الحِمل لكود الأشـتـو كانت آمنة (conservative) إذا أُخذ تحليل العنصر المحدود بعين الإعتبار. وأظهرت معادلات الأشـتـو قيم عالية للتحميل تصل إلى ٢٠% أعلى من نتائج العنصر المحدود.

وقد وجد أيضاً أن تأثير وجود الحُجب على عوامل توزيع الحِمل لقوى العزم معتمد على نوع العوارض ومواقعها. وتبين أن وجود الحُجب للعوارض الداخلية عَمِل على تخفيض عوامل توزيع الحمل للعوارض (Bulb Tee Girders)، بينما وجود الحُجب للعوارض الخارجية عَمِل على زيادة عوامل توزيع الحِمل للعوارض (Spread Box Girders).

يمكن الاستفادة من قدرة الجسر المحفوظة نتيجة التصرف اللدن إذا رُغب في ذلك. ونظراً إلى اللاخطية؛ فإن التصرف اللدن يمكن الاستفادة منه فقط إستناداً على كل حالة، وفي هذه المرحلة لن يكون مفهوم عوامل توزيع الحِمل فعالاً.